# The linking of process modeling of hopper-bottomed clarifier and computational fluid dynamics.

Lee, Brenda Ching Tsia

Swansea University
Prifysgol Abertawe

# The Linking of Process Modeling of Hopper-bottomed Clarifier and Computational Fluid Dynamics

Brenda Ching Tsia Lee

School of Engineering

Swansea University

Submitted to the University of Wales in fulfillment of the requirements for the Degree of

*Doctor of Philosophy*

2009



ProQuest LLC.
789 East Eisenhower Parkway
P.O. Box 1346
Ann Arbor, MI 48106 – 1346

# Certificate of Originality

This thesis is submitted to the Swansea University, under the supervision of Dr. T. N. Croft of Civil and Computational Engineering Centre, School of Engineering, Swansea University, in candidature for the degree of Doctor of Philosophy. The material in this thesis is the original work of the author except where acknowledgement to other authors is expressly made.

Signed,

.....

Brenda C. T. Lee

(Candidate)

Signed,

.....

Dr. T. N. Croft

(Supervisor)

Date: 30/10/2009

DECLARATION

This work has not previously been accepted in substance for any degree and is not being concurrently submitted in candidature for any degree.

Signed ..... (candidate)
Date 30/10/2009

STATEMENT 1

This thesis is the result of my own investigations, except where otherwise stated. Where correction services have been used, the extent and nature of the correction is clearly marker in a footnote(s).

Other sources are acknowledged by footnotes giving explicit references. A bibliography is appended.

Signed ..... (candidate)
Date 30/10/2009

STATEMENT 2

I hereby give consent for my thesis, if accepted, to be available for photocopying and for inter-library loan, and for the title and summary to be made available for outside organisations.

Signed ..... (candidate)
Date 30/10/2009

# Abstract

This study describes the investigation and development of bringing together the abilities of three-dimensional analysis using computational fluid dynamics (CFD) and drinking water treatment process simulator software. The main aim is to enhance the simulation of the performance of the clarification process of the hopper-bottomed clarifier (HBC) in the process model simulator.

The results of the CFD analysis is obtained by simulating the flow through a HBC model, built based on a real tank to obtain the hydraulic retention time (HRT) distribution of the tank. The model was built and refined stage by stage, and in the final model, the properties of the suspended sludge blanket in the model is defined by its solids concentration that varies with the depth of the tank.

The simulation of the clarification process of the process model simulator is based on the mass balance of sludge blanket in a constantly stirred tank reactor (CSTR) model, with limited consideration of the hydraulics behaviour of the tank. Output from the CFD analysis was fed into the process model simulator to allow consideration of the true HRT of the HBC when predicting the performance of the clarification process. Comparison of the results of the prediction before and after the coupling shows the benefits of it.

The enhancement of the precision of the prediction with the coupling was compared with real data of three cases with different raw water quality. This is to demonstrate that the results obtained is encouraging.

# Contents

# Acknowledgements

The accomplishment of this study would not be possible without them:

My supervisors, Colin Hayes and Nick Croft. Many thanks to Colin, for being the driver and the man behind the project, budding ideas and steering it into the right direction. For all the 'geeky' part of the work, nothing could be done without Nick, his patience and dedication; so for that and maybe beyond, I am very grateful.

WRc, David Shepherd and Jeremy Dudley, both of WRc, for their kind involvement and contribution to the project. I want to thank them also for their helpful insights throughout the four years. My gratitude also extends to Bristol Water and Jon Scott for the kind help in providing real data for the use of this work, that I could never do without.

My family - Mummy, Daddy, Cassandra and Daniel, Dimitri, Ken, and Ken's family. Thank you to each and everyone of your for the unceasing support and unconditional love. Thank you for being proud of me and mostly thank you for always believing in me.

My family in Wales - Michelle and Chong, Chris, Sim, May, Theresa, Soo, Ruth Diehl and Alvin. I can never thank any of you enough for the laughter, care and love that you bring with your friendship. I am also grateful to those in Swansea Chinese Christian church for the silent but constant support. I may not name all of you, but be assured that none is forgotten. Also not forgotten are fellow research friends for the pleasant friendships along the way.

Last in the list, but first in order, The Almighty. Thank You for the plan.

# List of Figures

# List of Tables

# Nomenclature

### Roman Symbols

| | |
|---|---|
| $A$ | tank area |
| $C$ | concentration of sludge blanket |
| $C_{min}$ | minimum blanket concentration |
| $C_{rem}$ | colour removed |
| $D_{Al}$ | alum dose |
| $D_{Fe}$ | ferric dose |
| $H$ | height of sludge blanket |
| $H_b$ | height of sludge blanket |
| $h_i$ | height of hopper section of HBC tank |
| $k_f$ | flocculation factor |
| $L$ | height of water in clarifier |
| $n$ | exponent of settling curve |
| $p$ | pressure |
| $Q$ | inflow rate |

$s$ sphericity of floc particles

$S_{Mx}$ viscious stress term in momentum source

$S_{raw}$ concentration of suspended solids in raw water

$S_t$ concentration of total suspended solids

$t$ time

$u$ $x$-component of velocity

$V$ tank volume

$V_{hopper}$ Volume of hopper section of HBC tank

$v$ $y$-component of velocity

$X$ concentration of settleable solids leaving tank

$X_i$ concentration of settleable solids entering tank

$w$ $z$-component of velocity

$z_0$ width of top of HBC tank

$z_i$ width of the base of HBC tank

$D_{poly}$ poly dose

**Greek Symbols**

$\mu$ dynamic viscosity of fluid

$\mu_{infty}$ apparent viscosity of sludge

$\nu$ instananeous upflow velocity

$\nu_{max}$ settling velocity of a single floc particle

$\nu_s$ instananeous hindered settling velocty of the blanket

$\nu_s$ settling velocity of primary particles

$\Phi$ mean blanket concentration

$\rho$ density of fluid

$\varphi$ flow variable

**Acronyms**

CFD Computational Fluid Dynamics

CSTR constantly stirred tank reactor

FVM Finite Volume Method

HBC hopper-bottomed clarifier

HRT hydraulic retention time

LHS left-hand side

RGF rapid gravity filter

RHS right-hand side

TSS total suspended solids content of sludge

WTP Water Treatment Plant

# Chapter 1

# Introduction

## 1.1 Computer Modelling and Simulation of Water Treatment Processes

There are increasing and continuous pressures on the operators of water treatment works to optimise their processes to a higher level. Optimisation of the performance of water treatment works requires a knowledge of the dynamic relationships between flow, water quality and treatment process design and their mode of operation. In practice, drinking water treatment plants are optimised based on rules of thumb, and the knowledge and experience of plant operators.

Computer simulation of treatment processes can be used for predictive control at treatment works, which is beneficial for water companies as they focus on reduction

of cost, and water efficiency. Process modelling tools are also designed to be used for training plant operators as it simulates the performance of the treatment processes in different operational control settings. This means that computer models enable training to take place on the desk, saving energy resources.

A process model is a computational model that simulates the actual treatment process based on mathematical and physical equations that define the process. The simulation therefore provides solutions that predict the output of the process, which in this case, is the water quality of the effluent of a treatment process. Process models have to be calibrated with the operating settings of treatment processes as initial conditions before a simulation. In each case, the yielded results of a simulation are validated using real data as to verify the accuracy of the model. This is done over a range of data before its accuracy is verified. When a model is validated, it can then be confidently used as a process model simulator.

While the application of process modelling of sewage treatment processes is well received, drinking water treatment simulators are not well accepted since its first introduction in the 1990s. This is due to the design of treatment tanks that are driven by jar tests, bench trials and rules of thumb [1]. However, the use of simulators is now slowly becoming common in the water industry as they prove to be useful.

## 1.2 Objectives of Research

The main aim of this research is to achieve greater precision in the simulation of performance characteristics of water treatment processes by bringing together the abilities of two computer modelling tools, a process model simulator and Computational Fluid Dynamics (CFD) . Both of these modelling tools have different features and thus give information on different aspects on the performance of a treatment process.

The simulation of a water treatment simulator does not include the possible effects of physical features of a process tank on the flow characteristics within a unit treatment. The output from CFD analysis, on the other hand, is able to demonstrate the variation of physical variables and their effects in the flow throughout a process unit. The fluid retention time of a treatment process tells a lot about its hydraulic performance and is the main focus of this work.

The coupling of a process model simulator and CFD analysis is a work that aims to achieve a hopper-bottomed clarifier (HBC) process model integrated with the understanding of the hydraulics regime, and its effect on its true fluid retention time. The linking will have several benefits, which are, more accurate simulation of performance characteristics, an enhanced capacity to investigate design features, and more powerful training tools.

This research work began with some exploration work done on the two modelling tools, water treatment simulator and CFD. With the objective to achieve, the capabilities of these tools needed to be known and understood. The ability and main

application of CFD modelling is generally known, therefore it started off by looking at the water treatment simulator software package, in the perspective of a user. Following the findings of the study, the use of CFD modelling in this research then took place to look at how its application in process treatment tanks and its results output could be used to investigate the hydraulic retention time (HRT) of treatment tanks.

The research then progressed on doing investigations on how to integrate the results of CFD simulations into process model simulators. This stage of the research commenced with building CFD models of process tanks. All real data and informations of treatment processes used in this research are provided by the Littleton Treatment Works of Bristol Water plc. The outcome of the CFD modelling work were then applied into a process model simulations of the HBC to investigate the effect of the coupling of the modelling tools. The results obtained are also compared to the real data.

The initial plan of this stage of the research was to include the investigations for all the process treatment tanks found in Littleton Treatment Works. As a starting point, the post-ozone tank was first modelled [2]. However as the work progressed, it was found that there were too many unknowns. The validation of the CFD simulation of the process also could not be easily done, causing this work to be discontinued.

As a sequent, the research work was then progressed on to model the HBC tank. The HBC process model is a model that still needs more understanding and investigation [1]. Hence, the research was then decided to focus on the HBC process tank. The engineering drawing of the HBC tank of Littleton Treatment Works is as show in Figure 1.1.

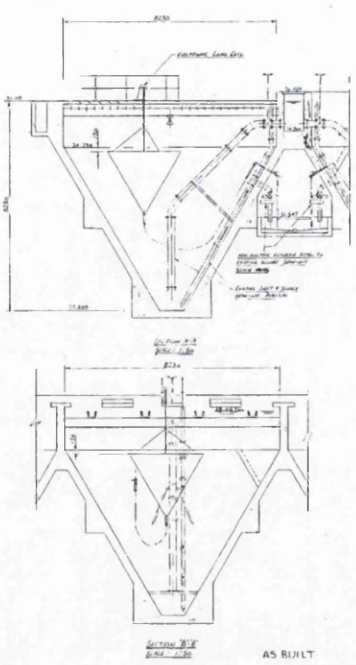


Figure 1.1: Engineering drawing of HBC in Littleton

## 1.3 Literature Review

Dudley et. al [1] made a review on the existing water treatment simulators and commented that the application of modelling in water treatment is not widespread due to several reasons. This is particularly due to the extensive data needed for model calibration and its restriction in modelling for cases outside the calibration range. There are a few existing water treatment modelling programs, namely OTTER, Stimela [3] which is developed by Delft University of Technology, Metrex [4] which is developed by University of Duisberg, Water Treatment Plant Model which is developed by United States Environmental Protection Agency and WatPro which is developed by Hydromantis, Inc [5].

OTTER is a multi-stage process modelling package that can be used to simulate the performance of a whole drinking water treatment plant,or even a single treatment process. It models the changes in a wide range of water quality parameters and is developed by the WRc for the use of engineers, rather than for research purposes. The process model included in OTTER are those typically found in the UK and USA, but not those used in Europe, for instance, water softening. [1]

Stimela is a program that is designed for the use of both practising engineers and researchers. It is an environment that uses MATLAB/Simulink, making is accessible and flexible [6]. Stimela models individual processes dynamically and may be freely accessed on the Internet for general use. Stimela is developed for application in the Dutch water industry.

Metrex also uses MATLAB/Simulink as a platform, but focuses its application for the use of research, specifically the particle removal process. It is not as flexible as Stimela due to its restriction of the MATLAB/Simulink environment. Metrex models treatment processes both analytically and numerically, and provides two level of simulations of which one is simulates in operation mode and the other supports the design process. Metrex is no more readily available as it is no more under development. [1]

The Water Treatment Plant (WTP) model was developed mainly for the use of practising engineer. It was initially developed in support of the Disinfectant/Disinfection Byproducts Rule [7]. The program calculates the effect of disinfections of the modelled treatment processes , but it is merely used to evaluate a design [8].

Similarly to WTP, WatPro focuses on modelling the disinfection processes and is developed mainly for the use of engineers. It includes the calculation of the by-products of disinfection process [9]. The models in WatPro are taken from WTP and its models for solids and turbidity removals are user specified, making it unsuitable to use for real operational work [1].

One most recent development of the water treatment process modelling is the TECHNEAU Water Treatment Simulator [10]. This program is intended to build a European platform for modelling of drinking water treatment processes. It uses OTTER, Stimela and Metrex as its foundation and will be made available on the Internet [1]. One part of the development project is also to develop new process models for those that need improvement, such as the coagulation/flocculation simulator.

As it is with the usage of process treatment simulators in water treatment plants, search on the literature on CFD modelling work also found that it is more widely used in modelling processes of wastewater treatment plants. This literature research, then, specifically looked into modelling of the clarifiers. Although the flow regime in the settling clarifiers is different from that of HBCs, the physical processes that occurs within the tank are the same, if not similar.

The effort to use modelling to design sedimentation tanks to replace empirical methods has the objective to achieve operational efficiency and optimisation of tank design [11]. A review was also done to investigate the usefulness of CFD modelling application [12]. The report highlights the ability of CFD to model the flow pattern or solids distribtution within the tank, something that the empirical models are not able to.

However, the usage of new mathematical models and the cost involved has limited the use of CFD modellling in the water industry. The review has also found gaps in CFD literature for properties of floc particles, flocculation, effect of flow on particle growth or breakup, and some of the geometries and design of clarifiers such as inlet pipe, slope of tank, and the hopper design.

Larsen [13] was the first to have applied a CFD model to several secondary clarifiers. Since then, many CFD modelling work was done for the purpose of studying the performance of the clarifiers (e.g. [14]). CFD simulation of the hydraulic behaviour of clarifiers are also used to look for means to improve the performance of the clarification process (e.g. [15]). Besides that, the use of CFD modelling is also utilised to look at the effect of change of design in clarifiers on the performance of the process (e.g. [16], [17]).

As mentioned in the review by Dudley et. al [1], the modelling of the process of disinfection for drinking water treatment is more thorough. Some examples of these are work done in modelling the UV treatment systems [18], [19] and ozone contactors [20]. Most of these work emphasise on the study of the flow distribution within process tank and its effect on the performance. Some were also intended to evaluate various designs and configurations of process tanks.

More recent application of CFD modelling can also be found in modelling the coagulation and flocculation process. The modelling of the process of flocculation within flocculator tanks or vessels was used to evaluate mixing efficiency (e.g. [21]) and some modelling work demonstrate the benefits of it [22]. The flow characteristics during the

process of coagulation was simulated [23] and particularly for this work, the results of the CFD modelling was used to study the efficiency of the process.

Work has also been initiated in modelling of clarifiers in drinking water treatment plant, however, these works mostly include the modelling of flat bottomed clarifier and circular sludge blanket clarifier. A recent example of this is a work done by Wu et. al [24], where the flow pattern through a circular sludge blanket clarifier was simulated using a three-dimensional model with a multi-phase flow.

Albeit that CFD published work done on a HBC was not found, an unpublished work was found, which was by BHR Group [25]. It was a case study to simulate the flow through an operating HBC so as to find the cause of dropping in performance of the clarifier during high demand [26]. The work was then carried further to adding of modifications to the design of the tank to curb the problem. The outcome of the work was reported to be beneficial, resulting in greater performance and thus reduction in operational costs.

The use of CFD application to flow problems in the water industry covers a large range, for instance, raw water reservoirs water treatment works, distribution systems, collection systems and sewage treatment works [22]. Provided that the prerequisites for calibrating and validating a CFD model can be met, CFD can be effectively utilised as a design tool in the industry [27]. However, there is still limitations on the approximation of the flow using CFD analysis for the clarification process due the fractal nature and settling characteristics of floc particles plus the effect of the density and porosity on drag force that require additional work. Besides that, it is also important to fully

understand the inter-relationships between chemical and biological reactions and the hydraulic conditions of the clarification process [22].

Before the use of CFD modelling, some studies developed mathematical model to simulate the clarification process in a HBC. An initial contribution to this study was by Ives [28], who proposed a model that was based on the principles of orthokinetic flocculation occurring within the sludge blanket. However, this model was found to have over estimated the efficiency of particle removal of the clarifier due to many simplifications made.

In 1979, Gregory [29] made an extensive review for the studies on the clarification process within a floc blanket, that took place until then. In his review, he commented that past studies on the process have not explained thoroughly the basics of the mechanism of the process. His report, therefore fills in the gaps by referring to unpublished work done by the WRc. However, Gregory's work focused on the experimental work and did not link his findings quantitatively.

Another model that simulates the sludge blanket clarification process was developed in 1999 [30]. This model was proved to be successful after its results was compared with experimental data that was obtained from a flat-bottomed clarifier. It is a model that is based on Gould's theory [31] of the operation of floc blanket clarifiers and can be used as an operation or design tool as it can be used to assess the effects of changes in the factors that affect the performance of the clarification process, for instance, the quality of raw water, its temperature, and flow rates.

The model developed by Head et. al [30] assumes that the blanket is completely mixed as it is simulated as a continuous stirred tank reactor (CSTR) . The clarification process in the HBC model in OTTER is based on this model. However, the evaluation of the performance of the process using this model was not tested before on a HBC. The difference in hydraulics behaviour of these two different types of clarifier may contribute to a different conclusion on this model when applied to a HBC.

## 1.4 Thesis Structure

The research work involved in this study is divided into two parts. The first part of the work involves the exploration work done on the two modelling tools mentioned, and the focus of the research. This is presented in Chapters 3 and 4. The second part of it consists of the work done in developing the HBC model and is presented in Chapters 5, 6 and 7 of this thesis. This is then followed by the investigation on the coupling of the modelling tools in Chapter 8 before the work is concluded in Chapter 9.

In Chapter 2, a detailed description of the HBC is elaborated. This is preceeded by an introduction to a typical drinking water treatment plant, stating the treatment processes involved that completes the works.

Chapter 3 introduces the modelling tool, OTTER, and exhibits its features of the application. It presents an investigation on getting to know the OTTER software and highlights the need to incorporate the knowledge of HRT in OTTER. In this chapter, a description of the HBC model in OTTER was also presented.

Chapter 4 explains the theory of CFD that is employed in PHYSICA, which is the modelling package being used in all of the CFD modelling work carried out for this research. The application of CFD modelling is demonstrated in simple tank cases and thus showcases the contribution of CFD analysis in this research.

Chapter 5 elaborates on the initial step of work that has been done in developing a CFD model of the HBC process tank. The chapter presents the two-dimensional model of the HBC tank and the investigation that looked at the flow path of discrete particles through the tank.

Chapter 6 presents the second part of the development of the CFD model of the HBC. Following the findings of the work presented in Chapter 5, a three-dimensional model of the HBC was built and simulated with an imposed sludge blanket.

Chapter 7 describes of the initial steps that were taken to employ the governing equations of HBC in OTTER into the final CFD model of HBC, improved from the model presented in Chapter 6. The results of this product is also being discussed in this chapter.

Chapter 8 reveals the final part of the research, where the findings obtained from the work explained in Chapter 6 is employed into the HBC modelled in OTTER. This fraction of work unveils the effect of the coupling of OTTER and CFD analysis.

Finally, conclusions on the contribution of the findings of this research and ideas on future work that can be done on this study are presented in Chapter 9.

# Chapter 2

# Introduction - Hopper-bottomed Clarifier

In this chapter, the functions and the mechanisms of the HBC in a drinking water treatment works are outlined. A brief description of different stages of water treatment processes are also described to give a better picture of the role that the HBC plays in a complete treatment process.

## 2.1 Drinking Water Treatment Processes

In the UK, water supply for domestic use must meet the definition of being "wholesome" [32]. This basically means that treated drinking water must meet the requirements of

the national regulations derived from the EU Drinking Water Directive (98/83/EC) [33]. The standards set out are based on advice from the World Health Organization.

Originally, the treatment of drinking water focused on improving the aesthetic qualities of drinking water [34]. Currently, the main requirements of treating drinking water is to remove pathogens and toxic chemicals. Therefore, the principal aim of water treatment is disinfection and the preceding treatment processes prepares the raw water for disinfection [32].

There are several stages of treatment prior to the process of disinfection, which are typically the coagulation, clarification and filtration processes. The selection of treatment processes are based on the nature of the source of raw water. The water supply in the UK is obtained from three type of sources; upland surface water, lowland surface water, and groundwater [32]. The different types of sources give water with different types of constituents that need to be removed, for example algae, colour and suspended matter.

The coagulation process is a process where coagulant is added to the raw water, then stirred for better mixing. Coagulants are normally salts of iron or aluminium. The commonly used coagulants in the UK are aluminium sulphate and ferric sulphate [32]. They are added to water to form floc particles that contain dissolved impurities. During the mixing, the process of flocculation takes place. Flocculation is a process where floc particles adhere to each other and grow.

Coagulated water is then treated by a clarification process, where the separation of

the solids from the water. The principal processes that can be used are sedimentation, flotation and filtration. These different treatment methods use different mechanisms to remove the solids from the water. The clarification process are meant to reduce the solids loading on subsequent filters.

In a filtration process, clarified water is passed through a porous medium, which is usually sand. Filtration has been in use since the nineteenth century [35] and is important in treating drinking water to achieve better clarity [36]. There are two types of filters, with the rapid gravity filter (RGF) being more commonly used to treat coagulated water, and the slow sand filter used without any prior coagulation. The RGF became more favourable since the 1930 due to its higher rate of process, which is 50 times faster than that of a slow sand filter [35]. The RGF is used for the removal of colour, aluminium, turbidity and iron, where as slow sand filters are used for the removal of algae and mineral turbidity [32].

Disinfection is a process aimed at killing potentially harmful organisms, as the removal of microorganisms may not be feasible with the treatments prior to this process. Disinfection are commonly achieved through chlorination, ozonation and ultraviolet radiation. To date, chlorine is the most commonly used disinfectant [35]. Each type of disinfectant has its advantages and disadvantages, depending on the water quality. Disinfectants used are expected to be at a concentration sufficiently toxic to microorganisms, but not to human and higher animals, have high killing rate and able to prevent the regrowth of microorganisms [35].

## 2.2 Introduction of HBC

It is common in the UK to use a combined flocculation and sedimentation tank. This process tank is called sludge blanket clarifier. In general, there are two types clarifier used in drinking water treatment works, flat-bottomed and hopper-bottomed.

### 2.2.1 What is A HBC?

A HBC, as shown in Figure 2.1, is a sludge blanket clarifier that is contained in a square hopper-bottomed process tank. A HBC tank is expensive to construct, and thus some HBCs are flat-bottomed with an inlet setting that distribute the inflow like a hopper-bottomed tank does [36].

The HBC is a process tank that follows after coagulation, before water is filtered. As it is with clarifiers, the clarification process that takes place in a HBC is used to reduce the solids loading on filters as coagulated water carry floc particles. Some treatment works also utilise HBC to remove precipitates from softening of lowland waters. [32]

The HBC plays an important role in treatment works as clarified water increases the effciency of disinfection. The clarifying process reduces the turbidity of coagulated water and is able to remove particles that are too fine to be removed by the process of sedimentation alone [36].

In a HBC, chemically coagulated water is treated by removing flocculated particles with the sludge blanket acting as a filter. Water is fed through from the bottom of the

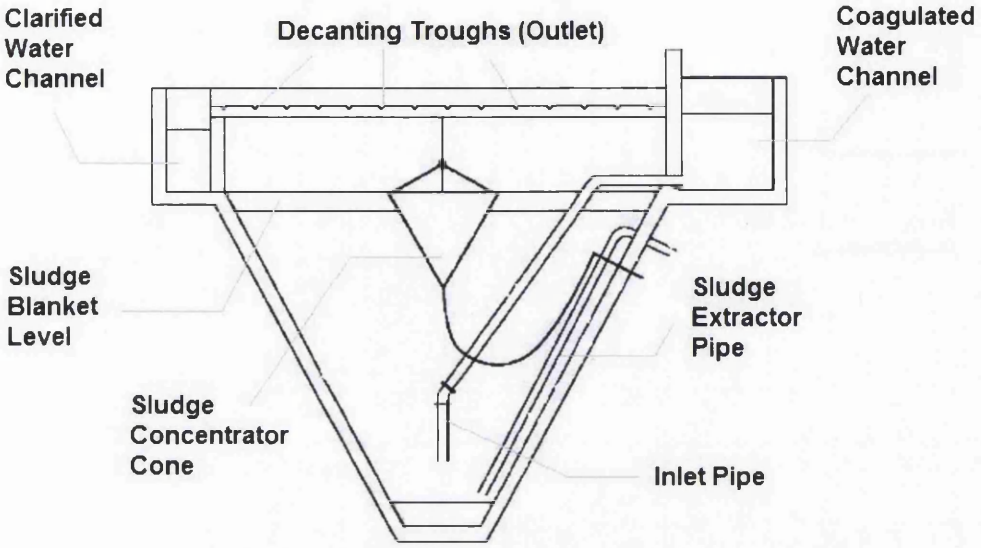


Figure 2.1: A labelled diagram of a hopper-bottomed clarifier

sludge blanket for this purpose. The sludge blanket is also known as the floc blanket as it formed by the acccumulation of floc particles that eventually forms a fluidised bed of sludge.

The passage of the flow through the tank exits through the decanting troughs at the top of the tank. These troughs are normally 1.0 m to 1.5 m above the surface of the sludge blanket. The sizes of the HBC tank that are available range from 0.6 m x 0.6 m to 50.0 m x 50.0 m. [37]

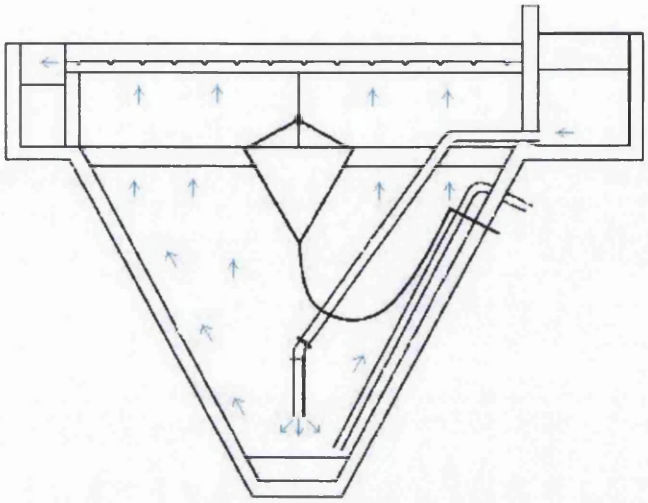

Figure 2.2: Diagram of HBC with flow direction through the clarifier

### 2.2.2 How Does a HBC Work?

The mechanism of the clarification process that occurs within the floc blanket of a HBC involves flocculation, entrapment and sedimentation of floc particles. The diagram in Figure 2.2 shows the progression of the flow through a HBC, where the blue arrows denotes the direction of the flow in the tank. Chemically coagulated water is fed into the tank from the inlet pipe that is situated near the base of the tank.

The inlet pipe introduces flow downward and due to the small aperture of the inlet, water jets in and hits the base of the tank in high velocity. The turbulence in the inflow prevents fine floc particles to agglomerate at this stage and may even cause the breaking of larger floc particles formed.

Water then flow upwards through the tank, approaching the suspended floc blanket. The speed of the upward flow decreases as the cross-sectional area of the tank increases. At this point, the process of flocculation starts to occur. The slowing down of the flow now allows fine floc particles to agglomerate. As this progresses, the flow lines are interrupted by the presence of the sludge blanket that is suspended near the outlet of the clarifier. The floc particles from the inflow also adhere to the particles that form the sludge blanket.

The sludge blanket is held suspended in the hopper section of the HBC tank by its own weight and the upthrust due to the flow. It is kept stable by bleeding the contained sludge into the submerged conical sludge concentrator. The desludging is normally controlled by the weight of sludge accumulated in the cone [32]. It also can be done periodically based on the height of the blanket or the solids concentration of the sludge blanket.

Water in the clarifier has to pass through the blanket that at this stage acts as a filter as it removes solids from coagulated water. The removal of solids occurs when suspended solids in the water is encouraged to adhere to each other and to the floc particles that form the sludge blanket. This phenomenon is also known as hindered settling of floc particles. Floc particles particles are therefore trapped and strained at this stage.

After passing through the sludge blanket, some degree of sedimentation of particles occurs just at the surface of the sludge blanket. The flow of the passage in this region is the lowest, which allows the settling of the floc particles.

The mechanisms of the clarification process occurring within the tank at different regions of the tank is as illustrated in Figure 2.3.

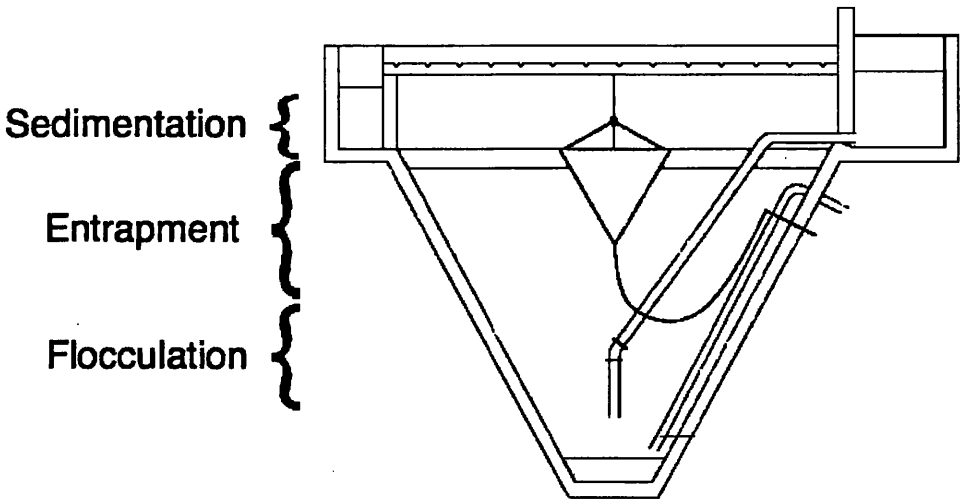


Figure 2.3: Mechanisms that occur within the HBC tank.

The flow progresses without any change in the speed of flow as the walls of the HBC tank in this region is straight-sided. Clarified water then overflows through the decanting troughs at the top of the tank.

## 2.3 The Significance of Hydraulic Retention Time of HBC

While the mechanism of flocculation and the behaviour of the aggregation of floc particles are not the same for any composition of floc particles, the process is time-dependent [29]. The clarification process of a HBC is governed by the physical process of floccu-

lation of floc particles within the tank. Since the main function of a HBC is to remove suspended solids from coagulated water, thus its level of performance is measured by its rate of solids removal [32].

The effciency of a HBC is also influenced by the upflow rate of water in the clarifier [29] and the rate of desludging sludge from the sludge blanket. These two factors govern the volume and the concentration of the sludge blanket, and thus its stability. A HBC is said to be performing well when it is operating at a sludge blanket concentration that gives maximum solids flux, which represents the rate of solids removal per unit surface area [32]. The concentration of sludge blanket also determines how much water is wasted during desludging.

The concentration of the sludge blanket and agglomeration process of the floc particles affect each other, where occurrence of flocculation within the blanket increases the concentration of the sludge blanket and the concentration of the sludge blanket affects the frequency of collision of floc particles. The rate of flocculation within the sludge blanket indicates the characteristic timescale of the clarifying process.

It is important to know and monitor the performance of the clarification process of a HBC to avoid entrainment of fine floc particles in the effluent. Poor performance of the process does not only impair the disinfection process, but also leads to increased frequency of backwashing of subsequent filters in a treatment works [32].

# Chapter 3

# OTTER - Water Treatment Modelling Software

This chapter introduces the process model simulator programme studied in this research, OTTER. It explains briefly the functions and use of OTTER in simulating a treatment works model. Since the focus of this research is on the HBC model, this chapter also includes a detailed description of the HBC model in OTTER.

A simple exploration of the software was also done, where OTTER was used to simulate two treatment works model that are arbitrary. The aim was to observe the results output for two treatment works model of different capacities.

## 3.1 Introduction

OTTER is a multi-stage process modelling tool, that was developed by the Water Research Centre (WRc). It was developed for water industry with the objective to optimise the performance of water treatment works. It is able to predict the water quality at each process stage in a treatment works. It also provides the function to dynamically simulate and thus analyse the performance of the different stages in a treatment works, and the interactions between treatment processes [38]. The software is useful for process engineers and scientists to use as an aid to study water treatment works and their performance at different operating settings.

OTTER requires an extensive set of data for calibration and these data is usually more than what is normally collected. This leads to difficulty for a model to adapt to a special requirement. It does, however provide sets of raw water profile of different sources, of which its determinands can be altered to best fit any simulation setting. Default values for parameters of model calibration are also provided if information is not readily available.

The software is well documented, have proven models and is backed by technical reports of WRc. It is validated based on the work that was done by WRc, mostly using data collected in Britain [39]. OTTER is therefore most suitable to be used for modelling works found in the United Kingdom and the default values that it provides are based on these data. OTTER is therefore, easier to use there is no available data for calibration. OTTER has been used in several water works studies [40], [41], [42], and used mostly in the UK and USA [1].

## 3.2 Modelling with OTTER

OTTER has a collection of individual process models for the most common water treatment processes. A treatment works model is made up of a set of interconnected water treatment process models, which are selected and built by a user.

For every selected process model, its model data can be edited or calibrated to the settings for a real works that is built on. The model data is edited using dialogues that allow changes in the categories of static data, operating data, model calibration, reporting options and results. Dialogues of each category appear as tabs in the user interface. These process models are connected together by streams. Streams are used in OTTER to symbolise channels or pipes.

Each works is comprised of a works definition, where the unit processes, sub-models if needed, and connections between unit processes are defined. Each works also comprises of one or more run definitions. A run definition contains the operational data, including raw water quality, usually varying over the simulation time.

A treatment works model built must have at least one source of raw water. OTTER provides more than fifty columns of water quality determinants that can vary over time. These determinants are water quality parameters that are categorised into groups, which are General, Total metals, Dissolved metals, Inorganics, Organics, Pesticides, Microbiological and Others. The group General includes determinands such as turbidity, temperature, colour, pH and solids. Whereas the group Others include determinands such as algae, chlorophyll, tase, odour, particle size and particle count. These

determinants can be tailored to individual circumstances and for most applications, only a small group of determinants is of interest.

When running a simulation, the start and end date and time can be specified, along with the timestep for the input and output. The time taken to complete a simulation run depends on these settings and the number of treatment processes there are in the works model. A treatment works model that consists of a coagulation tank, a clarifier, a filter and a chlorine tank, that is simulated for a duration of 30 days takes less than two minutes to complete.

When the values of the determinants are set for a simulation case, they are passed with the flow passing through the streams from source to process and from one process to another throughout the whole works, carrying any changes that occur when passing through individual processes.

The main results produced by OTTER consist of the predicted water quality determinands and flow rate values for all streams in the works over the duration of the specified simulation case. Most of the process models also produce resulted water quality after flow has passed through the process. The results for streams and processes are displayed in customised spreadsheets within the OTTER software. OTTER also enables result charts to be created based on the data ranges selected in the spreadsheets.

## 3.3 HBC Model in OTTER

This section specifically describes the HBC model in OTTER, which is the process model that the research focuses on. It includes an overview of the simulation of the clarification process in the model and how a user calibrates the model when running a simulation on OTTER.

The performance of HBC is modelled using the CSTR model. In OTTER, the CSTR model is used to characterise the hydraulic flow regime within the HBC.

The performance of the HBC in OTTER is governed by several factors. All of these factors affect the the stability of the sludge blanket in a HBC and are as follow :

1. The settling characteristics of the floc particles to obtain a hindered settling curve.
2. The concentration of the sludge blanket.
3. The flocculation factor of the floc particles. It is the measure of flocculation occuring within a HBC tank and denotes the ability of the blanket in trapping small floc particles.
4. The depth of the sludge blanket. This is controlled by the height of the sludge take-off point that is set by an OTTER user. A sludge blanket too shallow has poor solids removal, whereas a sludge blanket too deep has the risk of overflowing blanket when the flowrate increases.

OTTER calculates and simulate the changes of the depth of the sludge blanket

and its concentration in a HBC based on the given values for the first two factors mentioned above. With the dynamics of the sludge blanket being simulated, OTTER also calculates the percentage of solids removal of the HBC. [39]

### 3.3.1 The CSTR Model

CSTR stands for Constantly Stirred Tank Reactor and the model represents the sludge blanket in a HBC. A CSTR represents a perfectly mixed process tank, where the concentration of any component in every point of the tank, at any time, has the same concentration at the outlet. To describe a tank that is not perfectly mixed, the tank is represented by a series of CSTRs of equal volume. An OTTER user is allowed to choose the number of CSTR to represent the HBC when modelling in OTTER.

To have more than a CSTR to represent the sludge blanket in the HBC, the blanket is sectioned horizontally. The height of each section is determined by the number of CSTRs used, where each section must have the same volume.

There are a few assumptions made in the model when simulating the clarification process. They are:

- The sludge blanket is formed by two types of particles; primary particles, which are small particles, and fully grown particles.
- Desludging from the sludge concentrator cone is not simulated. The rate of desludging is defined by the flowrate of the sludge.

- Particles within the clarifier are all equally well removed.

#### 3.3.1.1 CSTR Model Equations

The simulation of sludge blanket in OTTER is not initiated with the forming of sludge blanket. OTTER assumes that the blanket has already been formed in a HBC, where its initial concentration need to be specified by the user. Otherwise, a preset default value would be used to proceed. The CSTR model simulates the changes in the height of the sludge blanket based on the Gould's model [31] and the removal of solids based on the work of [30, Head et. al].

In steady state conditions, the height of the sludge blanket remains the same through time. In such condition, the amount of solids trapped in the blanket is the same as the amount of the solids desludged. The change in the height of the blanket is mainly caused by the change in flow. Changes in flow rate causes changes in the volume and the solids concentration of the sludge blanket, and these effects vary the height of the sludge blanket.

The change in the height of sludge blanket is governed by:

$$\frac{dH}{dt} = \nu - \nu_s \tag{3.1}$$

where $H$ is the height of sludge blanket (m), $t$ is time (h), $\nu$ is the instantaneous upflow velocity (m/h), and $\nu_s$ is the instantaneous hindered settling velocity of the blanket (m/h).

The instantaneous upflow velocity, $\nu$, is calculated at the surface of the blanket [31].

The hindered settling velocity of the blanket is simulated using an equation that is similar to that presented by [43]. The equation is:

$$\nu_{max} = [1 - s(C - C_{min})]^n \tag{3.2}$$

where $C_{min}$ is the minimum blanket concentration at which blanket settles as discrete particles ($m^3$ of blanket / $m^3$ of water), $\nu_{max}$ is the settling velocity of a single floc particle (m/h), $s$ is the measure of sphericity of floc particles (dimensionless), and $n$ is the exponent of the settling curve.

The values for $C_{min}$ and $\nu_{max}$ are both given by the hindered settling curve that is used to calibrate a HBC model.

The removal of solids in the clarifier are simulated considering the removal by both process of flocculation and settlement that occur within the tank. The mass balance of the sludge blanket in a single CSTR is written as:

$$\frac{dX}{dt} = \frac{Q}{V}(X_i - X) - (\frac{k_f \Phi H}{100L} + \frac{\nu_{max} A}{V})X \tag{3.3}$$

where: $A$ is the tank area ($m^2$), $H$ is the height of the sludge blanket (m), $L$ is the height of water in the clarifier (m), $k_f$ is flocculation factor ($h^{-1}$), $\Phi$ is the mean blanket concentration (%v/v), $Q$ is the inflow rate ($m^3h^{-1}$), $X$ is the concentration of settleable solids leaving the tank ($gm^{-3}$), $X_i$ is the concentration of settleable solids entering the tank ($gm^{-3}$), $V$ is the tank volume ($m^3$), $\nu_{max}$ is the settling velocity of primary particles ($mh^{-1}$), and $t$ is time (h).

The concentration of settleable solids, $X$ and the volumetric concentration of the

blanket, $C$ is related by the density of floc, $\rho_{floc}$ where:

$$C = \frac{X\rho_{floc}}{1000} \tag{3.4}$$

The performance of a HBC model then can be predicted as the solids removal of its sludge blanket can be calculated. Following the solution of this calculation, the new concentration of the sludge blanket can be obtained and thus the new height of the sludge blanket.

### 3.3.2 Calibrating the HBC Model

In this part, the calibration of the HBC model in OTTER explained only covers the calibration of the HBC bank model. This is because, the single HBC tank model was not functional during the time this research was carried out. The HBC bank model is basically a group of HBCs that are in parallel. For each bank, there must be an influent, a clarified water outlet and a sludge outlet. The calibration of the HBC model of a treatment works in OTTER can be categorised into four types, which are the static data, bank operating data, individual tank operating data and the CSTR model calibration. Information presented is obtained from the documentation of the OTTER software, [39].

#### 3.3.2.1 Static Data

The static data of the HBC bank model represents the geometrical measurements of the HBC tanks. In this set of data, the number of the tanks that belong to the bank is specified. All HBC tanks that are grouped in the same bank are of the same size. The tank measurements that need to be specified are:

(a) Total depth of each tank, which is the height of water level contained in a HBC tank (m)

(b) Depth of hopper section (m)

(c) Tank surface area, which is the surface area of the top of the tank ($m^2$)

(d) Base area, which is the surface area of the base of the tank ($m^2$)

(e) Sludge take-off height, which is the height of the sludge take-off point measured from the bottom of the tank (m)

#### 3.3.2.2 Bank Operating Data

The operating desludging set up for whole bank is calibrated in this section and it includes:

- desludging option, which determines which of the three patterns of the occurence of desludging of the sludge blanket is chosen and they are:

    1. continous, where desludging is constant at a specified rate,

2. intermittent, where sludge blanket is desludged only when it is deeper than the sludge take-off point, and

3. timed, where desludging happens at a specified time at a specified rate.

- frequency, a specified number of times that desludging can occur for a day (only applies for timed desludging option)

- duration, of desludging, only when timed desludging option is chosen (h)

- rate, which is specified as a percentage of the inflow rate (%)

#### 3.3.2.3 Individual Operating Data

This is a set of data that is specific for each tank, and therefore need to be set for every tank. There are only two calibration settings that need to be done. Firstly, each tank can be specified whether or not it is operating for a specific simulation run. The second setting only applies when the timed desludging option is chosen for the bank, which is the desludge offset. The setting of this option enables the determination of when desludging occurs for a tank in relative to the rest in the same bank.

#### 3.3.2.4 Model Calibration

This part of the calibration refers to the CSTR model of the sludge blanket explained earlier in 3.3.1. The number of CSTR stages that represent the sludge blanket and parameters used in the blanket model equations are set in this section. These parameters are the initial and minimum blanket concentration, flocculation factor, solids:turbidity ratio, reference temperature for settling velocities, exponent factor of the hindered settling equation, and ratio of wet to dry solids that is contained in the sludge blanket. The required calibration data to describe the floc particles that form the sludge blanket are its maximum settling velocity, $\nu_{max}$ in equation shape factor, $s$, and density, $\rho_{floc}$. These parameters are applied in the equations (3.2) and (3.4).

#### 3.3.2.5 Output of HBC Model

The results obtained from a simulation with the HBC model tell of the performance of the bank in terms of the percentage of solids removal. Output from a simulation also reports on the mean concentration of the sludge blanket that is averaged for all HBC tank across the bank, and the average rise rate of the flow through each HBC tank.

## 3.4 Investigating OTTER

For the purpose of exploring the ability of OTTER, two treatment works model were built on OTTER. These models were used to run different simulation cases and the

results for each case was compared to compare the performances of both models. The two treatment works models are made up of the same treatment processes but are of different capacities and target HRT. Simulations were varied based on thirty two types of raw water qualities. For this study, only the values of turbidity of water are observed.

### 3.4.1 The Treatment Works Model

The two treatment works model are named as TW1 and TW2, where TW1 is the bigger works with constant flow of 200 Ml/day and TW2 has the capacity of 20 Ml/day. These models were not built with reference on any real treatment works, but based on selected HRT targets. The process models involved in these models are:

1. Source of raw water
2. Pump.
3. Coagulation tank
4. Flocculator
5. Hopper-bottomed clarifier bank
6. Rapid gravity filter bank
7. Chlorine contact tank
8. Final water

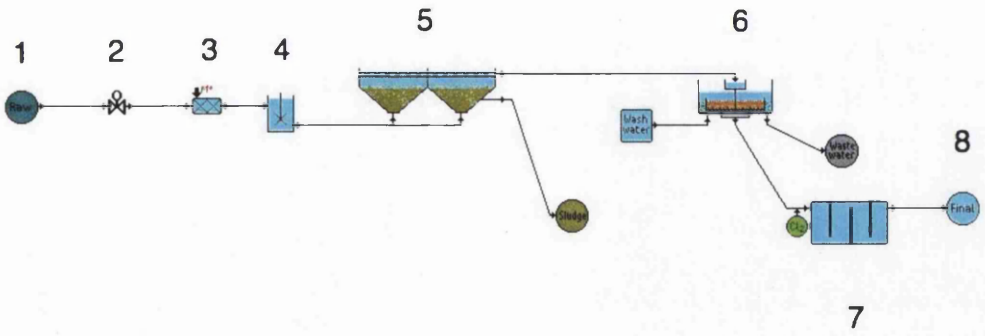


Figure 3.1: Treatment works model on OTTER

Figure 3.1 shows how the treatment works model appear in the user interface of OTTER.

#### 3.4.1.1 Operational Setting of TW1 and TW2

The setting up details for both TW1 and TW2 are tabulated in Table 3.1. The HRT of the flocculator, clarifier and filter for TW2 is half of that of TW1. While the chemicals used for the two works model are the same, the coagulant doses are different as to provide for the different flow rates.

### 3.4.2 Raw Water Profiles

There are in total thirty two raw water profiles that were used in this investigation. Every profile is numbered, from 1 to 32. Each profile was set to be a set of raw water quality data for a period of thirty one days, or a month.

These profiles are either sourced from the uplands or lowlands. The two different sources of raw water differ from each other in their values of pH and maximum turbidity. Raw water from an upland source has a pH value of 6.5 and turbidity at the maximum is 40 NTU. Raw water sourced from the lowlands has a higher pH of 7.5, and have the maximum turbidity of 100 NTU.

The minimum turbidity set for water of both sources was set to be 1 NTU for the purpose of this study. Each profile also could either occur during the winter time when the temperature is 4 deg C or during the summer time at 22 deg C. The apparent colour of the raw water were also varied, where the values are 5 Hazen and 40 Hazen.

The first sixteen water profiles are unique profiles that have the same random pattern in the change of turbidity. These profiles are tabulated with the respective determinands in Table 3.2.

The remaining water profiles are four different raw water profiles that had one of the determinands varied in four fixed patterns. For water profiles numbered 17 to 25, the pattern of the change in turbidity was varied, whereas for raw water profiles numbered 26 to 32, the apparent colour was varied. The varied patterns were assigned to the water profiles to observe the response of results predicted by OTTER. The four pattern types are:

1. A maximum turbidity peak (of varied determinand) occurring for a day, once during mid-month
2. A maximum turbidity peak (of varied determinand) occurring for a day, once

every week in the month

3. A maximum turbidity peak (of varied determinand) occurring for three days, once in the month

4. A maximum turbidity peak (of varied determinand) occurring for three days, once every week in the month

Table 3.3 lists raw water profiles 17 to 32 mentioned above and some of their determinands.

### 3.4.3 Results

The results of the simulations run for the purpose of this investigation were graphed and are attached in Appendix A.

For the convenience of observing the results without too much in detail, each raw water data profile and results obtained from the simulations of TW1 and TW2 have a reference number to simply describe the overall water quality (turbidity values). The reference number itself is not adequate to describe the pattern of any profile or results. It is merely a simpler way to identify the data that is represents.

The reference numbers were set in the format of:

(mean turbidity value)/(standard deviation of turbidity)/(maximum turbidity)

The reference numbers for water profile 1 to 16 and the corresponding results simulated with model TW1 and TW2 are tabulated in Table 3.4.

For water profiles 17 to 32, the reference numbers for both raw water and all simulation results are tabulated in Table 3.5.

### 3.4.4 Discussions and Conclusions

Table 3.4 and Table 3.5 are only showing the data representation raw and final water quality. The observation being discussed in this section is only based on the results presented in the above tables.

The simulation results for all profiles show that the performance of TW1 is better than TW2, especially for profiles with high turbidities. This is mainly due to the higher HRT of the process tank in TW1. The difference in target HRT of the treatment process tanks (except for chlorine contact tank) in the works model is as mentioned, 50 %. Profiles with low raw water turbidity show that the representation of the results for TW1 and TW2 are almost the same due to the very small difference in the results.

By observing the results of the simulation of raw water profiles with high values of turbidity, it shows that both works models perform better at higher temperatures. This is because at low temperatures, coagulation reaction rates can be low and it takes a longer period of time for efficient coagulation to occur.

During this investigation, the results are obtained with the condition that the sludge

blanket of the HBC in both treatment works model do not overflow. In order to achieve a stable sludge blanket, the rate of desludging of the sludge blanket needed to be adjusted. The desludging rate needs to be set accordingly to the raw water quality due to the high sensitivity of the stablity of the sludge blanket, and therefore each profile for a different treatment works model would need different desludging rate to prevent overflowing of sludge.

The setting of the desludging rate of the HBC affects the performance of the sludge blanket in its rate of solids removal. This means that the setting affects the performance of HBC and since each simulation needed different values of desludging rate, the performance of the HBC, even of the same treatment works model but of different raw water quality is not the same. For this reason, the results obtained from this study is subjective. If the setting of the desludging rate is made the same within a treatment works model, overflowing of the sludge blanket occurs. This is not favourable for the purpose of this study as it complicates the comparison of results.

The occurrence of the overflowing of the sludge blanket is shown in the results of the simulation of TW2 with low quality raw water profiles. With the high content of solids, the performance of TW2 has failed even with the maximum desludging rate allowed in OTTER, 20 %. For these cases, on some days, the turbidity of the outflow can be seen higher than that of the raw water as solids from the sludge blanket in the HBC is carried over thus increasing the solids loading through the treatment works.

The comparison between the performances of works model TW1 and TW2 should not be entirely based on the different turbidity values resulted from the simulations of

different values of turbidity. The performance of each works model is determined more than one factor. By taking the HBC as an example, the efficiency of the HBC is not only determined by its size, but also by its features, say the height of the sludge take-off in the tank.

Final water results of a treatment works model is an accumulative results of the series of treatment processes present in the works model. Because of this, the performance of works models may be better compared if done by comparing the performance of each treatment process.

## 3.5 Limitations and Strengths of OTTER

An OTTER model allows the input of a large amount of data for any simulation, but the user is not required to provide OTTER all of the information that is listed. For instance, there are more than fifty raw water quality parameters that are listed in OTTER but the user just has to specify the non-zero values. As for the individual processes settings of a works model, the default values can be used when there is insufficient information.

The default values provided in the OTTER software are based on empirical calibration. These default values are very useful as in most cases, not all information is available and they are accurate enough when used to simulate for treatments works in the Britain [1].

As mentioned earlier, OTTER provides the final water results in spreadsheets. The

raw water quality dialog is also presented in the form of spread sheets and this feature makes it easy for the user to import and export information to and from OTTER.

All individual treatment process in OTTER that requires mixing has a general assumption that complete mixing occurs. The works models simulated in OTTER do not take into account any hydraulic effects due to the structural geometry of any of the process tanks and the flow characteristics itself.

| Detail | TW1 | TW2 |
|---|---|---|
| Flow rate (Ml/day) / ( $m^3hr^{-1}$) | 200 / 8333.33 | 20 / 833.33 |
| Coagulation unit: | | |
| Coagulant | Aluminium Sulphate | Aluminium Sulphate |
| Maximum dose (mg/l) | 50.0 | 3.0 |
| Polyelectrolyte | Anionic | Anionic |
| pH adjustment | Sulphuric acid | Sulphuric acid |
| Flocculator: volume ($m^3$) | 8333.33 | 416.66 |
| Hopper-bottomed clarifier bank: | | |
| Number in bank | 10 | 2 |
| Total tank depth (m) | 10 | 10 |
| Tank surface ($m^2$) | 256 | 49 |
| Depth of hopper section (m) | 2 | 4 |
| Base area ($m^2$) | 169 | 9 |
| Rapid gravity filter bank: | | |
| Number of unit in bank | 20 | 2 |
| Filter unit depth (m) | 8 | 3 |
| Depth of gravel support (m) | 0.2 | 0.2 |
| Number of media layers | 1 (sand) | 1 (sand) |
| Media layer details | Default values used | Default values used |
| Filter surface area ($m^2$) | 209 | 138.88 |
| Weir height ($m$) | 2 | 2 |
| Chlorine contact tank: volume ($m^3$) | 8333.33 | 833.33 |

Table 3.1: Model Data and Calibration Setting for TW1 and TW2

| Profile No. | Temperature (°C) | Maximum Turbidity (NTU) | Apparent Colour (Hazen) | Source |
|---|---|---|---|---|
| 1 | 22 | 40 | 40 | Upland |
| 2 | 4 | 40 | 40 | Upland |
| 3 | 22 | 1 | 40 | Upland |
| 4 | 4 | 1 | 40 | Upland |
| 5 | 22 | 40 | 5 | Upland |
| 6 | 4 | 40 | 5 | Upland |
| 7 | 22 | 1 | 5 | Upland |
| 8 | 4 | 1 | 5 | Upland |
| 9 | 22 | 100 | 40 | Lowland |
| 10 | 4 | 100 | 40 | Lowland |
| 11 | 22 | 1 | 40 | Lowland |
| 12 | 4 | 1 | 40 | Lowland |
| 13 | 22 | 100 | 5 | Lowland |
| 14 | 4 | 100 | 5 | Lowland |
| 15 | 22 | 1 | 5 | Lowland |
| 16 | 4 | 1 | 5 | Lowland |

Table 3.2: Raw Water Profiles 1 to 16 for OTTER Investigation

| Profile No. | Temperature (°C) | Maximum Turbidity (NTU) | Apparent Colour (Hazen) | Source |
|---|---|---|---|---|
| 17 | 22 | 100 | 40 | Lowland |
| 18 | 22 | 100 | 40 | Lowland |
| 19 | 22 | 100 | 40 | Lowland |
| 20 | 22 | 100 | 40 | Lowland |
| 21 | 4 | 100 | 40 | Lowland |
| 22 | 4 | 100 | 40 | Lowland |
| 23 | 4 | 100 | 40 | Lowland |
| 24 | 4 | 100 | 40 | Lowland |
| 25 | 22 | 1 | 40 | Upland |
| 26 | 22 | 1 | 40 | Upland |
| 27 | 22 | 1 | 40 | Upland |
| 28 | 22 | 1 | 40 | Upland |
| 29 | 4 | 1 | 40 | Upland |
| 30 | 4 | 1 | 40 | Upland |
| 31 | 4 | 1 | 40 | Upland |
| 32 | 4 | 1 | 40 | Upland |

Table 3.3: Raw Water Profiles 17 to 32 for OTTER Investigation

| Profile No. | Raw Water | Results of TW1 | Results of TW2 |
|---|---|---|---|
| 1 | 32.839/7.412/40 | 4.025/0.741/8.012 | 16.505/9.207/29.895 |
| 2 | 32.39/7.412/40 | 4.131/0.730/8.066 | 36.587/5.7460.482/43.813 |
| 3 | 0.771/0.237/1 | 0.052/0.026/0.180 | 0.052/0.030/0.200 |
| 4 | 0.771/0.237/1 | 0.275/0.083/0.498 | 0.276/0.084/0.498 |
| 5 | 32.839/7.412/40 | 4.120/0.722/8.012 | 35.562/6.598/48.187 |
| 6 | 32.839/7.412/40 | 4.131/0.730/8.066 | 36.587/5.746/43.813 |
| 7 | 0.771/0.237/1 | 0.052/0.026/0.180 | 0.052/0.026/0.180 |
| 8 | 0.771/0.237/1 | 0.059/0.027/0.190 | 0.09/0.027/0.190 |
| 9 | 87.339/12.633/100 | 10.667/1.811/20.426 | 100.837/13.410/119.103 |
| 10 | 87.339/12.633/100 | 12.326/8.348/55.524 | 87.231/2.347/83.19 |
| 11 | 0.771/0.237/1 | 0.251/0.037/0.434 | 0.260/0.032/0.418 |
| 12 | 0.771/0.237/1 | 0.286/0.038/0.466 | 0.287/0.038/0.466 |
| 13 | 87.339/12.633/100 | 11.972/9.660/63.956 | 100.050/6.217/113.798 |
| 14 | 87.339/12.633/100 | 34.480/20.359/84.9 | 104.179/6.820/112.353 |
| 15 | 0.771/0.237/1 | 0.251/0.037/0.434 | 0.251/0.037/0.434 |
| 16 | 0.771/0.237/1 | 0.286/0.039/0.480 | 0.287/0.039/0.480 |

Table 3.4: Results of OTTER Investigation for Profiles 1 to 16

| Profile No. | Raw Water | Results of TW1 | Results of TW2 |
|---|---|---|---|
| 17 | 4.497/17.964/100 | 0.103/0.018/0.2 | 0.105/0.0259/0.244 |
| 18 | 16.784/37.097/100 | 0.103/0.018/0.2 | 0.105/0.026/0.244 |
| 19 | 10.361/29.827/100 | 0.103/0.018/0.2 | 0.105/0.026/0.244 |
| 20 | 39.187/49.128/100 | 0.103/0.018/0.2 | 0.105/0.026/0.244 |
| 21 | 16.484/16.759/100 | 1.710/0.223/2.916 | 11.260/2.462/14.066 |
| 22 | 23.645/30.296/100 | 1.710/0.223/2.916 | 11.260/2.462/14.066 |
| 23 | 21.484/26.562/100 | 1.710/0.224/2.916 | 11.260/2.462/14.066 |
| 24 | 46.000/43.785/100 | 1.710/0.224/2.916 | 11.260/2.462/14.066 |
| 25 | 0.768/0.241/1 | 0.052/0.026/0.180 | 0.052/0.026/0.180 |
| 26 | 0.772/0.236/1 | 0.052/0.026/0.180 | 0.052/0.026/0.180 |
| 27 | 0.768/0.241/1 | 0.052/0.026/0.180 | 0.053/0.030/0.200 |
| 28 | 0.768/0.241/1 | 0.052/0.026/0.180 | 0.066/0.023/0.186 |
| 29 | 0.768/0.241/1 | 0.058/0.059/0.190 | 0.056/0.028/0.190 |
| 30 | 0.768/0.241/1 | 0.058/0.028/0.190 | 0.066/0.023/0.186 |
| 31 | 0.768/0.241/1 | 0.058/0.028/0.190 | 0.059/0.029/0.200 |
| 32 | 0.767/0.241/1 | 0.072/0.024/0.194 | 0.072/0.025/0.200 |

Table 3.5: Results of OTTER Investigation for Profiles 17 to 32

# Chapter 4

# Computational Fluid Dynamics

Computational Fluid Dynamics (CFD) is a computer-based technique that simulates systems that involve fluid flow, heat transfer and many other related occurences. The results of CFD simulations provide qualitative and in some cases, quantitative prediction of fluid flow. It gives insight into flow patterns that are complicated, allowing the studying of flow systems that are difficult or even impossible to study using experimental technique, possible.

The use of CFD modelling enables scientists and engineers to perform numerical experiments, which are computer simulations using a computer. Its increasing application in the many industries has allow it to play important roles in the design, research and development, process optimisation and manufacturing of products. The CFD technique is well known to offer many advantages over experimental designs of fluid systems and they are [44]:

- reduction in design costs and time

- making studies of systems that are difficult or impossible to perform feasible

- provide practically unlimited results details

The use of CFD modelling in conjunction with experiment is also beneficial. Experimental measurements can be difficult, where typically measurements are only obtained at a small number of points but from the perspective of an engineer, these are 'real values'. If a computer model can duplicate the measured trends then there will be more confidence in its predictions when used as a predictive tool for examining cases that have not been part of the experimentation.

CFD analyses fluid flow systems with numerical algorithms. These algorithms give solutions to a fluid flow problem in predicting the progress of a circumstance quantitatively. The methodology in approaching fluid flow problems is the same for all commercial CFD packages. Thus, all CFD codes have the same basic analysis procedure and contain three elements: the pre-processor, solver, and the post-processor.

The CFD analysis can be solved with different numerical techniques, called the discretisation methods. In this research, the finite volume method was used. It is the most common method found in available CFD packages, given that is most well-established and validated for the use of CFD technique.

## 4.1 Modelling with CFD

The quality and accuracy of a CFD work are essentially based on three aspects, which are convergence, consistency and stability. In reality, however, the mentioned mathematical concepts are difficult to establish theoretically. Therefore the common alternatives used in practice for these three aspects are using methods that have the properties of conservativeness, boundedness and transportiveness. These three properties are included in all commercial CFD codes that are based on the finite volume method and the simulation results are generally accepted.

In order to obtain successful simulation results, an appropriate meshing or grid scheme of the domain geometry is important. A successful simulation result has the convergence of iterative process in terms of the magnitude of residuals, and grid independence. The solution of the iteration process is convergent when the residuals are very small. This can be faster achieved with settings of a good selection of relaxation factors and acceleration devices. Grid independence can be achieved through a process of gradually applying and refining the grid scheme of the geometrical domain, starting with coarse meshing until certain key results of interest do not change. [44]

## 4.2 The Theory: Finite Volume Method

The finite volume method (FVM) is a discretisation method commonly used for numerical solution of conservation laws. The basic steps of this method are: (1) the division

of the computational domain into finite volumes, known as grid generation, (2) the conservation law is applied to each finite volume, which requires the computation of the flux across the boundary of each finite volume, and (3) the solving of the resulting system of equations by an iteration method.

In FVM, the numerical fluxes, or the relevant properties for a finite volume is conserved from one discretisation cell to its neighbour. This can be expressed in words as [44]:

| | | |
|---|---|---|
| Rate of change of $\varphi$, with respect to time in the finite volume | = | Net flux of $\varphi$ due to convection into the finite volume |
| | + | Net flux of $\varphi$ due to diffusion into the finite volume |
| | + | Net rate of creation $\varphi$ inside the finite volume |

A finite volume can be either cell-centred or vertex-based [45]. The governing fluid flow equations are an account of the changes in the mass, momentum and energy of the finite volume due to the fluid flow across its faces.

The fluid flow equations are given by the Navier-Stokes Equations. The space and time $(x, y, z, t)$ variables are independent, whereas the properties of the fluid are dependent variables. These properties of the node of the finite volume are all written in functions of the independent variables, space and time.

The equations are a set of differential momentum equations and are written as

follow for the development of the FVM:

For $x$-component,

$$\rho\frac{Du}{Dt} = -\frac{\delta p}{\delta x} + div(\mu gradu) + S_{Mx} \tag{4.1}$$

For $y$-component,

$$\rho\frac{Dv}{Dt} = -\frac{\delta p}{\delta y} + div(\mu gradv) + S_{My} \tag{4.2}$$

For $z$-component,

$$\rho\frac{Dw}{Dt} = -\frac{\delta p}{\delta z} + div(\mu gradw) + S_{Mz} \tag{4.3}$$

where $\rho$ is the density of fluid, $u$, $v$ and $w$ are velocity vectors, $div$ is divergence, $grad$ is gradient, and $S_M$ is the viscious stress terms in the momentum source.

## 4.3 The CFD Software

The three elements of the CFD software used for this research is explained in this section.

### 4.3.1 Pre-Processor

Pre-processing in CFD modelling is the first step to input a flow problem into a CFD software.Figure 4.1 illustrates the input process that occurs in a pre-processor.

The pre-processor program used for this research is FEMGV [46]. With the input, FEMGV then translates the information into the form suitable for the use of PHYSICA

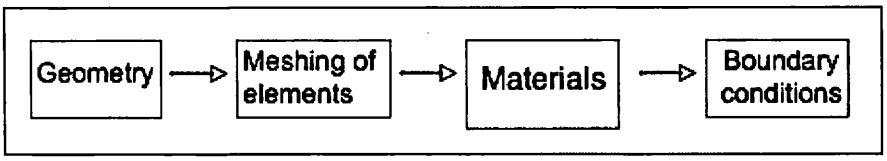


Figure 4.1: Flow diagram of input process in a pre-processor

as the solver. The input required in FEMGV is the location of the materials in the model, boundary conditions and loads within the mesh.

### 4.3.2 Solver

The solver being used throughout this research is PHYSICA [47]. It is a simulation software developed by Physica Ltd, UK and is designed for the simulation of fluid systems related to manufacturing processes. As of many other CFD commercial software, the discretisation procedure used to solve for Navier-Stokes equation used in PHYSICA is the FVM. Figure 4.2 shows the procedure.

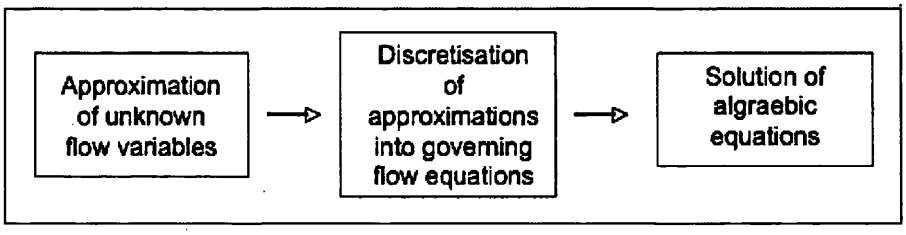


Figure 4.2: Flow diagram of numerical solving process in a solver

PHYSICA uses the Rhie-Chow interpolation [48] in its discretisation process and

the SIMPLEC algorithm to calculate the pressure field by default. The convection scheme used in PHYSICA is the HYBRID scheme and power law scheme [49]. [50]

The discretisation and solution procedure in PHYSICA is explained below, using the convection term as an example [50]: For a scalar quantity $\phi$, the volume integral of the convection term is transformed into a surface integral using the divergence theorem, as shown in equation (4.4).

$$\int_V div(\rho \underline{n} \phi) dV = \int_S \rho(\underline{u} \cdot \underline{n}) \phi_S \tag{4.4}$$

The surface integral is then divided to form a set of integrals over each face of a finite volume. the value estimated or each face is:

$$\sum_f \rho_f (\underline{u} \cdot \underline{n}_f A_f \phi_f \tag{4.5}$$

where $\rho_f$ is a value given in the upwind element. Thus:

$$\rho_f = \rho_P \qquad \text{if}(\underline{u} \cdot \underline{n})_f > 0.0 \text{and} \rho_f = \rho_A \qquad \text{if}(\underline{u} \cdot \underline{n})_f < 0.0 \tag{4.6}$$

The normal component of the velocity at the face is evaluated using the Rhie-Chow interpolation method [48]. The discretisation process may be completed by using arithmetic averaging as one of the methods to estimate the face value of $\phi$, which gives:

$$\phi_f = \alpha_f \phi_P + (1 - \alpha_f) \phi_A \tag{4.7}$$

Using the face value in equation (4.7), the convection term becomes:

$$\sum_f \rho_f (\underline{u} \cdot \underline{n})_f A_f [\alpha_f \phi_P + (1 - \alpha_f) \phi_A] \tag{4.8}$$

Similar steps are performed to discretise each of the terms in the conservation equation. Combining the terms from a single element gives an equation that relates the unknown value of the variable in the element to its neighbours in space and time. Combining the equations for all elements leads to an algebraic system of the solution, of which provides the unknown values of the variable in each element.

An iterative linear solver, such as those based on the conjugate gradient method, are employed to obtain the solution of the velocity, means that a loop over all variables until convergence is obtained or the specified maximum number of loops have been performed.

### 4.3.3 Post-Processor

FEMGV was also used as the post-processor for the CFD work done for this research. Post-processing is the process of examining and analysing the solutions of CFD simulations. At this stage, the flow field of the domain can be studied and its contours, vectors, streamlines and iso-surfaces can be displayed. Apart from that, the manipulation of the domain also can be carried out, together with many other features, such as particle tracking.

Today, post-processors offer outstanding graphic display capabilities and visualisation tools. FEMGV, being slightly dated does not have such extensive ability, but still provides the necessary functionality to examine the results of simulations.

## 4.4 Exploration of Modelling with PHYSICA

This section presents a study done to look at the use of CFD modelling in simulating flow pattern through tanks. In this study, three of 1 $m^3$ cubic tank models were used and each tank model has a different design to it. Two of these tank models have different number of baffles in them, and the remaining has none, enabling flow pattern through each tank to be different.

This study is intended to obtain information that can be calculated from the results simulation, which in this case is the HRT of fluid flowing through the tanks. It also investigates and demonstrates how different hydraulics of a tank can affect the its HRT.

### 4.4.1 Calculation of HRT

To calculate the HRT of the outflow in PHYSICA, a particle without mass is placed at the centre of each element. The passage of the particle is then calculated through the domain using Lagrangian tracking. At each tracking time step, the velocity of water is interpolated to the location of the particle. Details of the algorithm for a particle with mass can be found in [51].

### 4.4.2 Description of Tank Models

The cube tanks have the same circular inlet and outlet, which are 0.1 m in diameter with the centres located 0.2 m and 0.5 m from the top and the sides of the tank respectively.

The inlet and outlet for each tank are on opposite faces from each other.

Each of these models have varying physical features within it, and they differ in the number of baffles that are contained in each of the tank: Tank A has no baffle within it, Tank B has a baffle of 0.3 m high at the top of the tank at mid-span, and Tank C has three baffles of 0.8 m in height that are equally spaced, where the second baffle is at the base of the tank. Figure 4.3 illustrates these models.

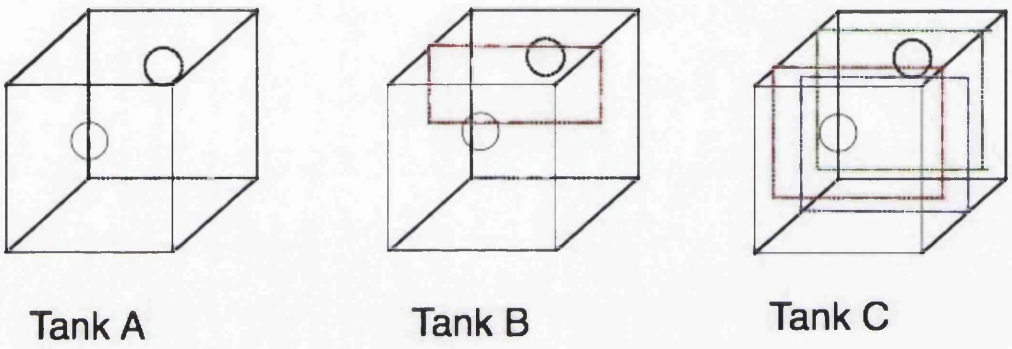


Figure 4.3: Diagrams of $1m^3$ tanks (not to scale).

#### 4.4.2.1 Model Settings

The grids for the meshes generated were the same for all of the models, where there were 62016 number of elements in each tank. The highest and the lowest cell width were 0.01250 m and 0.03125 m respectively. The boundary conditions at the inlet were set according to the flow rates, where in this study, was varied. The surface of the outlet has the boundary condition of 0.0 Pa gauge pressure.

The flow through each cube tank model was simulated with different inflow rates, which were 1.0 $m^3h^{-1}$, 2.0 $m^3h^{-1}$, 3.0 $m^3h^{-1}$, 4.0 $m^3h^{-1}$, and 5.0 $m^3h^{-1}$. This is to observe and compare the differences in resulting flow pattern due to the speed of the flow through the tanks.

All the simulation cases were run for a total of 1000 iterations to achieve a reduction of approximately 100 times in the mass residual. Details of the initial and final mass residuals for each simulation case is stated in the following section.

### 4.4.3 Results

The results of the simulation for all five flow settings of each tank are presented in both contour diagrams and graphs. The results for each tank are presented together, where in a figure, each row represents a different flow rate. The maximum value of the velocity contour presented for each flow setting is the same for better comparison. Each plot on a row uses the same contour range to allow a better comparison of the plots.

The comparison of the results for the simulations of different tanks is discussed in the following section, 4.4.4.

#### 4.4.3.1 Tank A

The initial and final mass residuals for all simulations with this model are tabulated in Table 4.1. The greater reduction in the mass residual for cases with lower flow rates indicates that these cases are more converged.

| Flow Rate ($m^3$) | Initial Mass Residual | Final Mass Residual |
|---|---|---|
| 1.0 | $2.773 \times 10^{-1}$ | $4.977 \times 10^{-4}$ |
| 2.0 | $5.5393 \times 10^{-1}$ | $9.100 \times 10^{-4}$ |
| 3.0 | $8.305 \times 10^{-1}$ | $5.610 \times 10^{-3}$ |
| 4.0 | 1.107 | $1.143 \times 10^{-2}$ |
| 5.0 | 1.384 | $2.419 \times 10^{-2}$ |

Table 4.1: Table of initial and final mass residual for each flow setting for simulations with model Tank A

The simulation results of this model are presented in Figure 4.4. Referring to the figure, the contour for resultant velocity mapped at the face of the inlet, diagrams labelled i, for all cases (a) to (b) show a similar pattern of the spreading of the flow as it enters the tank. Diagrams labelled (ii) show the streaming of the flow from the inlet on the left-hand side (LHS,) to the outlet on the right-hand side (RHS). For all cases, the slowing down of the streaming can be observed near the inlet before the flow speeds up again as it approaches the outlet. The results for all of the cases also show the remaining domain outside of the streaming shows very little, if not none, movement of flow.

Figure 4.5 presents the graphs representation of the HRT for all the cases. The first

five graphs in the figure labelled (i) to (v) are plots of percentage of outflow against the corresponding HRT. It can be observed that the higher the flow rate, the higher the percentage of the outflow that short-circuited to the outlet in the same range of HRT. Lower flow rates have a more varied HRT in the outflow. This may be due to the lower force in flow to overcome the stagnant fluid in the domain.

The last diagram in Figure 4.5 is a graph of percentage of domain not reaching the outlet against the flow rate settings for the simulated cases. This shows that the portion of stagnant water in Tank A is high for all cases as a result of the flow pattern through the tank. This graph shows the increase of water in the domain that actually flows out of the outlet, as the flow rate increases, with the exception of the case with the highest flow rate.

#### 4.4.3.2 Tank B

The values for the initial and final residual mass for each flow setting are tabulated in Table 4.2 below. Although the simulations for this model were run with the same number of iterations, the final mass residuals for all cases are lower than that of Tank A, denoting the better convergence achieved. The reduction of the mass residuals is at least 10000 times.

The results of the flow simulation for this model are shown in Figure 4.6. There are three columns of diagrams in this figure, where the first two rows are the resultant velocity contour plots on the face of the inlet and side view of the tank with the inlet

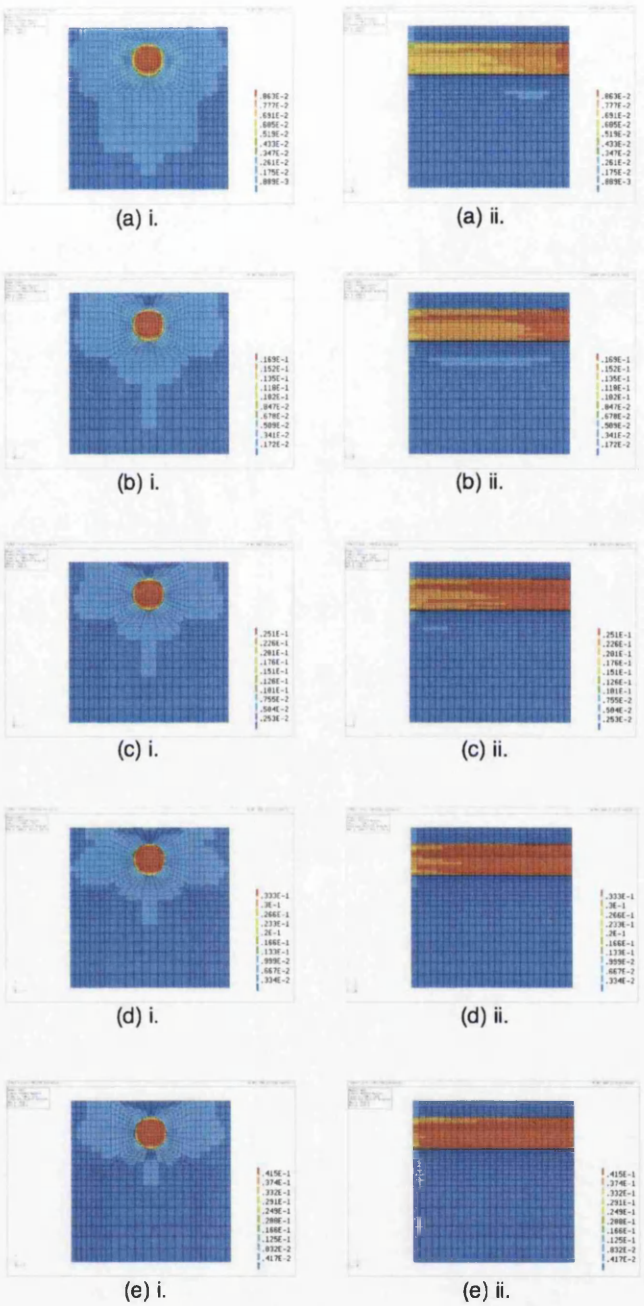


Figure 4.4: Simulation results of Tank A: (a) 1.0 $m^3h^{-1}$, (b) 2.0 $m^3h^{-1}$, (c) 3.0 $m^3h^{-1}$, (d) 4.0 $m^3h^{-1}$, and (e) 5.0 $m^3h^{-1}$; i- resultant velocity contour at face of inlet, and ii- resultant velocity contour across the tank with inlet on the LHS and outlet on the RHS.

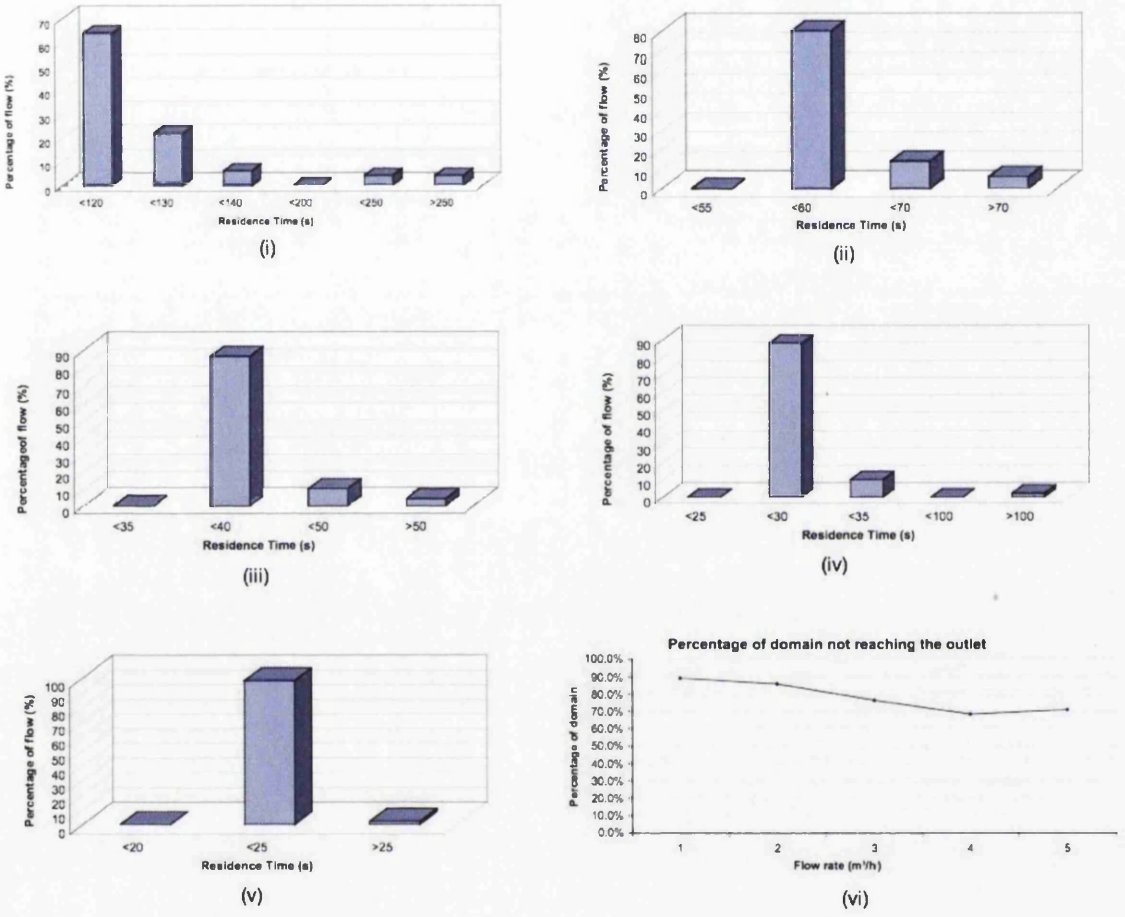


Figure 4.5: Chart representations of HRT results for Tank A, percentage of outflow against residence time: (i) 1.0 $m^3h^{-1}$, (ii) 2.0 $m^3h^{-1}$, (iii) 3.0 $m^3h^{-1}$, (iv) 4.0 $m^3h^{-1}$, and (v) 5.0 $m^3h^{-1}$; (vi) graph of percentage of domain reaching the outlet against flow rate.

| Flow Rate ($m^3$) | Initial Mass Residual | Final Mass Residual |
|---|---|---|
| 1.0 | $2.766 \times 10^{-1}$ | $2.675 \times 10^{-6}$ |
| 2.0 | $5.532 \times 10^{-1}$ | $6.524 \times 10^{-6}$ |
| 3.0 | $8.298 \times 10^{-1}$ | $1.006 \times 10^{-5}$ |
| 4.0 | 1.106 | $1.524 \times 10^{-5}$ |
| 5.0 | 1.383 | $1.792 \times 10^{-5}$ |

Table 4.2: Table of initial and final mass residual for each flow setting for simulations with model Tank B

on the LHS and outlet on the opposite. The third column of diagrams present the iso-surfaces of the resultant velocity of diagrams labelled iii.

Spreading of the inflow once entering the tank can be seen from the resultant velocity contour plots labelled i. The speed of the flow can be seen significantly decreased after that, as shown in the diagrams in row ii. The flow pattern through Tank B for the five cases can be observed to be similar as shown in the diagrams of row iii. The position of the baffle at the mid span can be easily spotted from these diagrams with the position of the iso-surfaces of very slow flow at two sides of the baffle and near the end of it. Some variation of speed can be seen near the base of the tank below the baffle and at the top of tank in the region surrounding the baffle. The dead zones of the domain around the corners of the tank also can be spotted from these diagrams.

The resulting HRT of these flow cases are plotted and presented in Figure 4.7. Diagrams i to v in this figure present the plot of percentage of outflow against the HRT of the flow through the tank for each case. Despite the similarities in the flow pattern

as observed in Figure 4.6, the trend in these graphs varies with the flow rate. The HRT within a tank of a flow rate setting varies widely. The inflow through this model comes in contact and mixes with water in the domain resulting in the range of HRT found.

The last graph presented in Figure 4.7 is a plot of the percentage of domain that remained in the tank against the flow rate of each case simulated. The results show that the percentage of the domain that reaches the outlet increases as the flow rate increases.

#### 4.4.3.3 Tank C

Table 4.3 lists the corresponding initial and final residual masses for each flow rate settings simulated with this model. The mass residuals for the simulations for this model are also lower than that achieved for simulations of Tank A. The values of the residuals were reduced to at least 10000 times from the initial values.

| Flow Rate ($m^3$) | Initial Mass Residual | Final Mass Residual |
|---|---|---|
| 1.0 | $1.386 \times 10^{-1}$ | $6.380 \times 10^{-6}$ |
| 2.0 | $2.773 \times 10^{-1}$ | $9.859 \times 10^{-6}$ |
| 3.0 | $4.159 \times 10^{-1}$ | $1.997 \times 10^{-5}$ |
| 4.0 | $5.546 \times 10^{-1}$ | $4.254 \times 10^{-5}$ |
| 5.0 | $6.932 \times 10^{-1}$ | $5.634 \times 10^{-5}$ |

Table 4.3: Table of initial and final mass residual for each flow setting for simulations with model Tank C

The simulation results for this tank are as shown in Figure 4.8, which has three

columns of diagrams for each row. All these diagrams are showing the contour plot of the resultant velocity of the flow. The first row, i, is the contour plot for the direction of the face of the inlet, while rows ii and iii are plots of the side view of the tank where the inlet is on the LHS and outlet on the RHS. The maximum resultant velocity for the range of contour values for diagrams on row iii are the same for all cases, which is $8.0 \times 10^{-4}$ $ms^{-1}$.

The streaming of the inflow entering the tank, as seen in the diagrams in row i of the Figure 4.8, only occurs at the bottom half of the inlet. The same streaming pattern also occurs at the outlet as shown in the diagrams of row ii. The speed of the flow is significantly reduced as the flow progresses. The contour plots in these diagrams also show a slight increase in the flow as it passes the opening of the baffles. Comparing the contour plot diagrams of row iii, the increase in the flow rate shows the reduction of portion of the domain that has very little flow.

Simulation results for this model show that the whole domain feeds to the outflow of the tank for all cases. Figure 4.9 presents the graphs that plot the percentage of domain against the HRT of the flow. The plots show that a large portion of the fluid through the tank has the retention time between 6000 s to 6005 s, where this portion of the domain increases as the flow rate increases.

Cases with lower flow rate values have higher higher percentage of flow that has the HRT of higher than 6030 s. The range of HRT of Tank C decreases as the inflow rate increases, where cases with the two highest inflow rate has the HRT only up to 6020 s.

### 4.4.4 Discussions and Conclusions

From the results presented in graphs for all the three tank models, the HRT of a tank of the same volume can be seen varied according to the flow rate and the flow pattern through the tank. The adding of baffles in the tank models changes the flow paths of water flowing through them.

The percentage of domain that does not feed to the outlet tells of the proportion of the tank containing self-sustaining vortices. This value was predicted to be high from the simulation of Tank A. High percentage of water stays in the tank due to short-circuiting of flow. This phenomenon is seen as the jetting of flow from the inlet passes through the tank straight to the outlet without much mixing with the water stored in the domain, as shown by the contour plot results.

The flow simulated with the model Tank B shows a different pattern, where the baffle in the middle of the tank directs the flow to the bottom at the mid-span of the tank before it progressing to the outlet. The results contour plot also show that the flow near the inlet slows down uniformly as it spreads and approaches the baffle. The same pattern can also be observed near the outlet, where flow speeds up uniformly. The design of Tank B proves to be more efficient than Tank A, with much lower percentage of the domain remains in the tank.

The HRT of Tank 3 is relatively much higher than that of Tank A and Tank B, as it has a longer path for the flow to reach the outlet. The additional baffles in this tank narrowed the passage for the flow to pass through, resulting in higher speed of

flow across the tank. Streaming or jetting of flow the tank is also not seen in the flow through Tank C due to the change in the flow path caused by the baffles.

With the higher speed in flow, the HRT for these cases are expected to be shorter. However, results show that despite of the difference, the dominant HRT for each case is the same, which is in between 6000 s and 6005 s. This could be caused by the increased number of corners in the tank due to the baffles, where flow could hit and circulate at before progressing towards the outlet. This phenomenon happens largely for higher flow speed cases due to the higher momentum in the flow through the narrow flow path.

Comparing the resulting HRT for all three tank models, Tanks C, which has three baffles, has the highest HRT. Results for the flow pattern of Tank C also show that the flow pattern in Tank C that the flow involves its whole volume, making it the most efficient tank, among the three models.

From this study, it is shown that there are two main factors that affect the HRT of a process unit: the operating flowrate and the physical feature of the tank. The difference in the results of the flow simulation for Tank A, B, anc C shows how different hydraulics condition affect the HRT of a tank. This goes to show the importance of knowing and understanding the hydraulics of a treatment process tank.

The use of CFD modelling and analysis to simulate flow through process tanks are already widely known. This simple study demonstrates how CFD results could give the HRT of a tank, which is the focal output of the CFD model of the HBC tank in this research.

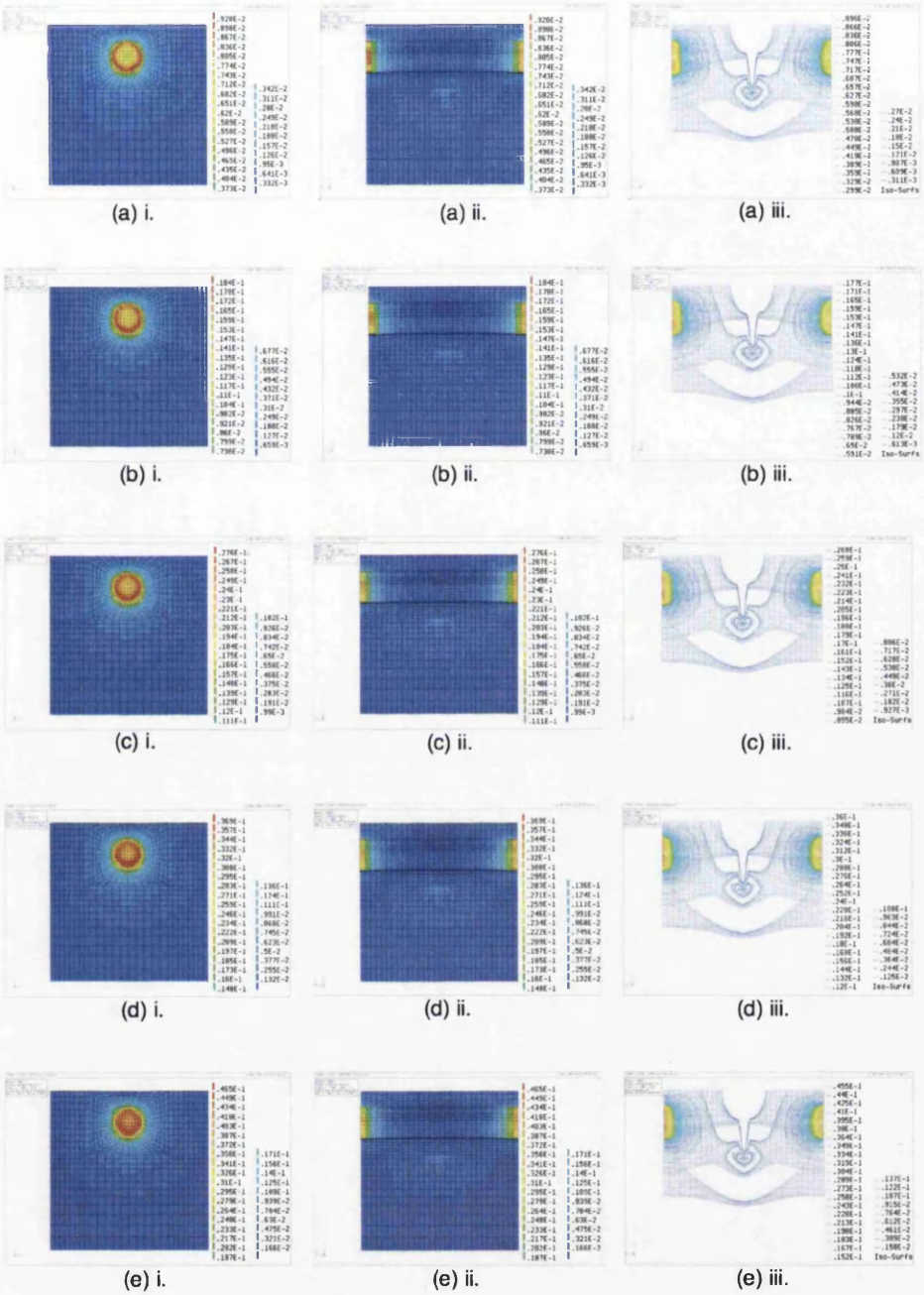


Figure 4.6: Simulation results of Tank B: (a) 1.0 $m^3h^{-1}$, (b) 2.0 $m^3h^{-1}$, (c) 3.0 $m^3h^{-1}$, (d) 4.0 $m^3h^{-1}$, and (e) 5.0 $m^3h^{-1}$; i- resultant velocity contour at face of inlet, and ii- resultant velocity contour across the tank with inlet on the LHS and outlet on the RHS, iii- iso-surfaces of resultant velocity of ii.

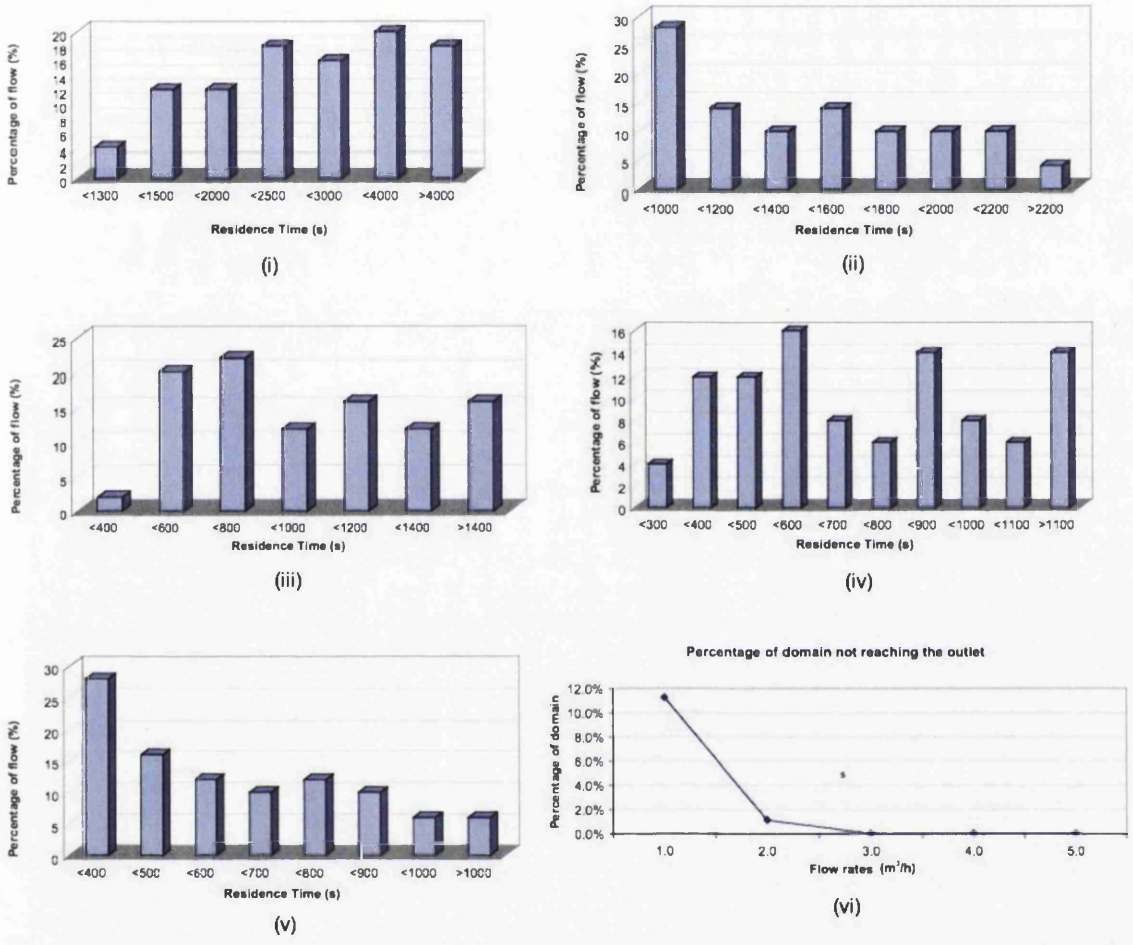


Figure 4.7: Chart representations of HRT results for Tank B, percentage of outflow against residence time: (i) 1.0 $m^3h^{-1}$, (ii) 2.0 $m^3h^{-1}$, (iii) 3.0 $m^3h^{-1}$, (iv) 4.0 $m^3h^{-1}$, and (v) 5.0 $m^3h^{-1}$; (vi) graph of percentage of domain reaching the outlet against flow rate.

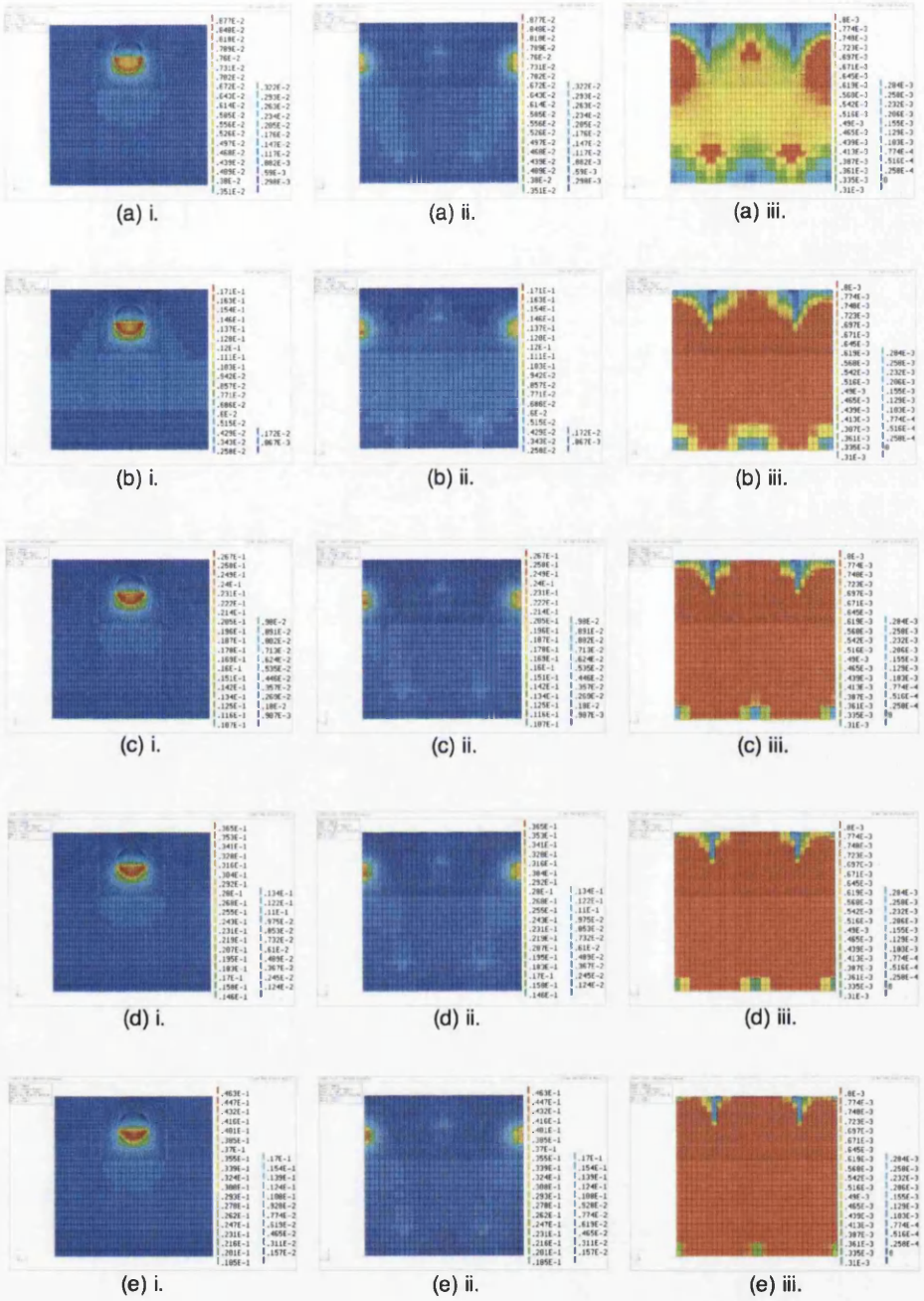


Figure 4.8: Simulation results of Tank C: (a) 1.0 $m^3h^{-1}$, (b) 2.0 $m^3h^{-1}$, (c) 3.0 $m^3h^{-1}$, (d) 4.0 $m^3h^{-1}$, and (e) 5.0 $m^3h^{-1}$; (i) resultant velocity contour at face of inlet, and (ii) resultant velocity contour across the tank with inlet on the LHS and outlet on the RHS, (iii) resultant velocity contour across the tank with velocity of 8.0 x $10^{-4}$ $ms^{-1}$.

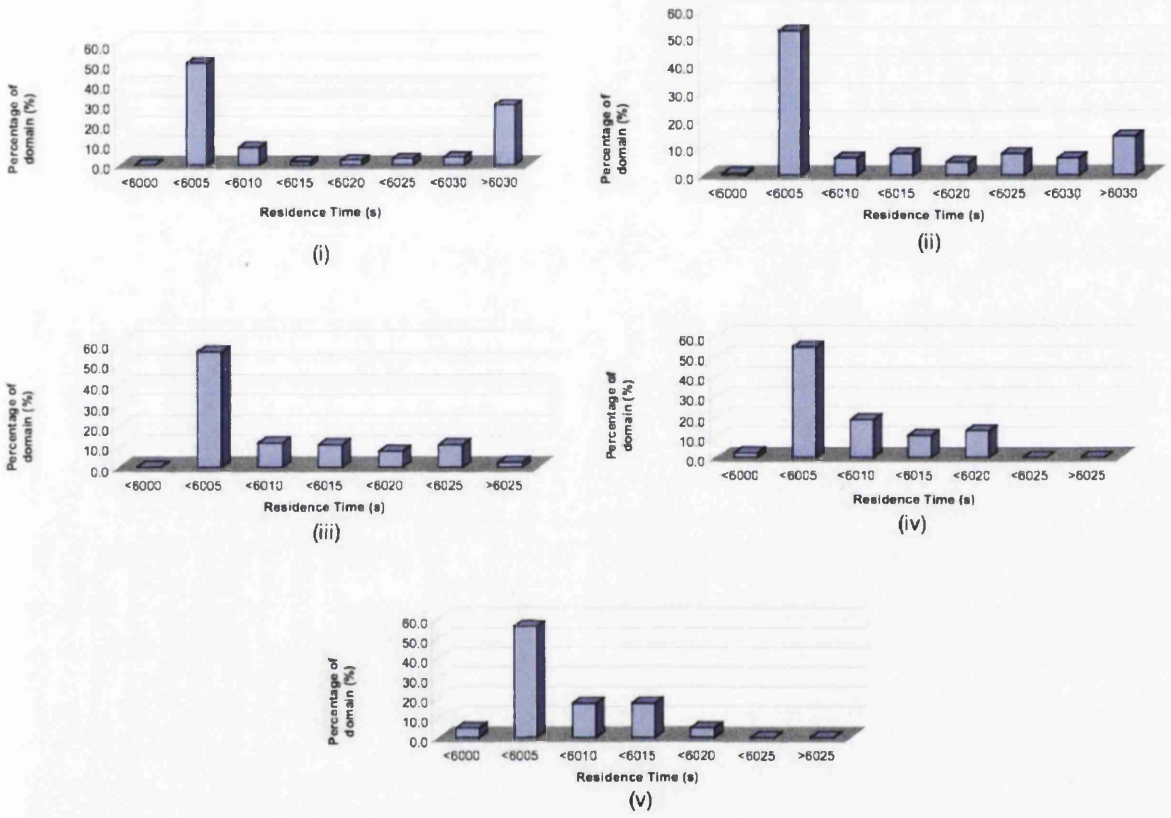


Figure 4.9: Chart representations of HRT results for Tank C, percentage of outflow against residence time: (i) 1.0 $m^3h^{-1}$, (ii) 2.0 $m^3h^{-1}$, (iii) 3.0 $m^3h^{-1}$, (iv) 4.0 $m^3h^{-1}$, and (v) 5.0 $m^3h^{-1}$.

# Chapter 5

# Development of CFD Models of HBC - Two-dimensional Model

In this study, the main objective of employing the CFD analysis is to ultimately obtain a more detailed representation of HRT distribution for the HBC. The CFD simulation of the simple cube tank models presented in Section 4.4 shows a stirred tank assumption is invalid in certain configuration. Both the HRT and the effective tank volume are dependent on internal features and the flow rates of the tank. For that reason, the CFD investigation work was initiated by first simulating flow of water through the HBC.

This chapter presents the first stage of the development of HBC models, elaborating on the outcomes of the work. Details of each CFD model are also presented together with discussion on the findings from the analysis and on the difficulties encountered.

The CFD analysis of the HBC tank was initiated by exploring the modelling possibilities with a two-dimensional model of a HBC. Simulations with a two-dimensional model is computationally less expensive, and thus allowing rapid examinations of modelling configurations. This was done to allow observation on parameters that are of significance to the flow simulation of a HBC.

While the main purpose of this investigation was to obtain the HRT distribution that requires simulation of the flow pattern of water flowing through the HBC, the two-dimensional model was used to simulate the behaviour of floc particles in the tank. The observation on the floc particles was an initial attempt to understand the physics of the forming of the sludge blanket suspension in the HBC. The analysis was done with floc particles of different physical properties, i.e. size, density and drag coefficient, so as to investigate how these properties affect the path pattern of floc particles in an operating tank.

## 5.1 Description of Model

The two-dimensional geometry of the HBC tank is symmetrical and thus gives the benefit of simplifying the model to a half, as illustrated in Figure 5.1. In this model, the trough features near the outlet were not included. The position of the sludge cone was also assumed to be in the middle of the tank to further simplify the model. What is shown in Figure 5.1 is basically the water domain of the HBC model.

Figure 5.2 shows the dimensions of the model.

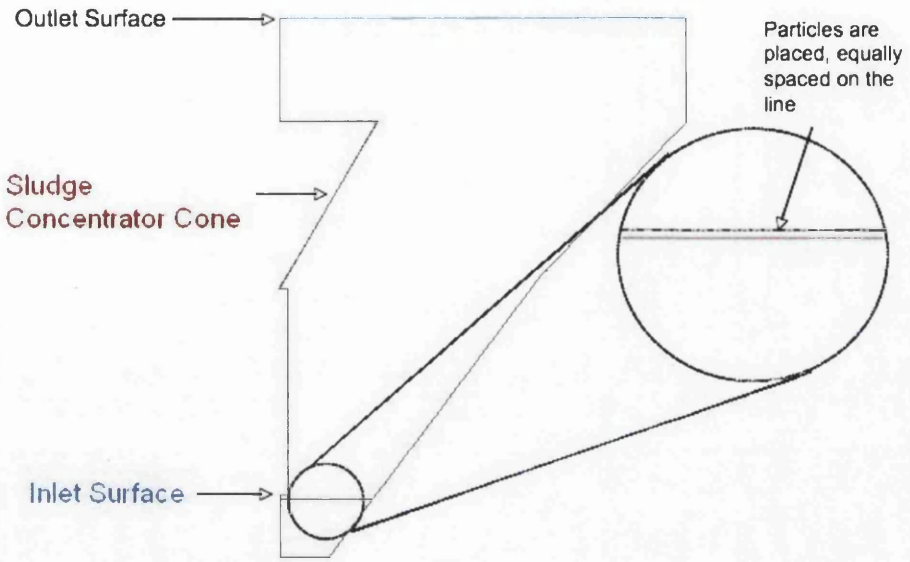


Figure 5.1: A labelled diagram of the two-dimensional CFD model of HBC (not to scale).

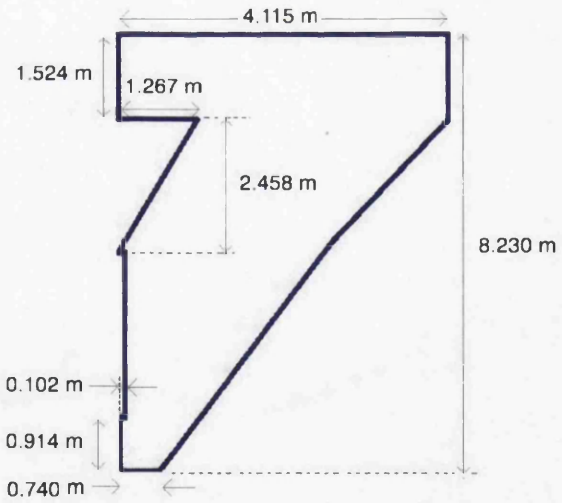


Figure 5.2: Dimensions of two-dimensional CFD model of HBC (not to scale).

### 5.1.1 Particle Tracking

For the purpose of investigating the behaviour of floc particles, particles were introduced into the domain. One hundred spherical floc particles were placed on the line across the width of the tank at the inlet level, as shown in Figure 5.1. The flow paths of the floc particles were calculated using particle tracking in PHYSICA, and the path that each particle takes were exported so they can be plotted on FemGV during post-processing.

The particle tracking routine is explained in Section 4.4.1. It basically evaluates the positions and velocities of particles placed in the tank as they are traced over time. When the line of where the particles and the number of particles are to be placed in the model have been specified, the particles are evenly distributed on the line. The physical properties of the particles, which in this case are the density and diameter of the particles also need to be specified.

Due to the high inflow, the particles that were placed directly just under the inlet and some of the adjacent particles, hit the base of the tank under the hydraulic force before flowing upwards to the outlet. However, some of the particles get trapped in the constant downward current near the base of the tank. These particles are allowed to bounce on the base for a thousand times before PHYSICA stops tracking them. These particles are referred as to be 'lost' during tracking.

### 5.1.2 Setting of Inflow

The model being two dimensional required an adjustment of the inflow velocity. In this model, the inlet of the tank is a slot which is infinite in the third dimension, where as, the inlet in three dimensions is a pipe. This adjustment is necessary due to the lower spreading rate of flow in the hopper section of the tank, resulting in a much higher outflow velocity than that is occurring in the real tank.

A depth could be attributed to each location in the mesh, that allows the change in cross-sectional area of the HBC to be consistent with the three-dimensional geometry. However, this is not possible in PHYSICA and it assumes unit depth over the whole mesh. This means that the flow rate can only be correct at one height. The flow at the inflow is adjusted so to have a closer outflow velocity for the benefit of the blanket formation.

If not adjusted, the flow velocity at any point of the tank apart from the inlet has a much higher velocity from the true flow. This results in high forces of flow jet through the tank. The high velocity flow exerts a high force towards the outlet, causing flow then flow downwards as only a certain volume of water can flow out of the tank. This is in contrary to what happens in the real tank, where flow is slower through time in the upward direction towards the outlet.

To achieve an outflow velocity of that found in the real HBC, the inflow of this model was reduced to 0.0287 $ms^{-1}$, whereas the true inflow velocity is 3.179 $m.s^{-1}$. This value for inflow was evaluated based on the ratio of the width across the tank at

the inlet and outlet levels.

The grid set up for the model provides the model with 11553 number of mesh elements. This gives a minimum cell width of 0.0504 m and maximum width of 0.0680 m. Analysis with this model was solved with the boundary conditions that were set at the inlet and the outlet. The boundary condition at the inlet states that the inflow velocity is constant. At the outlet, the boundary condition simply defines that the pressure is zero, which means that the outflow is under absolute pressure of 1 atm. This is set at on the top line of the model, indicating that the top surface of water is the outlet of the tank.

For all of the cases presented in the following section, simulations were run for a total of 5000 iterations with the application of false timestep of 0.01 s. With this amount of iterations, the yielded mass residual analysis is 9.803 x $10^{-5}$, reduced from initial mass residual of 2.928.

### 5.1.3 Particle Properties

The properties of the particles were set as the variables of the simulation of this model. The properties of the floc particles were varied to give different simulation cases to run. The three varying physical properties were the densities, sizes and drag coefficient of the particles. The results and observations of the effects of varying these physical properties of floc particles are presented in the next section of this chapter.

Table 5.1: Values of densities and sizes of particles

| Density ($kgm^{-3}$) | Size (m) |
|---|---|
| 1200 | $1.0 \times 10^{-5}$ |
| 1500 | $3.0 \times 10^{-5}$ |
| 1800 | $6.0 \times 10^{-5}$ |
| 2000 | $1.0 \times 10^{-4}$ |
| 2300 | $1.0 \times 10^{-3}$ |
| 2500 | - |

### 5.1.4 Varying Densities and Sizes of Particles

The size and density of floc particles are believed to be the two most important properties due to the ffect they have on the separation process of solids from the liquid [52]. Table 5.1 shows the five different values of densities and sizes of particles that were used in all the cases. For every density value, the sizes of the particles are varied, giving five combinations of different cases. There are therefore, in total, thirty simulation cases for varying these two properties of particles.

It was observed that the effective densities of particles formed under water treatment conditions decrease with their sizes increasing [53], [54]. Also, in practice, measuring the density of floc particles is not easy [52]. In this study, the increment in the densities is arbitrary, starting from a value slightly higher than the density of water. The highest value of the particle density, however, was chosen based on a survey presented in [52], where primary particles of a density 2500 $kgm^{-3}$ was used.

Particle size distributions are continuous until it reaches an upper limit and therefore the increment in sizes chosen for this study is also random. The range of particles sizes used in this study is quoted from a study looking at suspensions of particles reported in [55]. The upper limit of this range was chosen merely as a guide at this stage.

### 5.1.5 Varying Drag Coefficient of Particles

For this study, the drag coefficient of the particles were doubled because floc particles are not usually perfect spheres. It is assumed that the sphericity of a floc particle is 0.8, denoting the lack of sphericity [52]. Modifying the drag coefficient by an empirical factor, it is suggested that the drag coefficient value is almost twice the value of a sphere under Stokes Law, for low values of Reynolds number [54]. This case was done only with particles of density 1200 $kgm^{-3}$.

## 5.2 Results

The velocity contour plot of the resultant velocity is the same for all cases, which is as shown in Figure 5.3.

The results of the simulation of the two-dimensional HBC model are presented in diagrams that show the path taken by each particle. These paths are illustrated as lines that starts from the inlet level, where the particles are introduced at the beginning of a simulation. These are lines that show the pattern of their travel as they are dragged

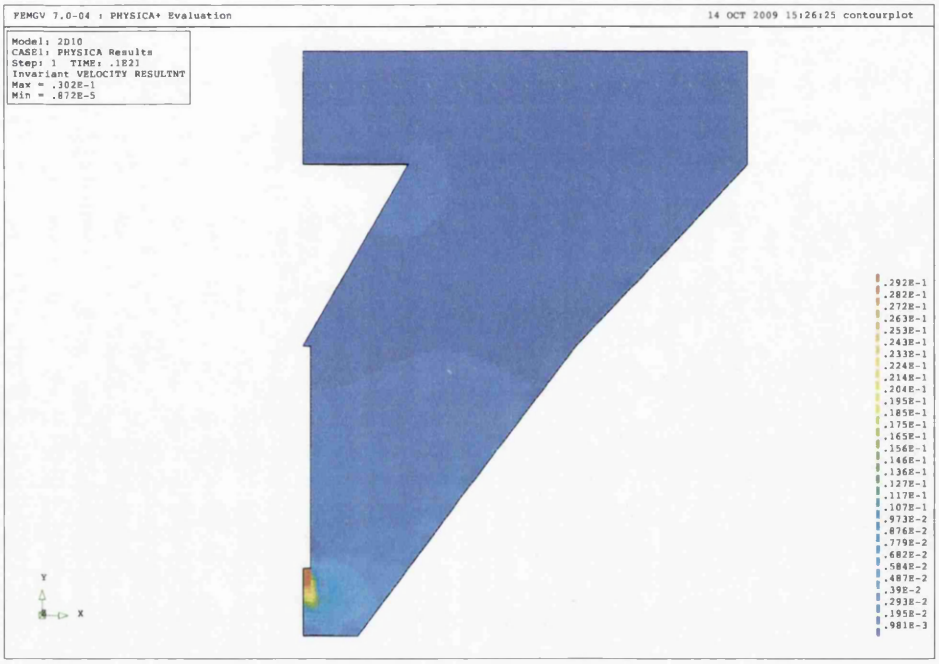


Figure 5.3: Diagram of resultant velocity contour plot of the domain

by the flow of water in an operating HBC.

As it was mentioned previously in 5.1.4, there are thirty simulations for varying the densities and the sizes of the particles. These simulations are grouped in six cases according to the density of the particles, Case 1 to Case 6. The simulation for different sizes of particles are then labelled from (a) to (e) in ascending order in each of these cases. In a result figure, the trend from (a) to (e) is arranged horizontally.

In displaying the path travelled by particles individually, FemView is able to display the paths of only up to twenty particles at one time. For this reason, for each set of simulation, there are five diagrams that are labelled from $i$ to $v$. The particles are numbered from 1 to 100, starting from the left-hand side of the tank, thus the diagrams for the path of:

- particles 1 - 20 are labelled as $i$,
- particles 21 - 40 are labelled as $ii$,
- particles 41 - 60 are labelled as $iii$,
- particles 61 - 80 are labelled as $iv$, and
- particles 81 - 100 are labelled as $v$.

In a result diagram, the trend from $i$ to $v$ is arranged vertically for every size variation.

Case 7 represents the simulation case for particles of density 1200 $\text{kgm}^{-3}$ that has

twice the drag coeficient of sphere particles.

The flow field of the water in the domain is generally uniform, with vortices just under the inlet due to the high speed of inflow. The flow proceeds upwards as its speed descends, which is expected until it reaches the top of the hopper section of the tank.

### 5.2.1 Varying Densities and Sizes of Particles - Case 1 to Case 6

#### 5.2.1.1 Case 1 - Density 1200 $kgm^{-3}$

The results of particle tracking for Case 1 is shown in Figure 5.4.

The uniform flow through the tank can be seen from the path pattern of particles (a) and (b), which have the diameters of 1.0 x $10^{-5}$ m and 3.0 x $10^{-5}$ m respectively.

The smaller particles merely floats, or flow along with the flow of water through the HBC tank. It can be observed from Figure 5.4, the larger the particles, the more they are resistant to the upward flow drag.

For smaller sized particles, their initial positions in the tank across the inlet level affect their path through the tank. Those that are placed just under and near the inlet were retained in the vortices before being dragged by the flow to the outlet. As for the rest, they flow towards the outlet without any delay, which may denote shorter retention time. The largest size of particles, (e), of diameter 1.0 x $10^{-3}$ m, can be seen not getting trapped in the flow circulation that occurs just under the inlet, unlike


Figure 5.4: Case 1 - Path pattern of particles in a two-dimensional HBC model: (a) diameter 1.0 x $10^{-5}$ m, (b) diameter 3.0 x $10^{-5}$ m, (c) diameter 6.0 x $10^{-5}$ m, (d) diameter 1.0 x $10^{-4}$ m, and (e) diameter 1.0 x $10^{-3}$ m

those of smaller diameters. The particles merely settle down to the base of the tank, regardless of their initial positions.

#### 5.2.1.2 Case 2 - Density 1500 $kgm^3$

Figure 5.5 presents the results of the particle tracking of Case 2. In this case, PHYSICA stopped tracking the particles of the largest diameter, 1.0 x $10^{-3}$ m, as explained in 5.1.1. This simply means that these particles stayed at the base of the tank.

Results are showing that the trend of the path pattern that the particles take are the same as Case 1 as the diameter of the particles increases. However, with higher densities, smaller sized particles also show signs of being influenced by their own weight. Some of the particles of diameter 3.0 x $10^{-5}$ m, labelled as (b) in Figure 2.4 can be seen settling down despite of the upward flow in the tank. The particles do not get dragged by the flow of water as much as those in Case 1.

The effect of the initial positions of the particles on the path they take shows the same trend as that observed in Case 1.

#### 5.2.1.3 Case 3 - Density 1800 $kgm^{-3}$

The results of Case 3 is shown in Figure 5.6. Again, in this case, the tracking of the largest sized particles was stopped due to the settling of the particles on the base of the tank.

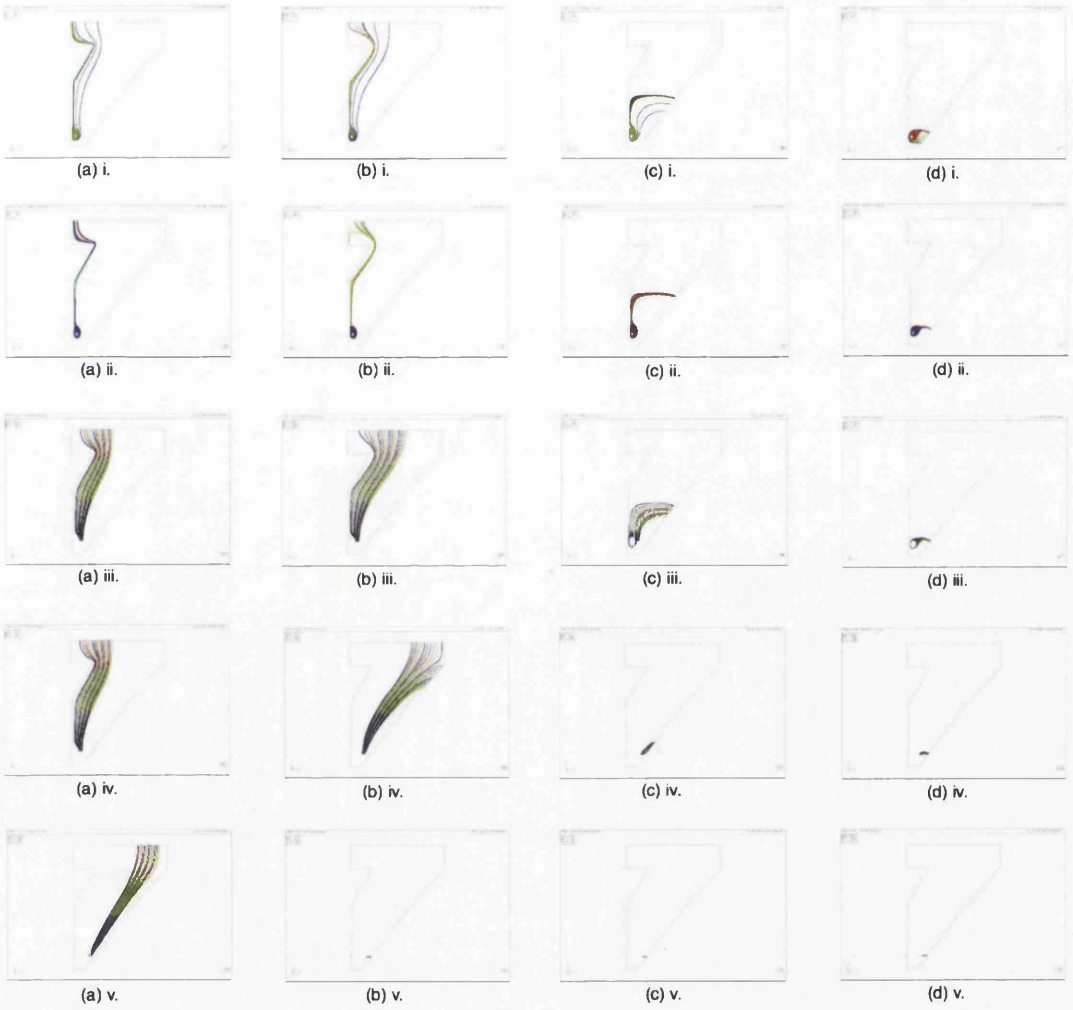


Figure 5.5: Case 2 - Path pattern of particles in a two-dimensional HBC model: (a) diameter 1.0 x $10^{-5}$ m, (b) diameter 3.0 x $10^{-5}$ m, (c) diameter 6.0 x $10^{-5}$ m, and (d) diameter 1.0 x $10^{-4}$ m

The increase in density of the particles in this case has the same effect on the path pattern as that in Case 2, when compared to Case 1. The path pattern of all particles, except for particles with the smallest diameter (a), 1.0 x $10^{-5}$ m, show more of the effect of their weight in causing the particles to settle.

It can be seen that more of the larger particles, (c) and (d) of diameter 6.0 x $10^{-5}$ m and 1.0 x $10^{-5}$ m respectively, are trapped in the vortices under the inlet. In Figure 5.6, particles in (c)iii and (d)iii show that the particles are retained in the vortices before moving upwards and settle, as opposed to the particles in (a)iii and (b)iii, that owed directly upwards with water in the domain.

#### 5.2.1.4 Case 4 - Density 2000 kgm$^{-3}$

Simulations for this case yielded to results presented in Figure 5.7. The path pattern for the particles of the largest size, 1.0 x $10^{-3}$ m, are also not shown in this case due to the same reason mentioned in the previous case.

When compared to the results of Case 3 in Figure 5.6, there is no obvious difference in the path pattern of particles of the smallest diameter, (a). However, for the rest of the particles, more settling of the particles can be seen, at the same time, showing the same trend in the pattern as the size of the particles increase.


Figure 5.6: Case 3 - Path pattern of particles in a two-dimensional HBC model: (a) diameter 1.0 x $10^{-5}$ m, (b) diameter 3.0 x $10^{-5}$ m, (c) diameter 6.0 x $10^{-5}$ m, and (d) diameter 1.0 x $10^{-4}$ m

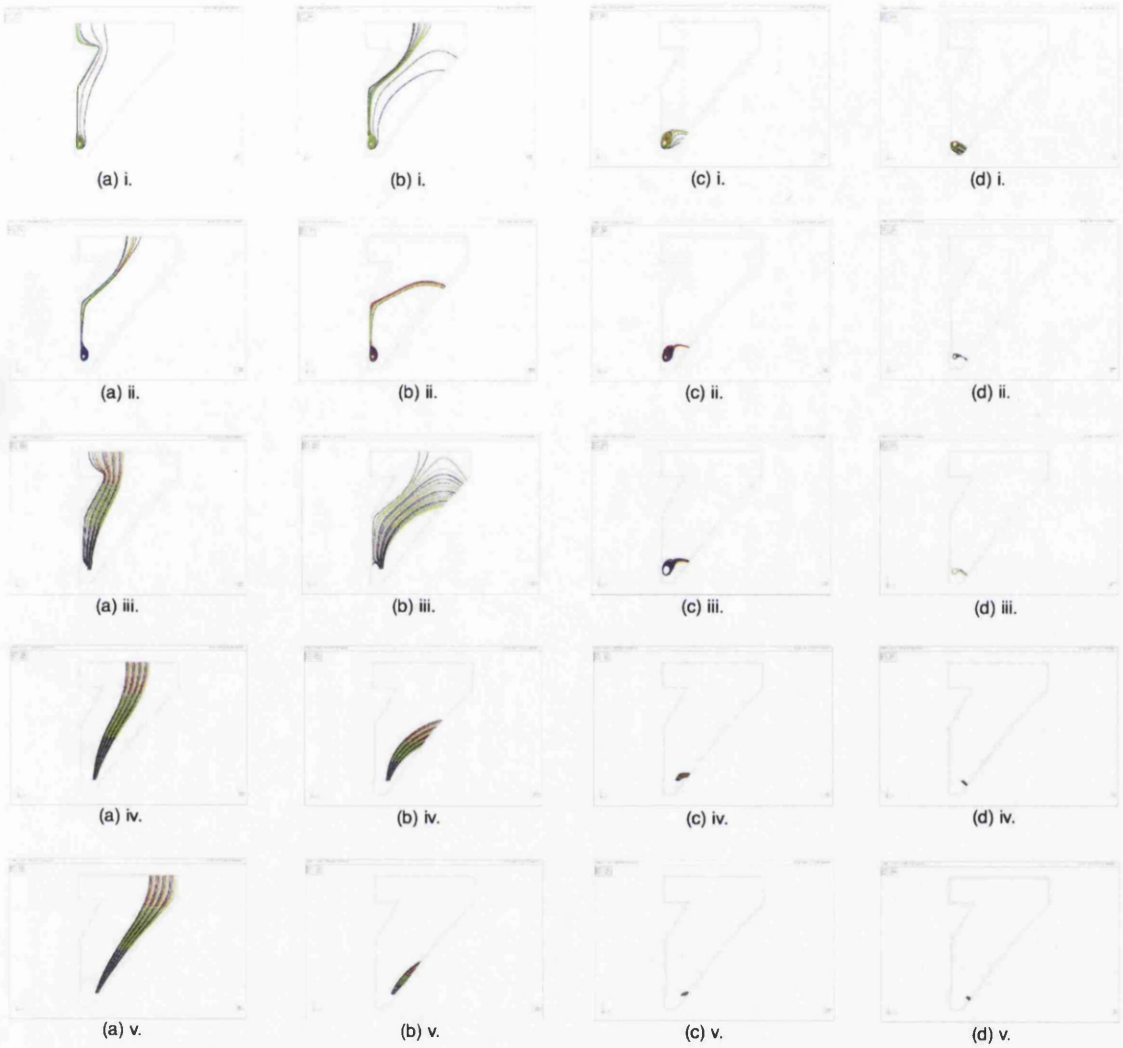


Figure 5.7: Case 4 - Path pattern of particles in a two-dimensional HBC model: (a) diameter 1.0 x $10^{-5}$ m, (b) diameter 3.0 x $10^{-5}$ m, (c) diameter 6.0 x $10^{-5}$ m, and (d) diameter 1.0 x $10^{-4}$ m

#### 5.2.1.5 Case 5 - Density 2300 $kgm^{-3}$

The results for this case is shown in Figure 5.8 below. As of the case above, the tracking of the largest sized particles was not completed due to the settling of the particles. Similarly, the observation on the difference of path pattern of the particles is the same as that of cases mentioned above. The path pattern of particles (b) of diameter 3.0 x $10^{-5}$ m, show more settling of the particles, with none was dragged by the flow of water to the outlet. Also, more particles can be seen retained in the vortices just under the inlet in (b)iii of Figure 5.8.

Particles of the smallest size, (a) are still showing similar path patterns with an exception of those furthest from the inlet. Some particles can be seen settling when approaching the top of the hopper section, where the flow begins to be at its lowest.

#### 5.2.1.6 Case 6 - Density 2500 $kgm^{-3}$

This case sets the highest density of particles, Figure 5.9 presents its results. The path pattern for the particles of the largest diameter was also not produced.

The path pattern results of this case is very much similar to that in the previous cases. This comes only with one exception that can be seen in the path pattern of particles (b) of diameter 3.0 x$10^{-5}$ m, where particles can be seen carried less with the flow before they start to settle.

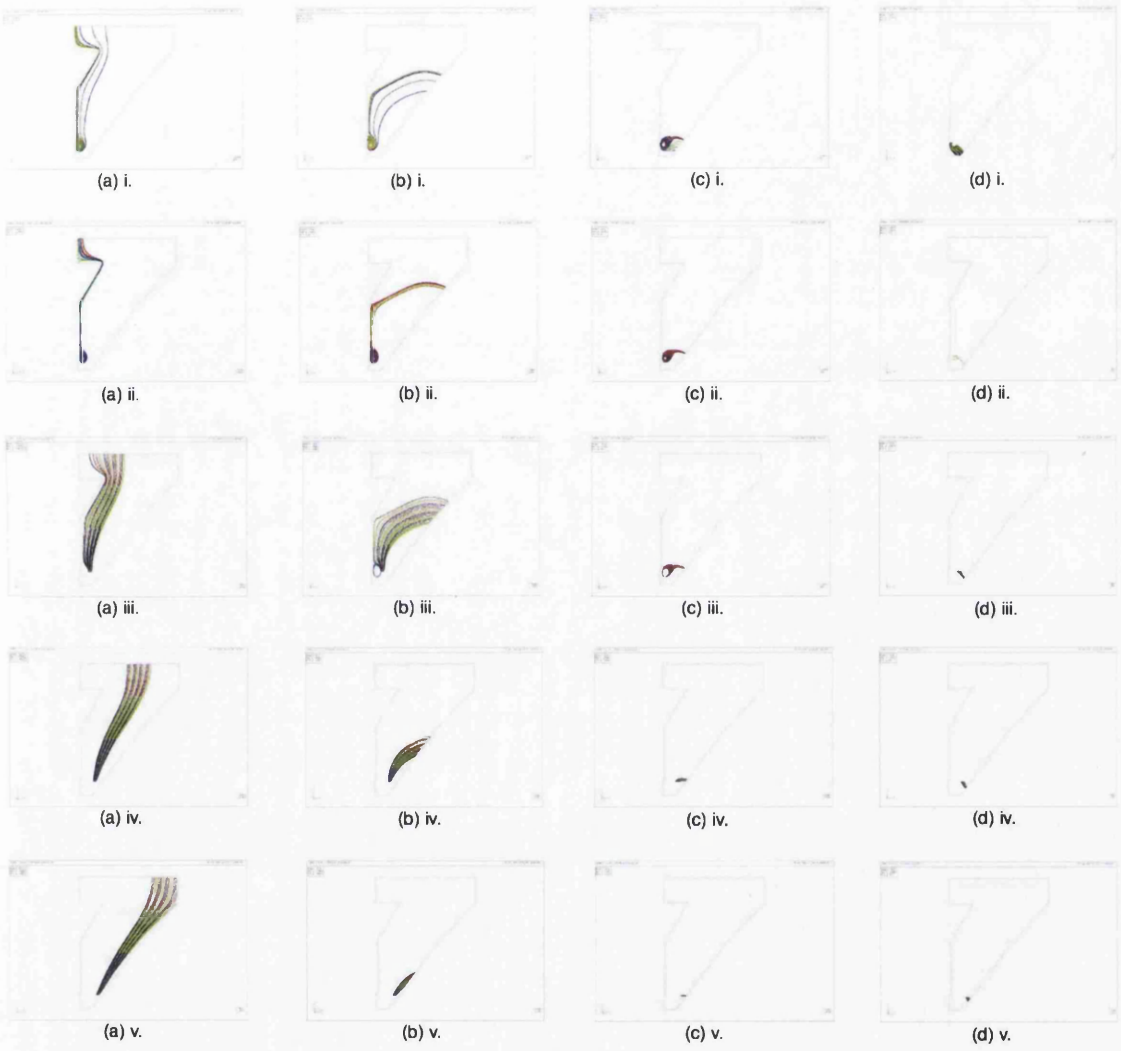


Figure 5.8: Case 5 - Path pattern of particles in a two-dimensional HBC model: (a) diameter 1.0 x $10^{-5}$ m, (b) diameter 3.0 x $10^{-5}$ m, (c) diameter 6.0 x $10^{-5}$ m, and (d) diameter 1.0 x $10^{-4}$ m

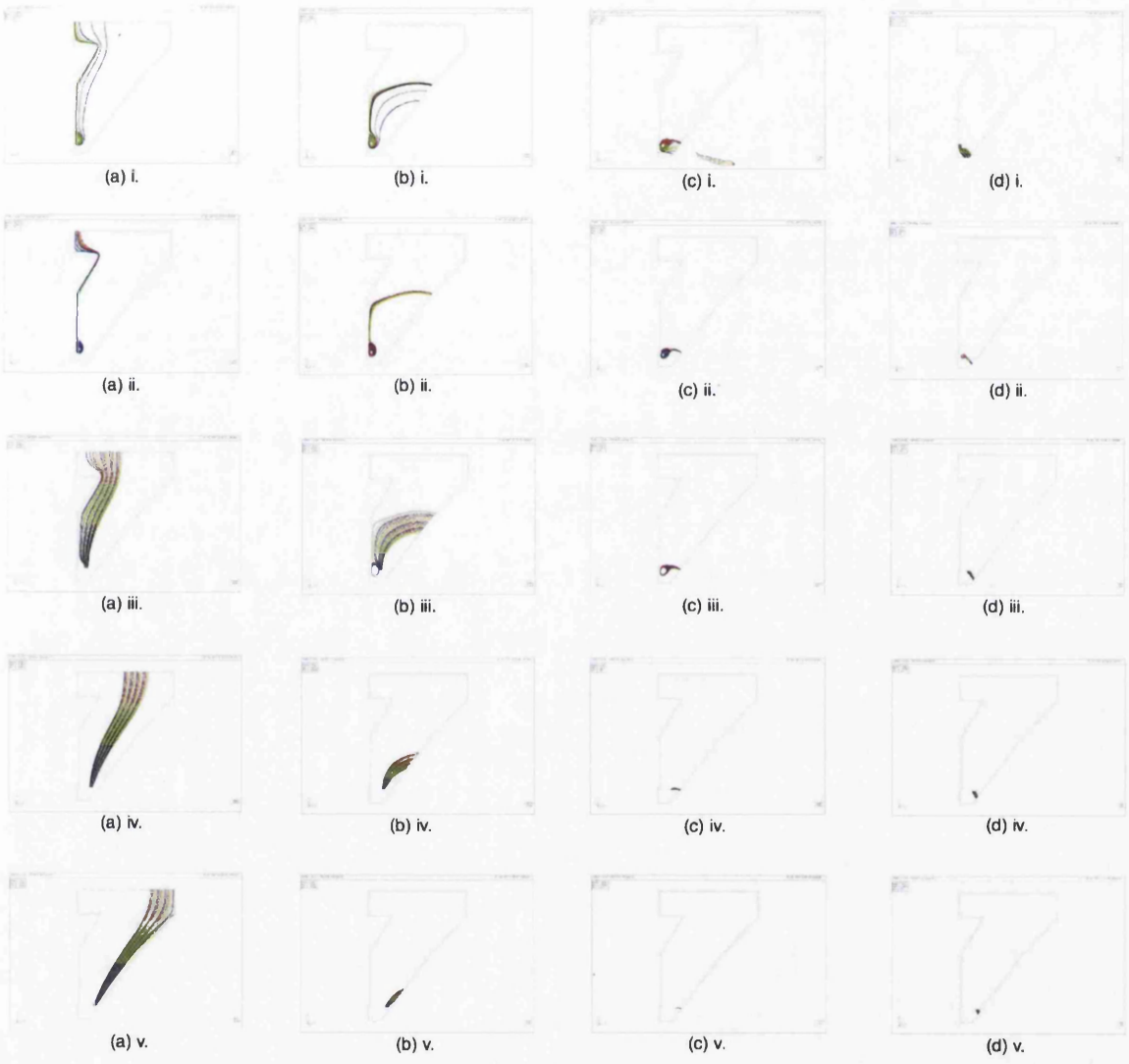


Figure 5.9: Case 6 - Path pattern of particles in a two-dimensional HBC model: (a) diameter 1.0 x $10^{-5}$ m, (b) diameter 3.0 x $10^{-5}$ m, (c) diameter 6.0 x $10^{-5}$ m, and (d) diameter 1.0 x $10^{-4}$ m

### 5.2.2 Varying Drag Cofficient of Particles - Case 7

For this case, the density of the particles was 1200 $kgm^{-3}$ and the drag cofficient of these particles have been doubled, compared to the particles in 5.2.1. The results of this simulation case is shown in Figure 5.10 below.


Figure 5.10: Case 7 - Path pattern of particles in a two-dimensional HBC model: (a) diameter 1.0 x $10^{-5}$ m, (b) diameter 3.0 x $10^{-5}$ m, (c) diameter 6.0 x $10^{-5}$ m, (d) diameter 1.0 x $10^{-4}$ m, and (e) diameter 1.0 x $10^{-3}$ m

In comparison to the results of Case 1 shown in Figure 5.4, the increase in the

drag coefficient of particles does not have any significant impact on the resulted path pattern, as shown in Figure 5.10.

## 5.3 Discussions

### 5.3.1 Varying Densities and Sizes of Particles

The path that a particle takes is governed by the forces acting on it. These forces are drag, which is directed commonly in the flow direction, and gravity, which affects the buoyancy of the particle. In this study, these two forces act in the opposite directions to each other, where the weight of the particle pulls the particle downwards due to gravity, and the thrust from the flow, upwards. The travelling path of a particle, therefore is determined by the net of these forces.

For all densities, the change of the flow path pattern of the particles as the their sizes increase shows a similar trend, where the larger particles resist more of the drag force acting on them. This can be explained with the drag force on a particle is strongly affected by the surface area of the particle, where as its buoyancy, is affected by its volume. Small particles have large area compared to volume, allowing the drag force acting on them to dominate.

The increase in size increases the volume of the particles faster than the surface area of the particles and hence the buoyancy of the particles start to become dominant. Furthermore, the magnitude of the thrust from the flow acting on the particles decreases

as the upward flow through the tank decreases in speed. The descent in this force continues until the flow reaches the top of the hopper section before it remains constant. This change in the magnitude of the drag force allows the buoyancy of the particles to be more and more dominant as the flow through the tank progresses. This explains the trend that was observed across the change in size, where larger particles settle sooner.

For particles of the same size, the increase in the density of the particles, increases weight. Whilst it does have an affect on the drag force, observation from the results have shown that it is less significant. The increase in weight of the particles has made buoyancy of the particle to be dominant.

### 5.3.2 Varying Drag Coefficients of Particles

Increasing the drag coefficients particles increases the magnitude of the drag force acting on a particle. From the drag equation below, equation (5.1), the drag force on the particles was doubled when the drag coefficient of these particles were doubled.:

$$F_d = \frac{1}{2} C_d A_c \rho_w \nu_s^2 \tag{5.1}$$

where:

$F_d$ = drag force acting on the floc particle (N)

$C_d$ = drag coefficient of a particle (dimensionless)

$A_c$ = surcafe area of the particle perpendicular to the direction of drag force ($m^2$)

$\rho_w$ = density of water ($kgm^{-3}$)

$\nu_s$ = velocity of the particle relative to water ($ms^{-1}$)

Therefore the larger sized particles were expected to be carried further into the flow before settling. However, no significant changes was observed in path pattern of particles in Case 7. This shows that the change in the drag force on the particles is relatively small compared to the weight of the particles.

## 5.4 Conclusions

This investigation on the behaviour of floc particles through the flow in a HBC has shown that the path pattern that a particle takes is governed hugely by its physical properties. However, the physical properties of a particle does not remain constant as they agglomerate as the flow progresses through the tank. The physical properties of a floc particle also varies with the raw water quality and the type of coagulant used.

Modelling the path pattern of discrete particles is also not practical at this stage as the number of floc particles entering the HBC is not a data that can be obtained. Also, as previously mentioned, the quantity of the particles also changes due to the occurring flocculation process, making the use of particle tracking not practical.

In order to model the formation of the sludge blanket, the growth and interaction of the floc particles need to be included in the simulation. The flocculation process is complicated and the simulation of the process is high in computational cost. This adds on to the large number of unknowns and hence no further work was carried out on the behaviour of floc particles.

The adjustment of the inflow setting done on this model means that the speed of the flow through the tank does not equal to the true flow speed of a real HBC tank until it proceeds to the top of the hopper section of the HBC. As explained before, using the real inflow speed would also cause the same problem due to the different resulted flow distribution in the tank. This leads to the investigation being brought forward to three-dimensional modelling of the HBC.

# Chapter 6

# Development of CFD Models of HBC - Three Dimensional Model

This chapter continues to outline the development work on the CFD model of the HBC. It presents the three-dimensional model of the HBC.

The aim of this work is to observe the flow pattern that occurs through the HBC tank during operation. The main advantage of the extension from the two-dimensional model to a three-dimensional model is that the flow rate is consistent with the flow rate found in the physical HBC at all heights. Consequently the prediction of a realistic fluid flow throughout the clarifier should be possible. In this work, different simulation cases were run at different inflow settings to observe the effects that the speed of the flow has on the flow pattern.

The modelling of the formation of the sludge blanket has been shown complicated in the previous section, hence in this work, a sludge blanket was imposed on the model. This work was also done with cases that have different thicknesses of sludge blanket for each flow setting. The thicknesses of the blanket was varied to investigate the effect that the sludge blanket has on the flow pattern.

In this chapter, this study is presented in two stages, Stage 1 and Stage 2.

## 6.1 Stage 1

### 6.1.1 Description of Model

The three-dimensional model of the HBC tank is a full model, as shown in Figure 6.1. However some simplifications were applied for the use of this work. Some of the physical features of the tank were simplified and for initial stage of flow simulation, the characteristic of the sludge blanket was also made simple.

There are three physical features of the tank that have been simplified when the model was built. They are the desludging cone, the inlet pipe and the outlet of the tank.

The desludging cone was modelled as a solid cone, therefore the cone merely acts as an obstacle to the flow in the tank, thus nothing is effectively solved in the concentrator cone. This model also does not simulate any desludging into the cone.

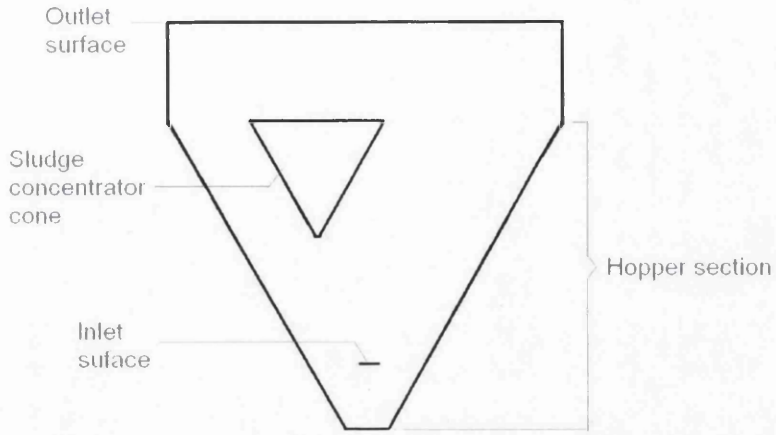


Figure 6.1: A labelled diagram of three-dimensional CFD model of HBC (not to scale).

In this model, the inlet is a face of where the mouth of the inlet pipe is located. The body of the inlet pipe was completely ignored as it is relatively small compared to the whole domain and does not significantly affect the flow pattern in the tank.

Due to the nature of the inlet that is located within the domain, some recirculation of flow was found to be occurring in the region near it. This has led to the lack of flow feeding into the domain. This is because an internal face has element on either side and thus some information was being conveyed through the inlet from the element adjacent to it at the top. This led to a small inaccuracy in the mass flow rate through the domain. For this reason, the elements right above the face of the inlet were removed in order to have the inlet as a boundary face, instead of an internal face.

Water exits the actual tank by overflowing into a number of trough located at the

top of the HBC. To simplify the geometry these troughs have not been included. This reduces it to be the top surface of the water in the tank. This means that the flow through the tank was simulated to overflow at the surface as its outlet. The reason behind this is that it was assumed that there is effectively plug flow in the upper part of the clarifier.

The dimensions of this model is illustrated in two diagrams, Figure 6.2 and Figure 6.3. Figure 6.2 shows the dimensions of the tank on the y - x axis, whereas Figure 6.3 shows the dimensions of the tank on the y -z axis.

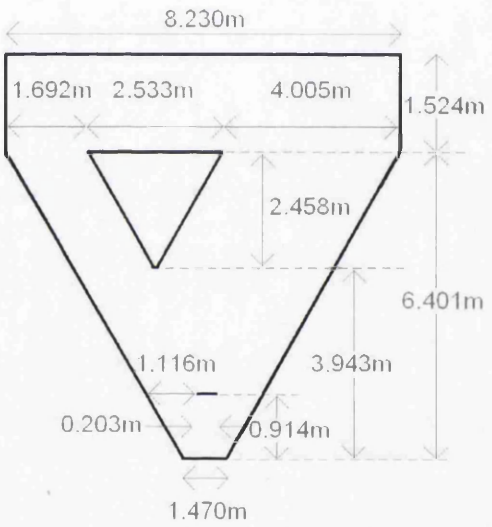


Figure 6.2: Dimensions of three-dimensional CFD model of HBC on the y -x axis (not to scale).

The sludge blanket imposed in this model is a layer that is submerged in the HBC tank. The surface of the sludge blanket is situated at the top level of the hopper-section of the tank and its thickness is then varied from this level downwards. This layer of

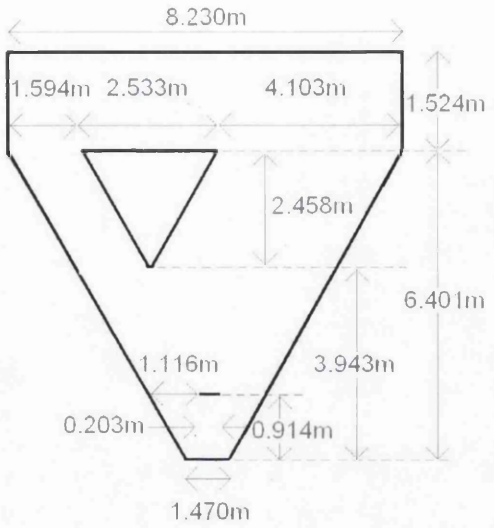


Figure 6.3: Dimensions of three-dimensional CFD model of HBC on the y - z axis (not to scale).

sludge is actually a layer of viscous fluid that has the viscosity of a thousand times more than water, a value that was randomly picked. This is to imitate the resistance that the sludge blanket as on the flow through the tank, due to the suspended solids that form the sludge layer. This simplified sludge blanket is hence a distinct layer from the water domain, unlike what can be found in a real tank that actually has ascending solids concentration, and thus the effective viscosity increases with height up to the top of the hopper section.

### 6.1.2 Simulation Model Settings

The boundary conditions set at the inlet varies according to the inflow values, but were kept constant for each case. The pressure at the outlet, which is top surface of water domain was set as zero gauge pressure, which defines that the surface is at an absolute pressure of 1 atm.

The density of mesh used for this model was chosen based on the observation of the flow field after 1000 iterations. This was done by increasing the number of meshes at a time, and the chosen density of mesh is the one where no significant difference in results is obtained when the number of meshes increased. The comparison presented are for three mesh sizes. These simulations were run with the lowest flow rate and blanket thickness of 0.46 m.

Table 6.1 below tabulates the detail of the three different mesh densities that were used for this purpose.

| Mesh Type | Number of Elements | Minimum Element Width (m) |
|---|---|---|
| 1 | 44016 | 0.051 |
| 2 | 108252 | 0.034 |
| 3 | 192448 | 0.025 |

Table 6.1: Details of Tested Mesh Densities

The results diagrams for the tested mesh types for the first 1000 iterations are as shown in Figure 6.4 for the lowest flow rate.

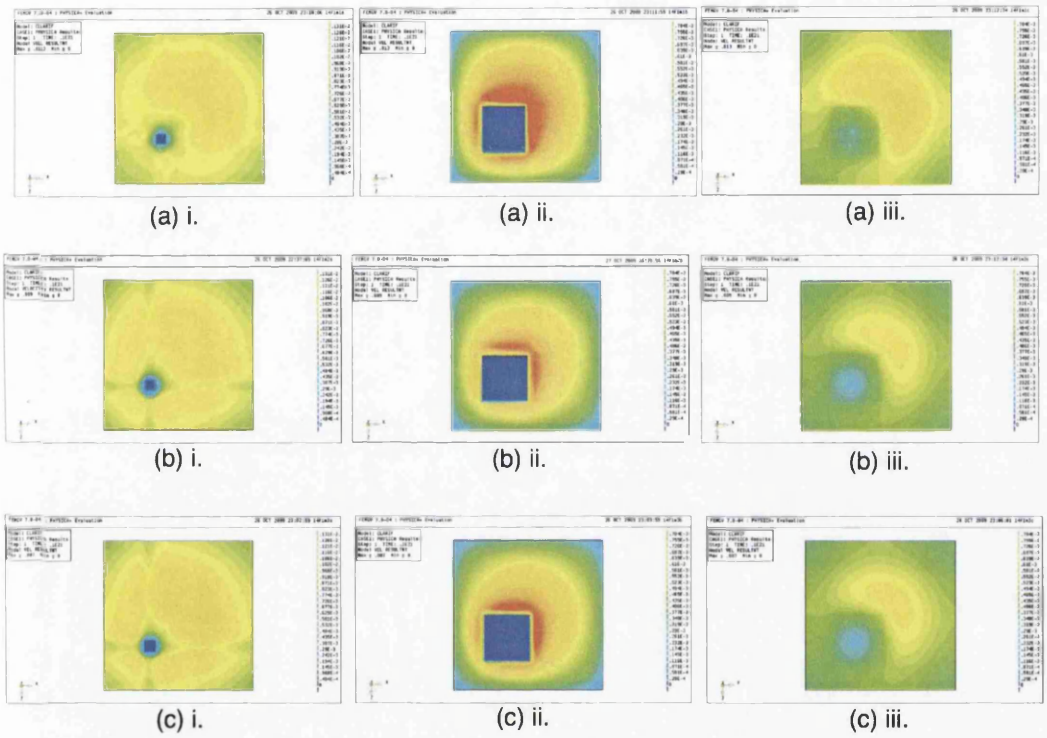


Figure 6.4: Resultant velocity contour plot for flow rate 0.033 $m^3s^{-1}$: (a) Mesh Type 1, (b) Mesh Type 2, and (c) Mesh Type 3; at three different levels - (i) 2 m below the hopper section of the tank, (ii) top of hopper section of the tank, (iii) outlet surface.

Results obtained using Mesh Type 1 and Mesh Type 2 show obvious differences in the regions of where flow is higher. However, when comparing results obtained with the mesh density of Mesh Type 2 and Mesh Type 3, no significant difference can be observed. To ensure mesh independence, results obtained from using Mesh type 2 and Mesh Type 3 were further compared with an additional of 500 iterations and are presented in Figure 6.5.

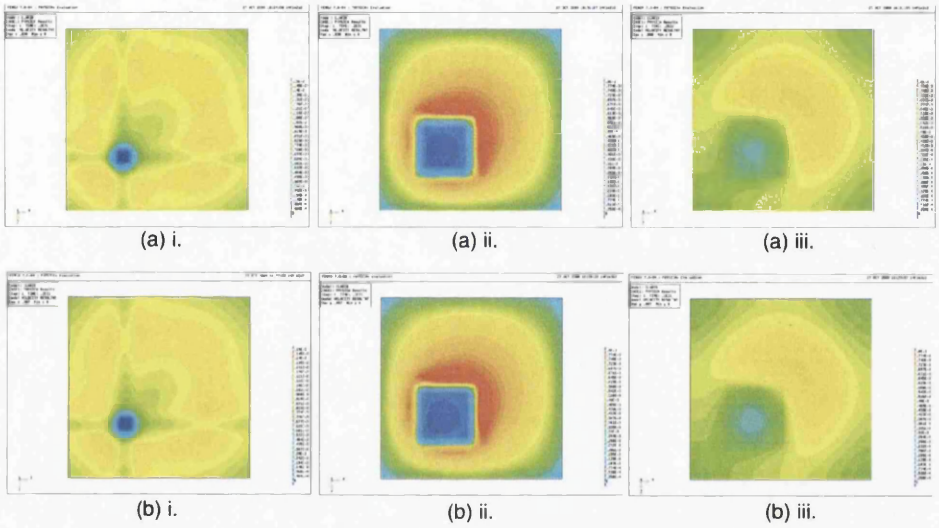


Figure 6.5: Resultant velocity contour plot for flow rate 0.033 $m^3s^{-1}$: (a) Mesh Type 2, and (b) Mesh Type 3; at three different levels - (i) 2 m below the hopper section of the tank, (ii) top of hopper section of the tank, (iii) outlet surface.

After 1500 iterations, results from both mesh densities still do not show any significant difference. Therefore, the density of Mesh Type 2 was chosen for the simulation of the model for all cases presented below.

### 6.1.3 Varying Inflow and Thickness of Sludge Blanket

With the simplification employed onto the sludge blanket in the model, it leaves only two factors that would significantly affect the flow pattern through tank. The speed of the inflow into the HBC determines the rising rate of the flow through the HBC and the pattern that it takes as the flow distributes to the expanding cross-section. The submerged sludge blanket, on the other hand, acts like a cushion to the flow, hence its thickness may affect the flow pattern in the tank as different thicknesses means that the flow is dampened at different degrees.

The inflow rate was varied based on the possible number tanks that would be operating at the same time. At Littleton, the clarifiers are grouped into three banks, with two banks consisting of four clarifiers and the third bank containing six clarifiers. For the purpose of this work, three combinations were chosen for this investigation. These combinations are chosen based on having any one, two and all three banks operating at the same time. This yields the possibility of having four, six, eight, ten and all fourteen clarifiers running at any one time, and the chosen inflow rates used are when four, ten and eighteen operate at the same time.

The thickness of sludge blanket was however varied at random intervals to give six different thicknesses. This layer is to imitate to the most concentrated part of the sludge blanket in the HBC with minimum thickness of 0.46 m. The maximum thickness of the blanket is 2.0 m, which takes up about 30 % of the height of the hopper section of the HBC model. These values are merely arbitrary.

The values for the variables mentioned above are listed in Table 6.2 below. The thickness of the sludge blanket was varied for each flow setting and therefore gives a total eighteen simulation cases.

| Inflow Rate ($m^3s^{-1}$) | Thickness of Sludge Blanket (m) |
|---|---|
| 0.033 | 0.46 |
| 0.058 | 0.60 |
| 0.117 | 1.00 |
| - | 1.20 |
| - | 1.50 |
| - | 2.00 |

Table 6.2: Values of Inflow Rate and Thickness of Sludge Blanket

### 6.1.4 Results and Discussion

The flow pattern through the tank is presented in Figure 6.6 and Figure 6.7. The contour plots presented in these figures are direction contour of the vertical flow.

The vertical flow contour plots show that the flow in the tank circulates in the domain and only streaming flow at the corners of the tank is feeding the outlet. The circulation of the flow is denoted by the downward flow region in the middle section of the tank.

The flow pattern given by the simulation is not what was expected at the beginning of this study. The occurrence of the circulation may be due to the higher speed of the

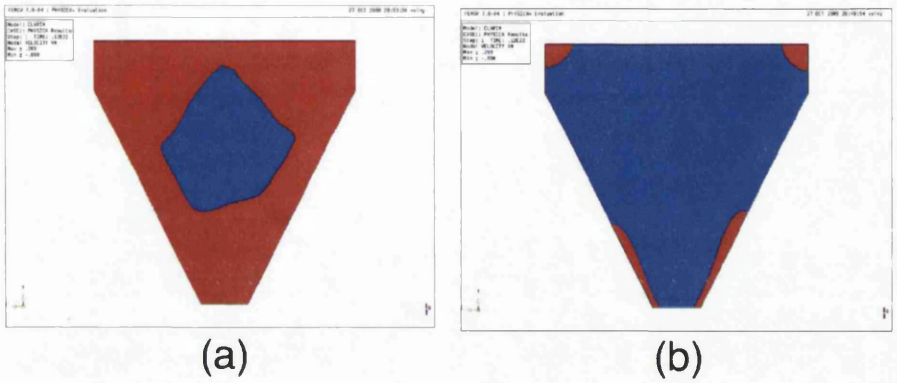


Figure 6.6: Vertical direction flow contour: (a) on the y-x axis, and (b) on the y-z axis.

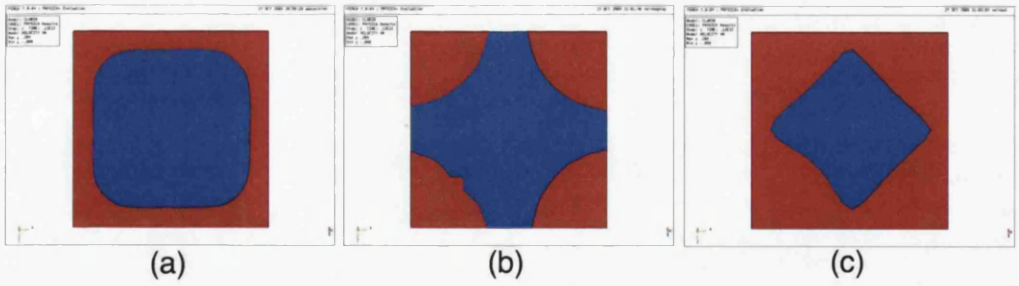


Figure 6.7: Vertical direction flow contour: (a) just above the inlet level, and (b) top of the hopper section of the tank. (c) at the outlet.

streaming flow at the corners of the tank, together with the boundary condition at the outlet being at atmospheric pressure. The streaming flow may be flowing out of the tank at a higher volume, causing feeding of flow into the tank in the middle section. Due to this finding, this part of the work was taken to the next stage. In the next stage, the CFD model was refined to achieve the correct flow pattern through the tank.

## 6.2 Stage 2

### 6.2.1 Description of Model

In this stage of the work, the CFD model of the HBC was improved, whereby the trough features at the outlet was included. The mesh of the sludge concentrator cone that previously acts like a solid obstacle to the flow in the tank was deleted, reducing the number of elements in the model. The rest of the dimensions of the model remain the same.

Figure 6.8 presents the troughs that were built on the model and engineering drawing of the trough details of the UFC. The height of the outlet at the top of the trough is 0.02 m and water flows through it like flowing over a weir. The dimensions of the troughs on the CFD model is illustrated in Figure 6.9.

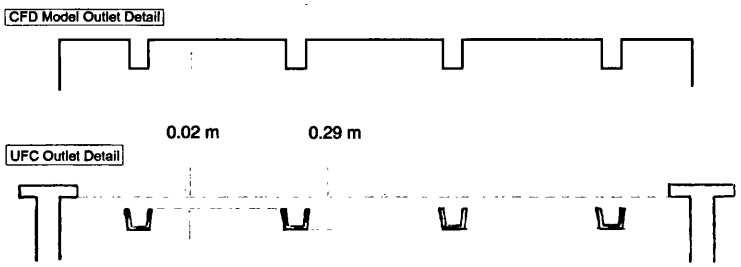


Figure 6.8: Top: Trough outlet detail on CFD model of UFC. Bottom: Engineering drawing of trough details of UFC.

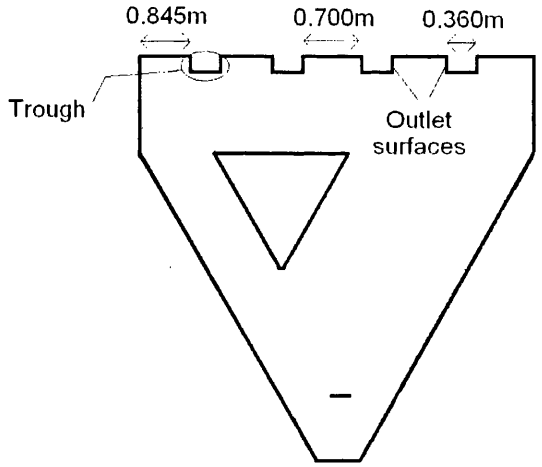


Figure 6.9: Trough details on the UFC model

### 6.2.2 Simulation Model Settings

As it is with the previous model, the boundary conditions at the inlet differ accordingly with the flow rate of each case and gauge pressure at the outlet is kept at zero.

Each case was run with a false time step of 0.03 . The value of the false timestep is decided based on the nearest value to the time step of the width of the smallest element divided by the highest velocity in the domain, and small adjustment to achieve better efficiency. However, each was run for different number of iterations and resulted in different residual values at the end of simulation. These values are also stated later in the chapter with the results of each case. The simulations were run until the final mass residual for each case is at least 1000 less than the initial mass residual and does not change significantly with added iterations.

The size of the mesh elements used for this model is the same as the one used in Stage 1. However, the number of elements have increased due to the change in the physical feature of the outlet. The number of elements generated for this model is 119160.

To ensure mesh independence, the results obtained from this size of mesh was compared with a denser mesh, Mesh Type 3, as described in Table 6.1, after 1000 iteration. The simulation was run with the flow rate of Case 1.

The comparison of the contour of resultant velocity at two different heights of the tank is presented in Figure 6.10. Results in the figure for both mesh types show no

significant difference.

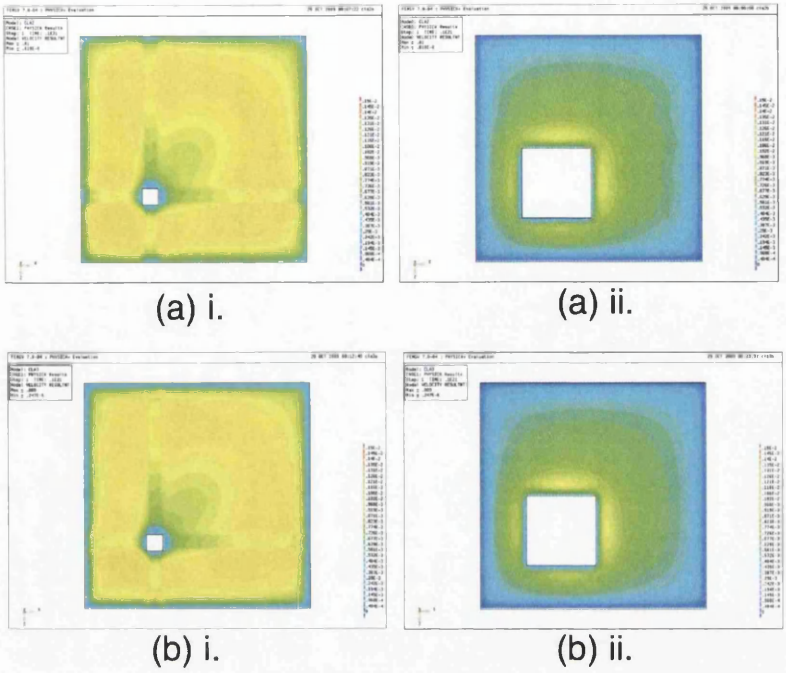


Figure 6.10: Resultant velocity contour plot for flow rate 0.033 $m^3s^{-1}$: (a) Mesh Type 2, and (b) Mesh Type 3; at two different levels - (i) 2 m below the hopper section of the tank, and (ii) top of hopper section of the tank

The variation of each simulation is as explained in Section 6.1.3.

### 6.2.3 Results

The results of the simulations for all of the cases are grouped according the the flow rate setting. The results for each simulation were captured at three different levels of the tank, labelled as (a), where the lowest level being 2 m below the top of the hopper section of the tank. The second level, labelled as (b) is at the top of the hopper section

of the tank and the third, labelled as (c) at the outlet surface. The width of the tank in (a) is 3.582 m and 8.230 m for diagrams of (b) and (c). Results shown below is the invariant resultant velocity of the flow. In every case, the same maximum level for the contour is used.

Discussion of the results are presented in Section 6.3 to allow a comparison over the range of simulations.

#### 6.2.3.1 Case 1 - Flow Rate 0.033 $m^3s^{-1}$

The velocity at the inlet for this case was 0.8025 $ms^{-1}$. The flow pattern through the tank for this model is shown in Figure 6.11, in the form of contour plots of the vertical flow. Diagrams on row (a) in the figure show the contour plots of the side view of the tank and on row (b) are diagrams of cross-section of the tank at different heights. The shown plots are results of simulation with blanket of 1.50 m thick.

The contour plots show that flow from the inlet flow downwards to the base of the tank before progresses upwards towards the outlet. There is a small region with upward streaming flow near the walls of the tank at the bottom of the tank and flow across the tank above the inlet level does not show significant streaming. Circulation of flow also can be observed around the troughs, where there are regions of downward flow as shown in diagram (a)i of Figure 6.11.

Figure 6.12 shows the direction contour plots of the flow near and at the outlet. From the figure, flow circulation can be seen occurring near the walls of the troughs and

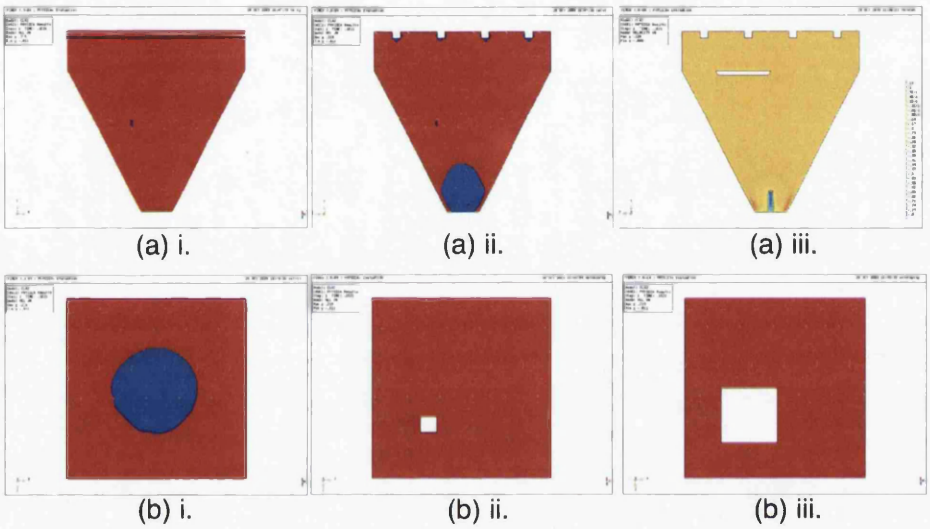


Figure 6.11: Vertical direction flow contour: (a)i. on the y-x axis, (a)ii. on the y-z axis , (b)i. just above the inlet level, (b)ii. mid-height of hopper section, and (b)iii. top of hopper section; (a)iii. vertical flow contour plot on y-z axis.

flow in the rest of the section simply flow upwards towards the outlet. In diagram (c) in this figure, contour of the z-component of the flow shows how flow progress towards the outlet faces at the side of the troughs.

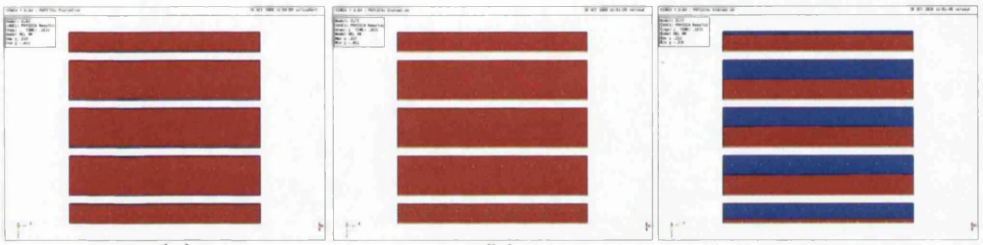


Figure 6.12: Direction flow contour: (a) vertical flow under troughs, (b) vertical flow at outlet level, and (c) z-component flow at outlet level.

The initial mass residual was 3.313 x $10^{1}$. Graph of the values of final mass residual on a logarithmic scale plotted against the number of iterations for this case is shown in Figure 6.13. The simulations were run for 3500 iterations for this case, when sufficient convergence is achieved.

The final residual mass for each of the simulation of different thickness of sludge blanket are tabulated in Table 6.2.3.1. The maximum velocity for all contour plots is 1.5 x $10^{-3}$ $ms^{-1}$.

The simulation results for this case is presented in six figures, Figure 6.14 to Figure 6.19, where each figure shows the contour plots for each blanket thickness.

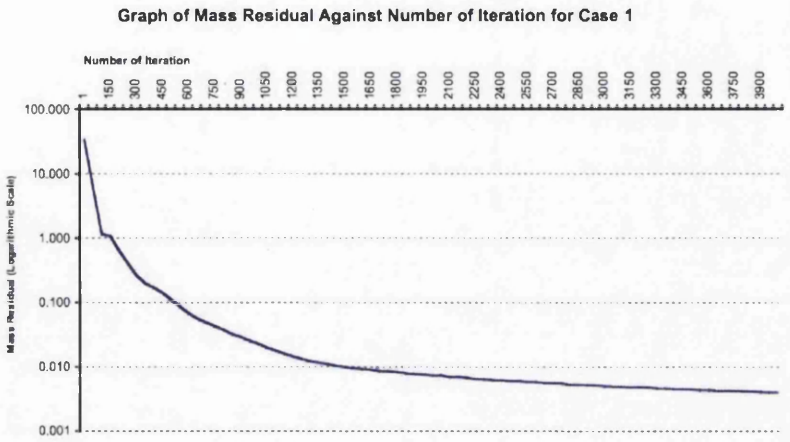


Figure 6.13: Case 1 - Graph of final mass residual against number of iteration on a logarithmic scale.

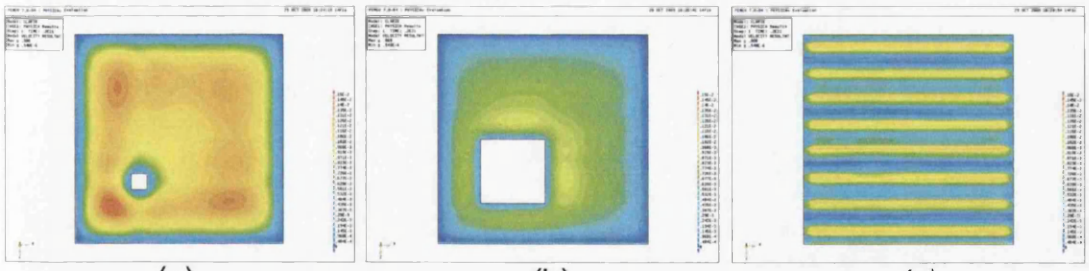


Figure 6.14: Resultant velocity contour plot for Case 1 , blanket thickness of 0.46 m. Levels of tank: (i) 2 m below the hopper section of the tank, (ii) top of hopper section of the tank, (iii) outlet surface.

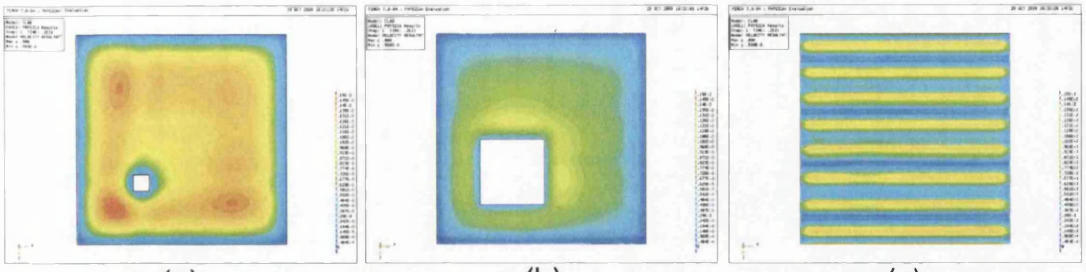


Figure 6.15: Resultant velocity contour plot for Case 1 , blanket thickness of 0.60 m. Levels of tank: (i) 2 m below the hopper section of the tank, (ii) top of hopper section of the tank, (iii) outlet surface.

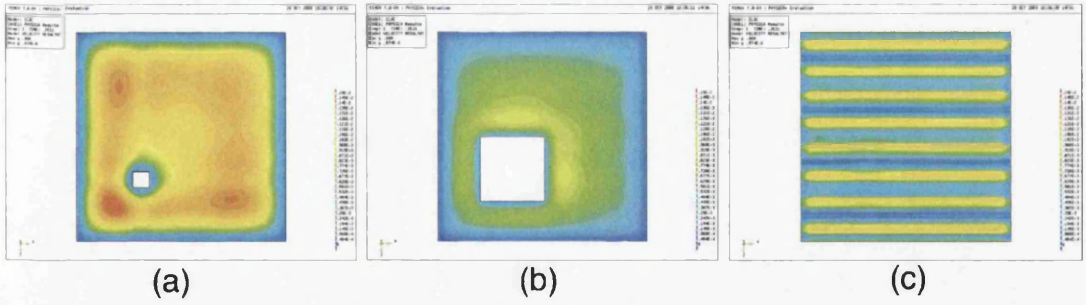


Figure 6.16: Resultant velocity contour plot for Case 1 , blanket thickness of 1.00 m. Levels of tank: (i) 2 m below the hopper section of the tank, (ii) top of hopper section of the tank, (iii) outlet surface.

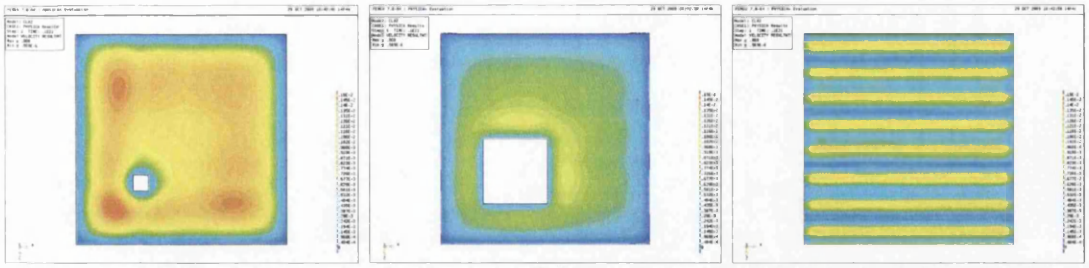


Figure 6.17: Resultant velocity contour plot for Case 1 , blanket thickness of 1.20 m. Levels of tank: (i) 2 m below the hopper section of the tank, (ii) top of hopper section of the tank, (iii) outlet surface.

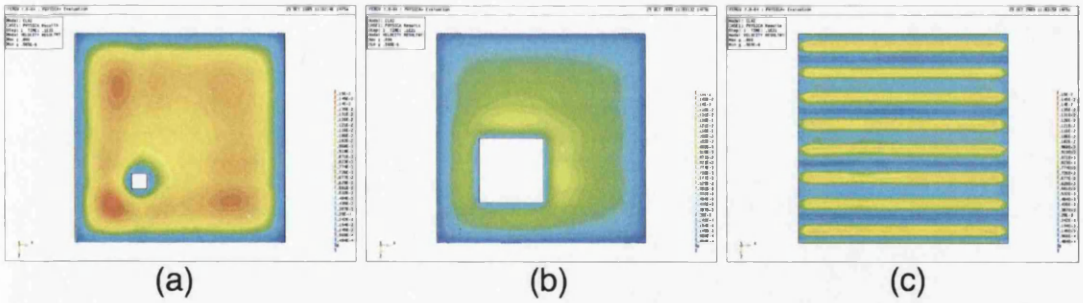


Figure 6.18: Resultant velocity contour plot for Case 1 , blanket thickness of 1.50 m. Levels of tank: (i) 2 m below the hopper section of the tank, (ii) top of hopper section of the tank, (iii) outlet surface.

| Thickness of Sludge Blanket (m) | Final Mass Residual |
|---|---|
| 0.46 | 4.369 x $10^{-3}$ |
| 0.60 | 4.377 x $10^{-3}$ |
| 1.00 | 4.386 x $10^{-3}$ |
| 1.20 | 4.324 x $10^{-3}$ |
| 1.50 | 4.371 x $10^{-3}$ |
| 2.00 | 4.313 x $10^{-3}$ |

Table 6.3: Case 1 -Thickness of sludge blanket and corresponding final mass residual

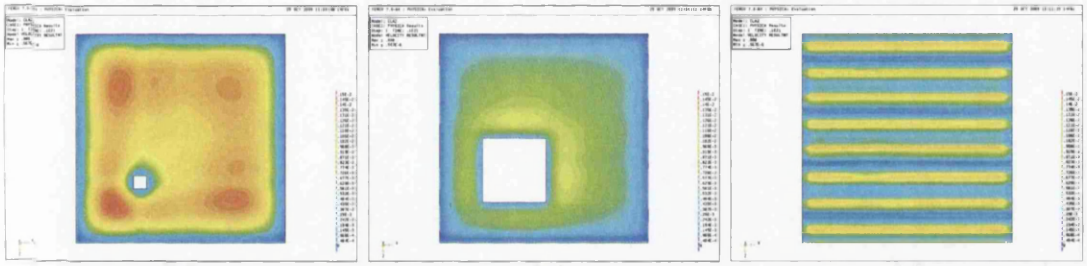


Figure 6.19: Resultant velocity contour plot for Case 1 , blanket thickness of 2.00 m. Levels of tank: (i) 2 m below the hopper section of the tank, (ii) top of hopper section of the tank, (iii) outlet surface.

### 6.2.4 Case 2 - Flow Rate 0.046 $m^3s^{-1}$

For this case, the velocity at the inlet was 1.228 $ms^{-1}$. Shown in Figure 6.20 is the graph of the final mass residual on a logarithmic scale plotted against the number of iteration for this case. The maximum velocity for all contour plots is 2.5 x $10^{-3}$ $ms^{-1}$.

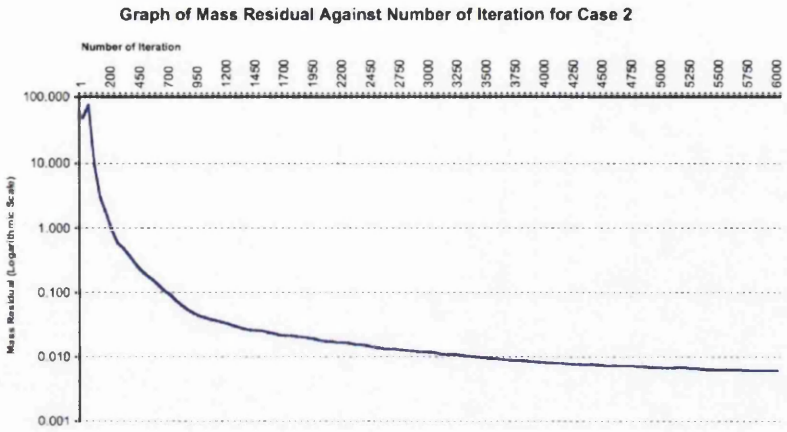


Figure 6.20: Case 2 - Graph of final mass residual against number of iteration on a logarithmic scale.

The simulations were run for a number of 5500 iterations with an initial mass residual of 4.640 x $10^1$. The final residual mass for each of the simulation of different thickness of sludge blanket are tabulated in Table 6.2.4.

Figure 6.21 to Figure 6.26 show the results for the simulations grouped in this case. Each figure show three contour plots of the resultant velocity of a blanket thickness.

### 6.2.5 Case 3 - Flow Rate 0.117 $m^3s^{-1}$

For this case, the velocity at the inlet was set as 2.807 $ms^{-1}$. Figure 6.27 presents the plot of the resulted final mass residual on a logarithmic scale against the corresponding number of iteration.

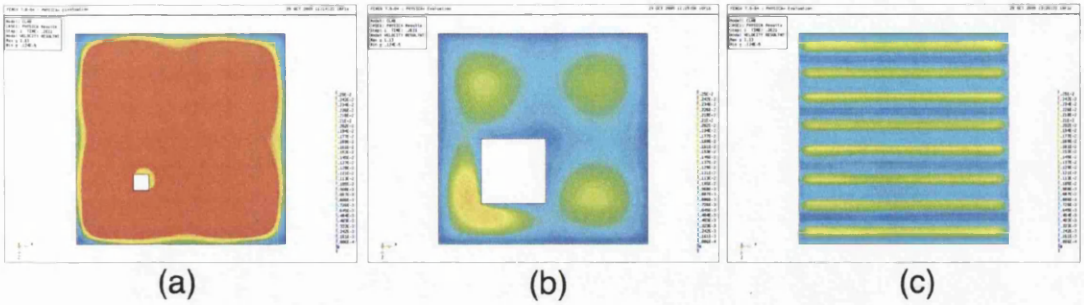


Figure 6.21: Resultant velocity contour plot for Case 2 , blanket thickness of 0.46 m. Levels of tank: (i) 2 m below the hopper section of the tank, (ii) top of hopper section of the tank, (iii) outlet surface.

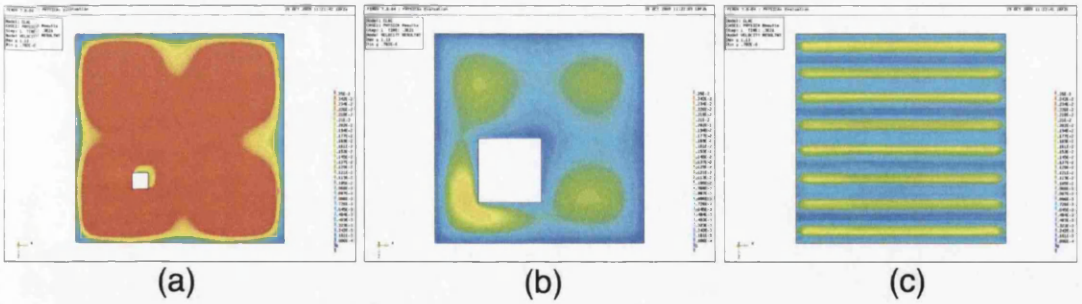


Figure 6.22: Resultant velocity contour plot for Case 2 , blanket thickness of 0.60 m. Levels of tank: (i) 2 m below the hopper section of the tank, (ii) top of hopper section of the tank, (iii) outlet surface.

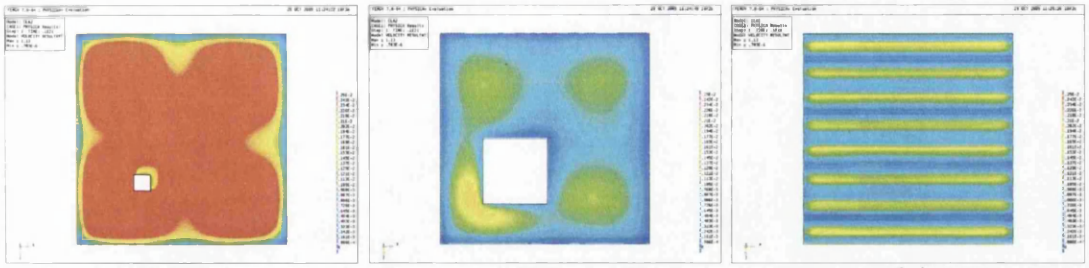


Figure 6.23: Resultant velocity contour plot for Case 2 , blanket thickness of 1.00 m. Levels of tank: (i) 2 m below the hopper section of the tank, (ii) top of hopper section of the tank, (iii) outlet surface.

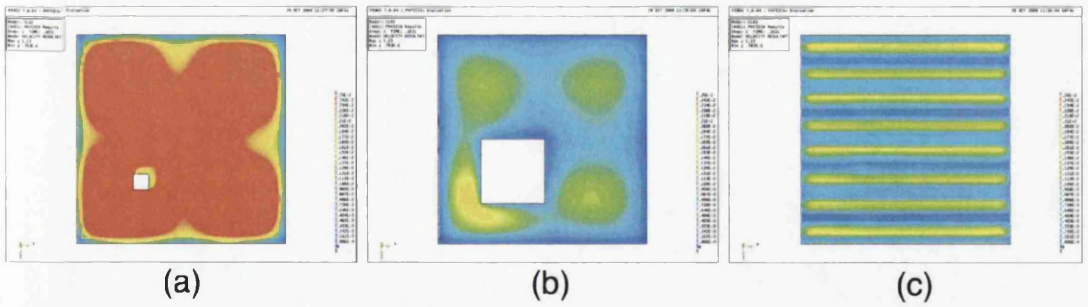


Figure 6.24: Resultant velocity contour plot for Case 2 , blanket thickness of 1.20 m. Levels of tank: (i) 2 m below the hopper section of the tank, (ii) top of hopper section of the tank, (iii) outlet surface.

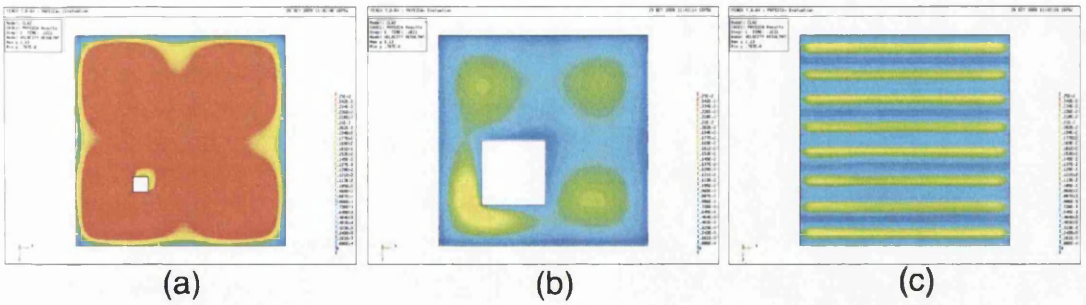


Figure 6.25: Resultant velocity contour plot for Case 2 , blanket thickness of 1.50 m. Levels of tank: (i) 2 m below the hopper section of the tank, (ii) top of hopper section of the tank, (iii) outlet surface.

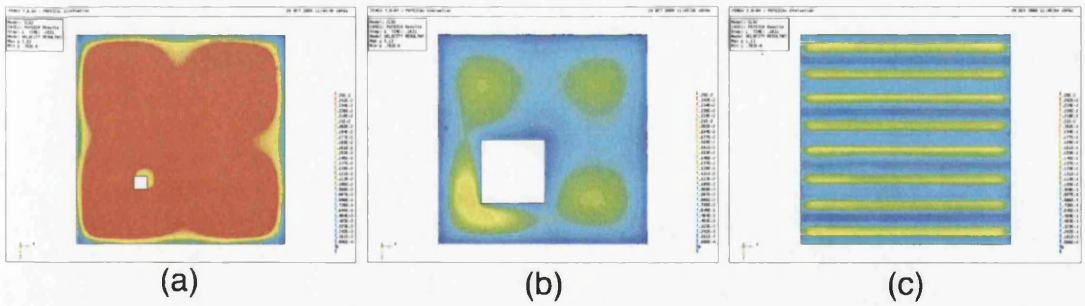


Figure 6.26: Resultant velocity contour plot for Case 2 , blanket thickness of 2.00 m. Levels of tank: (i) 2 m below the hopper section of the tank, (ii) top of hopper section of the tank, (iii) outlet surface.

| Thickness of Sludge Blanket (m) | Final Mass Residual |
|---|---|
| 0.46 | 6.236 x $10^{-3}$ |
| 0.60 | 6.271 x $10^{-3}$ |
| 1.00 | 6.351 x $10^{-3}$ |
| 1.20 | 6.312 x $10^{-3}$ |
| 1.50 | 6.271 x $10^{-3}$ |
| 2.00 | 6.381 x $10^{-3}$ |

Table 6.4: Case 2 -Thickness of sludge blanket and corresponding final mass residual

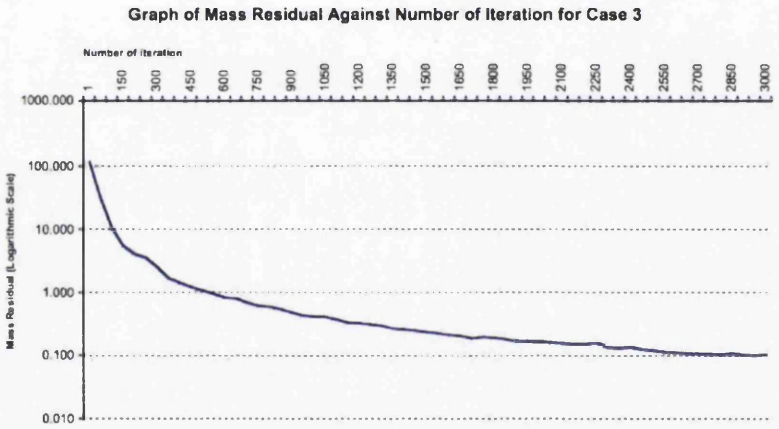


Figure 6.27: Case 3 - Graph of final mass residual against number of iteration on a logarithmic scale.

The simulations were run for 2700 iterations with an initial mass residual of 1.162 x $10^2$. Table 6.2.5 below tabulates the thicknesses of the sludge blanket with the corresponding final mass residuals for the simulations of this case.

| Thickness of Sludge Blanket (m) | Final Mass Residual |
|---|---|
| 0.46 | 1.072 x $10^{-1}$ |
| 0.60 | 1.046 x $10^{-1}$ |
| 1.00 | 1.058 x $10^{-1}$ |
| 1.20 | 1.097 x $10^{-1}$ |
| 1.50 | 1.052 x $10^{-1}$ |
| 2.00 | 1.073 x $10^{-1}$ |

Table 6.5: Case 3 -Thickness of sludge blanket and corresponding final mass residual

Figure 6.28 to Figure 6.33 show the results for the simulations grouped in this case. Each figure shows three contour plots of the resultant velocity of a sludge blanket thickness. The maximum velocity for all contour plots is 5.0 x $10^{-2}$ $ms^{-1}$.

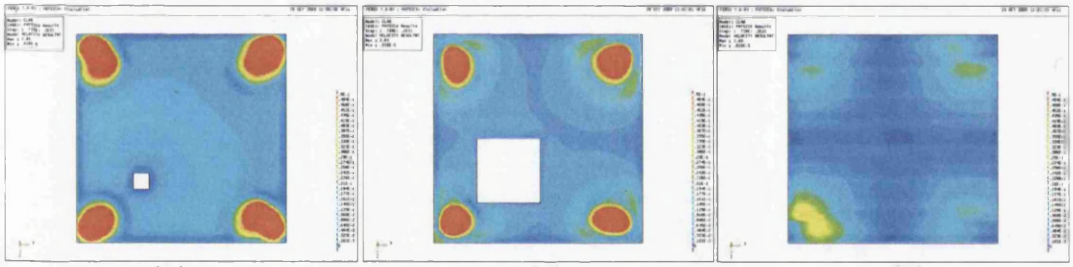


Figure 6.28: Resultant velocity contour plot for Case 3 , blanket thickness of 0.46 m. Levels of tank: (i) 2 m below the hopper section of the tank, (ii) top of hopper section of the tank, (iii) outlet surface.

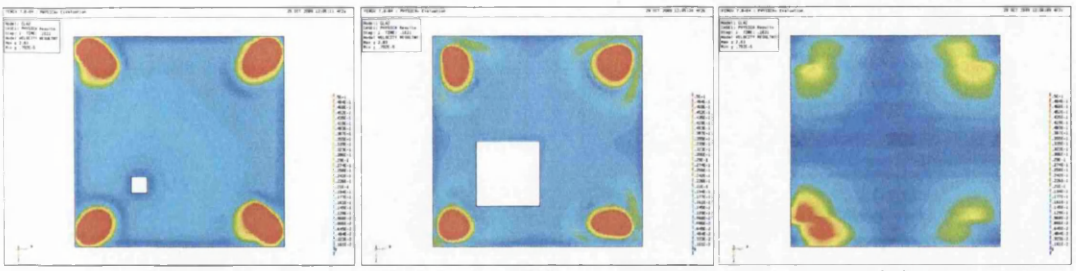


Figure 6.29: Resultant velocity contour plot for Case 3 , blanket thickness of 0.60 m. Levels of tank: (i) 2 m below the hopper section of the tank, (ii) top of hopper section of the tank, (iii) outlet surface.

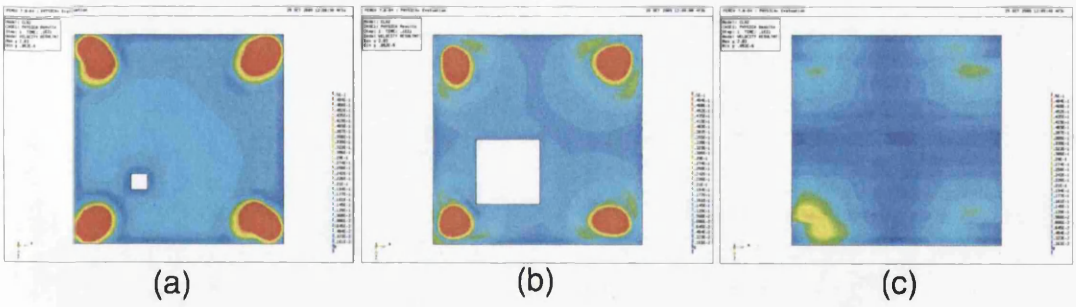


Figure 6.30: Resultant velocity contour plot for Case 3 , blanket thickness of 1.00 m. Levels of tank: (i) 2 m below the hopper section of the tank, (ii) top of hopper section of the tank, (iii) outlet surface.

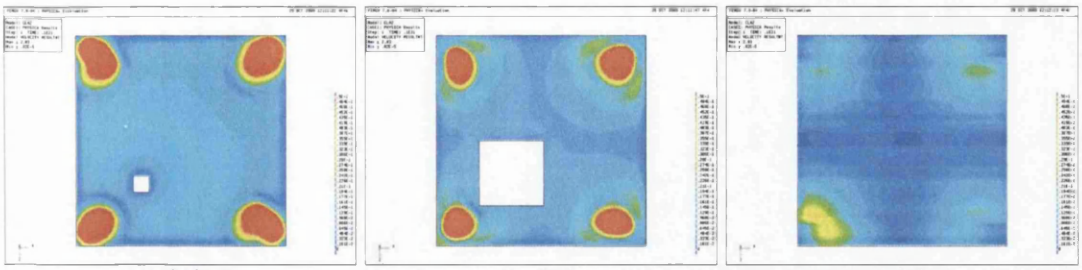


Figure 6.31: Resultant velocity contour plot for Case 3 , blanket thickness of 1.20 m. Levels of tank: (i) 2 m below the hopper section of the tank, (ii) top of hopper section of the tank, (iii) outlet surface.

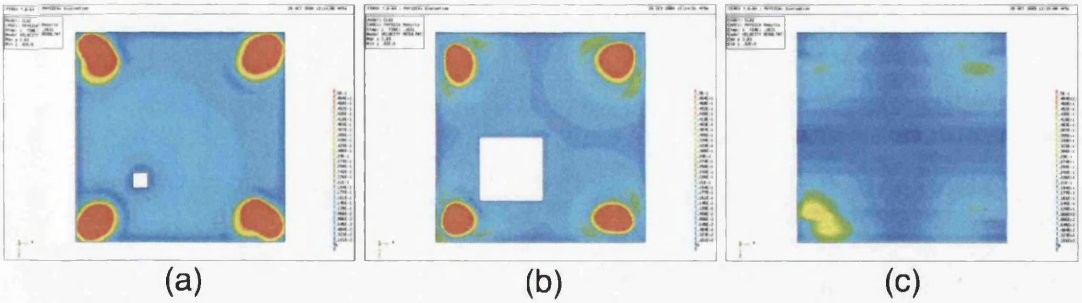


Figure 6.32: Resultant velocity contour plot for Case 3 , blanket thickness of 1.50 m. Levels of tank: (i) 2 m below the hopper section of the tank, (ii) top of hopper section of the tank, (iii) outlet surface.

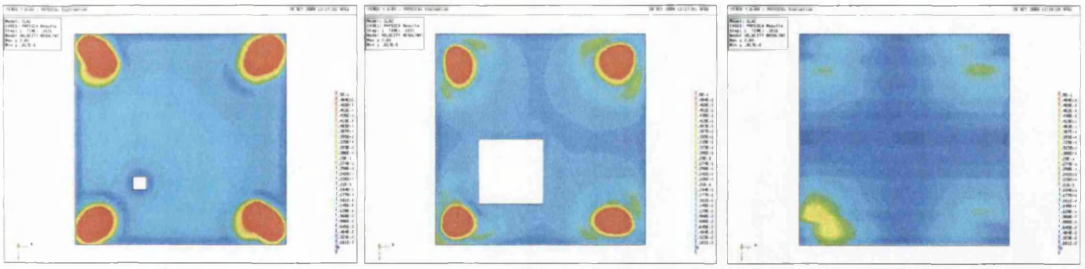


Figure 6.33: Resultant velocity contour plot for Case 3 , blanket thickness of 2.00 m. Levels of tank: (i) 2 m below the hopper section of the tank, (ii) top of hopper section of the tank, (iii) outlet surface.

## 6.3 Discussions

The contour plot results for all flow cases generally show a similar pattern. Flow through the tank progresses from the bottom of the tank with flow near the walls of the tank and around the cone is at the lowest speed due to friction from the walls. The speed of flow also decreases as it flows through the hopper section as the cross-sectional area of the flow increases. As flow approaches the troughs, it speeds up towards the outlet at the top of the troughs.

For Case 2 and 3, steaming of flow can be observed near the the four corners of the tank. This is because as the flow through the tank approaches the cone, the flow moves around the cone as it acts as a stationary obstacle to the flow. The cone helps accelerate the flow close to it. The streaming at the corner nearest to the cone is shown to be more prominent and this is because the flow area in this region is the lowest.

It was expected that as the thickness of the sludge blanket increases, the flow across the section would be more uniform. This is because simulation cases with thicker sludge blanket are cases where flow has passed through a bigger part of the domain that is more viscous. The higher viscosity of the sludge blanket exerts higher internal friction in the flow and this dampens the difference in the speed of flow of the fluid and thus reduces the accelerated streaming occurring in the domain. However, no significant difference can be observed. This may be due to the low speed of flow, making the effect less obvious.

Contour plots for flow just under the trough simply show that flow that progress to the outlet increases in speed as the troughs reduce the flow area. However, for Case 3, the streaming of flow near the four corners of the tank can still be observed at this level due to the higher speed of flow in this case.

## 6.4 Conclusions

The simulation results obtained from this study have shown that the physical properties of the sludge blanket affects the flow pattern through the tank. The viscosity of the sludge reduces the streaming of higher flow speed that flows through the tank and this reduces the possibility of flow short-circuiting through the HBC tank.

However, in this model, the blanket does not rise in regions of faster flow. This would help diffuse the flow as part of the convective force of the fluid would need to balance the desire of the sludge blanket to move back to a 'flat' state. This may be a

factor that reduces the flow near the corners of the tank.

The exclusion of the simulation of the desludging of the sludge blanket means that the loss of flow through the cone was ignored in the simulation. Another shortcoming of the model is that the properties of the imposed sludge blanket is constant for all cases which is not realistic. The viscosity of the sludge blanket in a real HBC varies with the height of the tank and is a function of the flow rate.

This work, therefore encourages a further study on the properties of the sludge blanket to simulate a better approximation on its effects on the flow through a HBC tank. This will also results in better approximation of the HRT of the tank.

# Chapter 7

# Hydraulic Retention Time Profile

Following up the work done as presented in the previous chapter, this chapter presents the three-dimensional model of the UFC, with some development to the model. The development work involves changes in the imposed sludge blanket in the model. The main objective of this work is to refine the model to achieve a better approximation in the simulation of flow through the UFC tank.

With this improvement to the model, the expectation is that it yields a better approximation of the HRT of flow going through the tank. In the work presented in this chapter, the HRT profile for each case was obtained following the resolution of the flow pattern through the UFC tank.

## 7.1 Development of Model

In this part of the study, a sluge blanket model based on the one included in an OTTER model of the UFC was employed. In operating UFCs, sludge blanket are usually kept stable and any change of depth or volume of the sludge blanket is relatively insignificant with respect to the flow through the tank. Therefore, the mathematical equations behind the CSTR model of the sludge blanket used in OTTER was employed into the CFD model of UFC to obtain the solids concentration of the sludge blanket when it is stable.

Equations that were employed into the sludge blanket of this model are equations that are used in OTTER to simulate the clarifying process of the UFC, as explained in 7.2. They are used to evaluate the performance of the sludge blanket as the process of entrapment of the blanket is being simulated. With these equations, the solids concentration of the sludge blanket can be obtained. The solids concentration of the sludge blanket affects the viscosity of the sludge blanket and hence affects the flow pattern of water through the UFC tank. Simulation of the flow through the UFC tank only commences after these parameters are calculated.

The outlet of this model was modified, where troughs were added to it to model the actual feature of the outlet of the real UFC. The enhancement of the outlet feature of the model was done for the purpose of achieving a better simulation of the outflow at the top of the tank. In the previous model, the assumption was that the whole of the top surface of the UFC was set to be a constant pressure. Due to this, water could be lost, or gained over this surface, which may be the cause of the streamlines around the

desludging cone. Since the flow in this model does not overflow at top surface of the tank, but at the side of the troughs, there may be some difference in the flow pattern near the top of the tank. The details of the trough is presented in ??.

On this model, some changes were made on the domain to increase the efficiency of the simulation. These changes are explained in 7.3.

## 7.2 Employment of Sludge Blanket Equations

A sludge blanket modelled with the CSTR model is divided into layers, depending on the number of CSTR used to represent the blanket. The solids concentration within a layer is the same throughout the layer. With the CSTR equations included in the model, PHYSICA is able to calculate the different solids concentration for each CSTR layer of the sludge blanket. The solids concentration at each CSTR layer is important for the flow simulation through the UFC tank as it differs at each level of the blanket. This means that the solids concentration is a function of the vertical height of the UFC tank in PHYSICA.

### 7.2.1 Evaluation of Concentration of Sludge Blanket

The initial solids concentration of the sludge blanket in the model was calibrated to the sludge blanket of an operating UFC of Littleton at different depths. The following set of equations explained below were used to calculate the solids concentration of the

sludge blanket when operating for different cases used for this study and was done for ten loops, which is sufficient to achieve a sludge blanket with little fluctuations in its solids concentration, before the simulation of flow.

The sludge blanket in the UFC model is modelled to be always in a stable condition, whereby an overflowing of the sludge blanket would not occur. The desludging of the sludge blanket is kept sufficient to avoid any overflowing by setting it to occur whenever the total depth of the blanket exceeds the height of the hopper section of the UFC tank. When desludging is needed, the volume and solids concentration would then be recalculated.

The number of CSTR used for the purpose of this part of the study was set to be three. Hence, the sludge blanket was divided into three layers of the same volume and the height of each layer was recalculated at each time step.

With the specified solids concentration for each CSTR layer, the concentration of the sludge blanket of the layer as expressed in $\%v/v$ can be found with this equation:

$$X_b = \frac{10\Phi\rho_f}{\varphi} \tag{7.1}$$

where $X_b$ = solids concentration (mg/l), $\Phi$ = concentration of sludge blanket, based on the thirty minutes settled volume of solids [29] $\rho_f$ = density of floc particles (g/l), and $\varphi$ = Ratio of wet to dry solids.

With the known solids concentration of the sludge blanket, the removal of solids at each time step can be evaluated by integrating the mass balance equation, equation 3.3, as mentioned in 3.3.1. The new solids concentration of the sludge blanket is therefore

given by:

$$X_{b(j)} = X_{b(j-1)} + X_i - X_j \tag{7.2}$$

where $X_i$ is the concentration of solids entering the clarifier in mg/l, $X$ is the concentration of solids leaving the clarifier in mg/l, and $j$ is the current time step.

Following this, the settling velocity of the sludge blanket, $v_s$ can hence be found from the hindered settling curve, defined by the equation (3.2) in 3.3.1. Next, the change of height of the sludge blanket can be found using the equation (3.1) in 3.3.1.

The values of the constants used in this set of equations were set based on the default values given by OTTER. Table 7.1 below presents the constants used and their corresponding values.

| Constant | Value |
|---|---|
| $\rho$ | 1005 g/l |
| $\varphi$ | 300 |
| $C_{min}$ | 9.0 $m^3/m^3$ |
| $v_{max}$ | 0.00157 m/h |
| $s$ | 1.0 |
| $n$ | 2.43 |
| $k_f$ | 0.00347$h^{-1}$ |

Table 7.1: Table of default values used in the CSTR model equations.

### 7.2.2 Implementation of Viscosity Change In Model

With the employment of the sludge blanket equations in the model, the domain is divided into four regions, as shown in Figure 7.1, regions A, B, C and D. The regions A, B and C in the hopper section of the tank represent the sludge blanket in the domain, and region D represents clarified water. The sludge blanket is divided into three, as three CSTR stages were used, as mentioned in Section 7.2.1. The height of each region of the sludge blanket is determined by its volume, where the volumes of all three regions are the same.

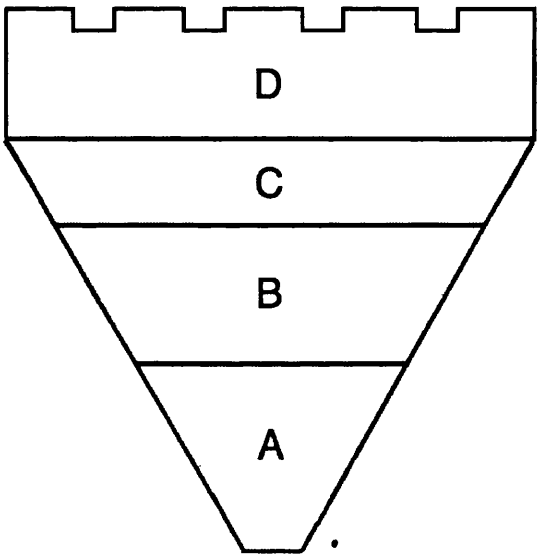


Figure 7.1: Diagrams of regions A, B, C, and D in the domain.

As explained in the previous section, Section 7.2.1, each region has its own solids concentration. Therefore, the viscosity of the fluid in each region differs accordingly. In

PHYSICA, the y-axis position of the centroid of each element is located. From there, the viscosity of the element is then determined according to he region that its centroid lies in.

### 7.2.3 Evaluation of Viscosity of Sludge Blanket

Due to the lack of publication that covers the rheological study of chemical sludge, the references used are based on work done on anaerobic sludge. The viscosity of sludge is known to be greatly affected by it solids content [56], [57]. Hence, the viscosity of the sludge modelled in the clarifier model is determined by the equation below that gives the relationship between viscosity and the solids content of the sludge [58].

$$\mu_\infty = 0.9699e^{0.099TSS} \tag{7.3}$$

where $\mu_\infty$ in mPa.s is the apparent viscosity of the sludge and TSS is the total suspended solids content of the sludge in the unit of g/l. The value of TSS is the value of $X_b$ in the unit of g/l, which can be found using equation 7.2.

The values of the TSS of the sludge blanket in this model varies from 0.130 g/l to 0.388 g/l, resulting with a sludge blanket that is only slightly more viscous than water.

## 7.3 Model Description

The dimensions of the model remains the same as that in the previous model, as shown in Figure ?? in the previous chapter. Again, this model does not simulate desludging of the sludge blanket.

### 7.3.1 Simulation Model Settings

The grid for the model gives a total number of elements 360896. The smallest width of cell is the elements at the outlet, which are 0.001 m, and the widest cell is 0.010 m.

Due to the vast range of velocity within the tank, all simulations were run for 2000 simulations with a false timestep of 2.0 before proceeding to reach a solution with a good convergence. This is to allow for a quick simulation of flow through the tank to be achieved. The details of the simulations following this step is stated together with the corresponding results in 7.4.

For each simulation, another value of false timestep is used after the 2000 iterations. This false timestep is different for every case and is decided based on the nearest value of the width of the cell at the inlet divided by the inflow velocity, which is expected to be the highest speed of flow in the domain.

The simulations are run until the final mass residual is at least 1000 times less than that of the initial value. The mass residuals are not normalised and therefore cases with higher flow rates have higher higher residuals. All simulations were run up to the

number of iterations where the difference in the HRT results for every 250 iterations are less than 6 s.

#### 7.3.1.1 Varying Inflow Rate

The flow rate settings for the cases run with this model are kept the same as the settings used for previous work done with the three-dimensional model, only with additional of two variations. The added variations of inflow is the rate at which when there are six and then clarifiers operating at the same time. The flow rate values are: 0.033 $m^3s^{-1}$ (0.12 Ml/hr), 0.046 $m^3s^{-1}$ (0.17 Ml/hr), 0.058 $m^3s^{-1}$ (0.21 Ml/hr), 0.077 $m^3s^{-1}$ (0.28 Ml/hr) and 0.117 $m^3s^{-1}$ (0.42 Ml/hr).

#### 7.3.1.2 Varying Turbidity

With the calculation of the solids concentration of the sludge blanket included in this model, the turbidity of the inflow was varied. The turbidity of the raw water used are based on the real raw water quality data of Littleton, together with the corresponding doses of coagulant used at the treatment works. The resulting concentration of suspended solids in the coagulated water is found by using the equation used in OTTER [59]:

$$S_t = 2.9D_{Al} + 1.9D_{Fe} + S_{raw} + 0.2C_{rem} + D_{poly} \tag{7.4}$$

where $S_t$ is concentration of total suspended solids in mg/l, $D_{Al}$ is alum dose in mg Al/l, $D_{Fe}$ is ferric dose in mg Fe/l, $S_{raw}$ is concentration of suspended solids in raw

water in mg/l, $D_{poly}$ is poly dose in mg/l, and $C_{rem}$ is colour removed in Hazen units.:

In the simulations presented in this chapter, the type and dosage of coagulant matches those used at Littleton Treatment Works. Confidentiality agreements do not permit details of either the type or dosage of coagulant to be included in the thesis.

| Turbidity (NTU) | Solids Concentration of Coagulated Water (mg/l) |
|---|---|
| 5.2 | 19.19 |
| 10.7 | 32.60 |
| 20.0 | 42.03 |

Table 7.2: Values of turbidity of raw water and corresponding solids concentration in coagulated water.

## 7.4 Results

The results obtained from the simulations are presented below. For each simulation case, the results presented are the contour plots of invariant resultant velocity and chart representations of the HRT. These are grouped according to the flow rate settings. The details of the simulation runs are also included below.

The contour plots for each case presented are captured from the same three levels as those presented in Chapter 5, for comparison purposes. The HRT results are values

taken from the outlet elements of the model. Adjacent to the outlet, there are in a total of 1024 elements.

Discusions of the results are presented in the next section, 7.5.

### 7.4.1 Case 1 - Flow Rate $0.033 m^3 s^{-1}$

The inflow velocity for this case is 0.8025 $ms^{-1}$. The simulations for the cases were run for an additional of 12750 number of iterations with a false timestep of 0.02 and the initial mass residual is 3.308 x $10^1$. The final mass residual for every simulation of this flow rate is tabulated in Table 7.3.

| Turbidity (NTU) | Final Mass Residual |
|---|---|
| 5.2 | 2.917 x $10^{-2}$ |
| 10.7 | 2.499 x $10^{-2}$ |
| 20.0 | 1.599 x $10^{-2}$ |

Table 7.3: Case 1 - Final mass residual for each turbidity case

The flow mechanism through the HBC tank for this case is shown in Figure 7.2, where the particle tracking feature in FemGen was used. Particle tracking feature displays solid lines that represent the paths of the flow for a specified selection of centroids to start the tracking. In this case, some centroids that are just under the inlet level were chosen.

The particle tracks start at the height of just under the inlet level. As the flow

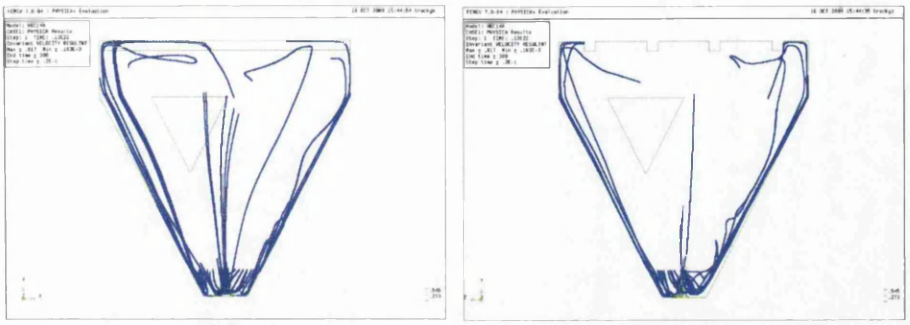


Figure 7.2: Particle tracks for flow beginning from under the inlet level: (a) on the y-x axis, and (b) on the y-z axis.

progresses from that level, some tracks near the inlet show that the occurrence of flow circulation can be observed at the bottom of the tank, where flow is downward coming from the inlet and speed is high. Flow near to the walls of the tank, does not get trapped in the circulation and moves upward towards the outlet.

Particle tracks near the top of the tank also show some occurrences of flow circulation at the corners where the troughs are due to the small aperture of the outlets. Flow that progresses to the middle section of the tank also can be seen circulating.

Figure 7.3 shows the contour plots of the y-component of the flow near the walls of the tank. The contours only show the direction of the flow with no information of its magnitude.

Flow circulation occurring in the middle section of the tank is shown in the first two diagrams presented in Figure 7.4. In these diagrams, vertical flow direction contour is

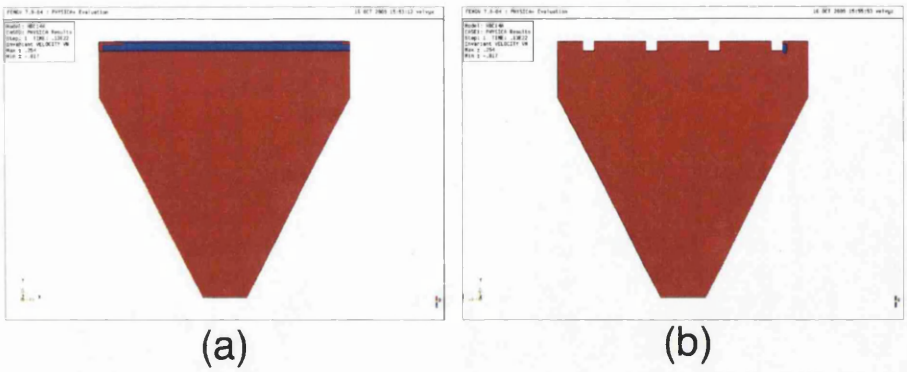


Figure 7.3: Vertical direction flow contour: (a) on the y-x axis, and (b) on the y-z axis.

shown at cross-sections of the tank at two different heights. The third diagram shows the direction contour of the z-component of the flow at the outlet. Flow can be seen flowing out of the trough apertures in the diagram.

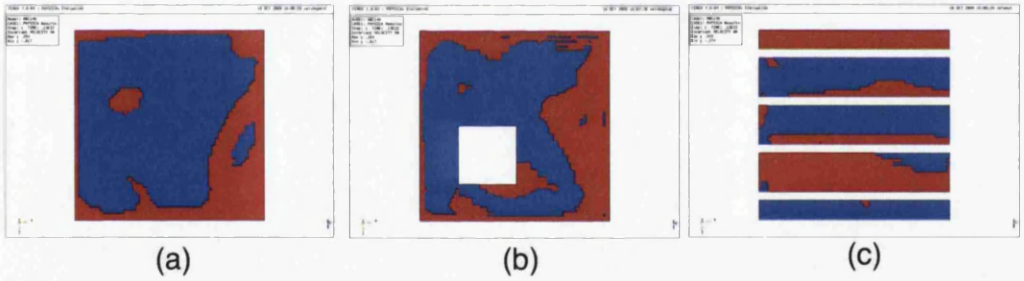


Figure 7.4: Vertical direction flow contour: (a) mid height of the hopper section of the tank, and (b) top of the hopper section of the tank. (c) flow contour for z-component of the flow at the outlet.

Although downward flow is shown in the middle section of the tank, the magnitude of this flow is lower than the upward flow. This is shown in Figure 7.5, which is a contour plot of the vertical flow at the top of the hopper section of the tank.

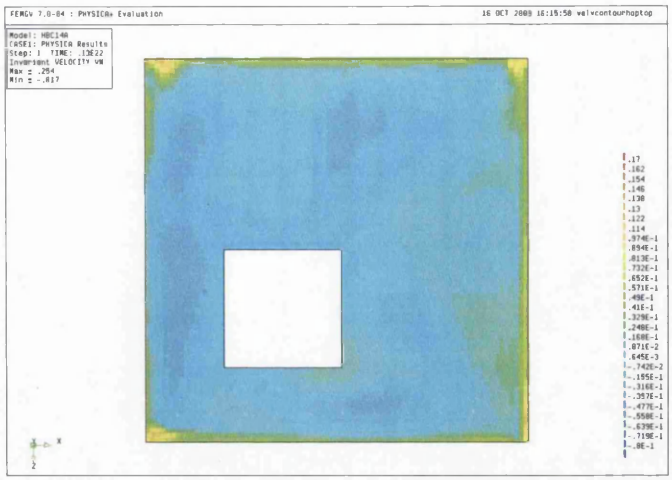

Figure 7.5: Contour plot of vertical flow at the top of the hopper section of the tank.

The contour plots of the resultant velocity are presented in Figure 7.6 and the HRT of the three simulations are shown in the form of bar charts in Figure 7.7.

### 7.4.2 Case 2 - Flow Rate 0.046 $m^3s^{-1}$

The inflow velocity for this case is 1.22 $ms^{-1}$. With a false timestep of 0.02, the simulations were run for a number of 14000 iterations. The initial mass residual is 4.632 x $10^1$ and the final mass residual is as tabulated in Table 7.4.

| Turbidity (NTU) | Final Mass Residual |
|---|---|
| 5.2 | 4.105 x $10^{-2}$ |
| 10.7 | 4.891 x $10^{-2}$ |
| 20.0 | 4.103 x $10^{-2}$ |

Table 7.4: Case 2 - Final mass residual for each turbidity case

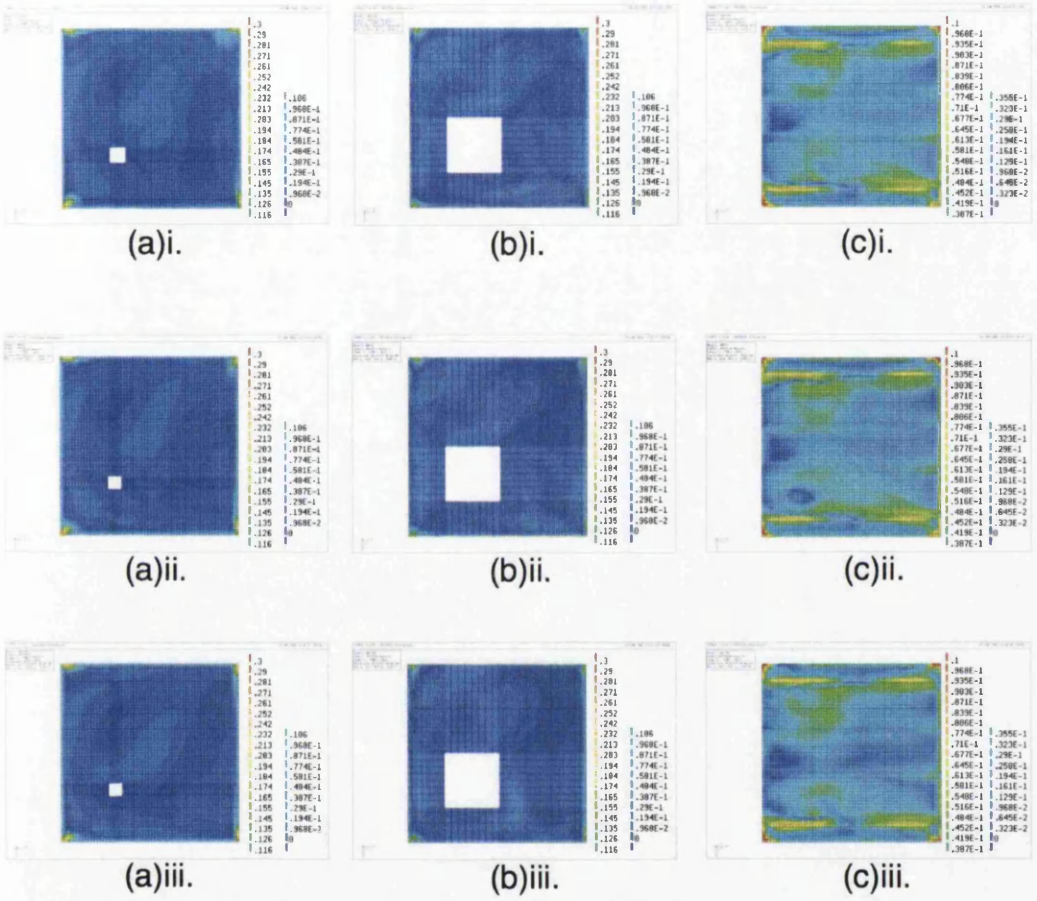


Figure 7.6: Invariant resultant velocity for Case 1 - Levels of tank: (a) 2 m below surface of sludge blanket, (b) top surface of sludge blanket, (c) bottom of troughs; turbidity: (i) 5.2 NTU, (ii) 10.7 NTU, (iii) 20.0 NTU.

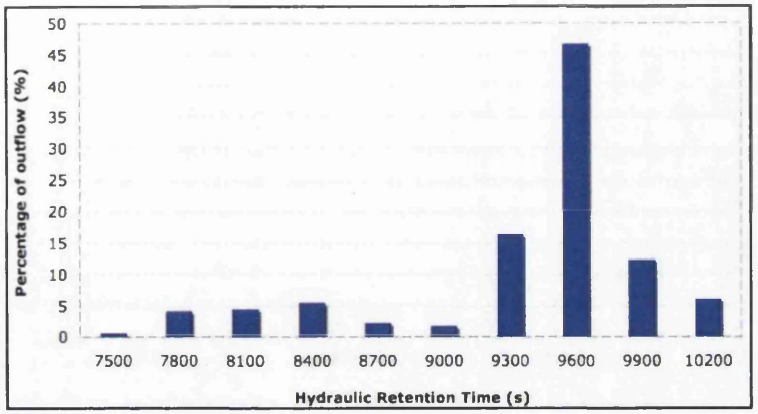


(a)

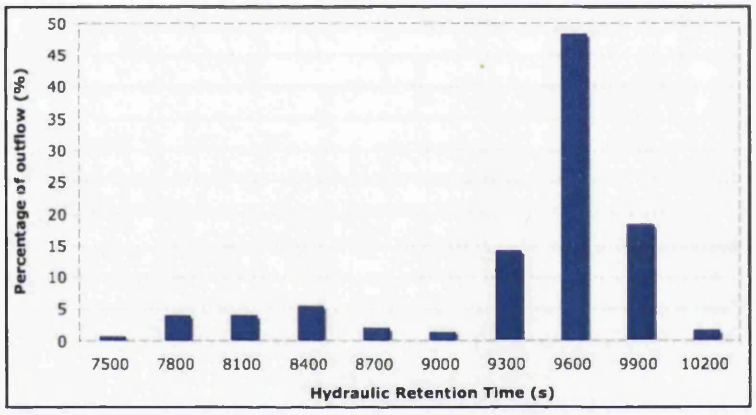


(b)

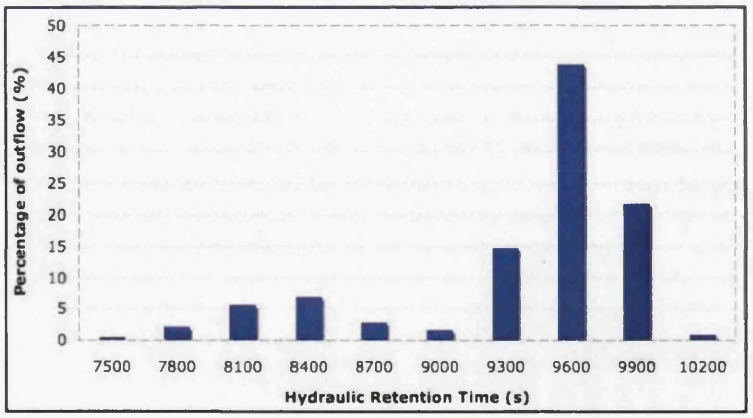


(c)

Figure 7.7: Case 1 - Charts of hydraulic retention time for (a) 5.2 NTU, (b) 10.7 NTU, and (c) 20.0 NTU

Figure 7.8 presents the contour plots of the resultant velocity for three cross-sections of the UFC tank. The charts for the HRT of the simulations are shown in Figure 7.9.

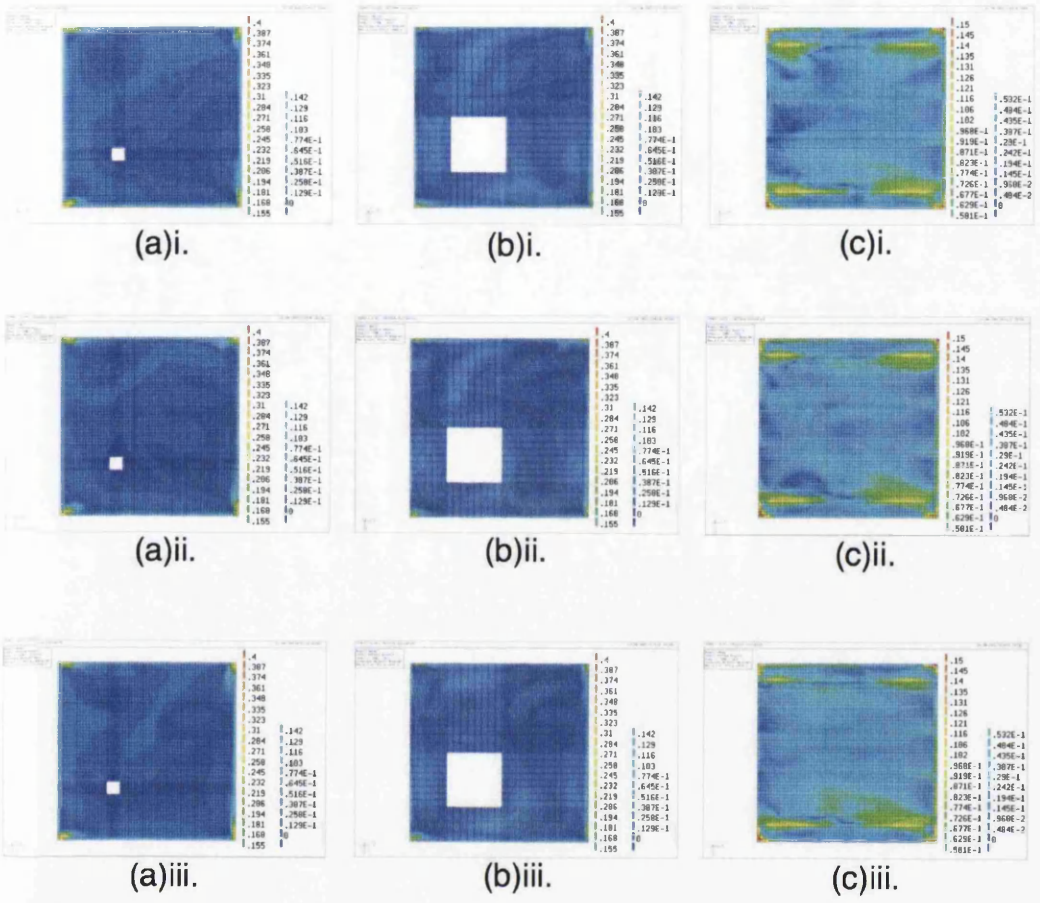


Figure 7.8: Invariant resultant velocity for Case 2 - Levels of tank: (a) 2 m below surface of sludge blanket, (b) top surface of sludge blanket, (c) bottom of troughs; turbidity: (i) 5.2 NTU, (ii) 10.7 NTU, (iii) 20.0 NTU.

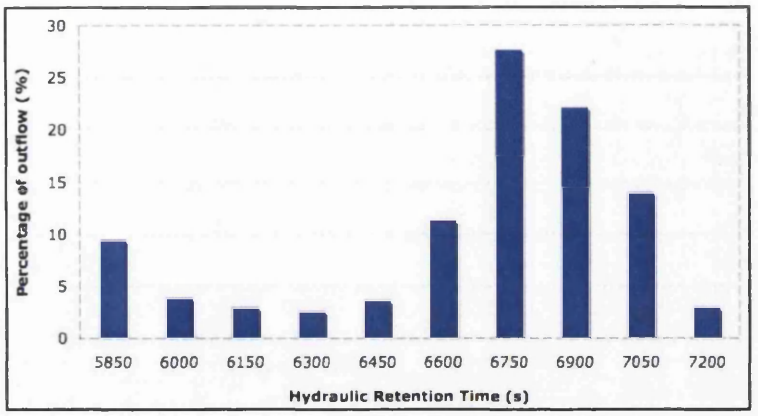


(a)

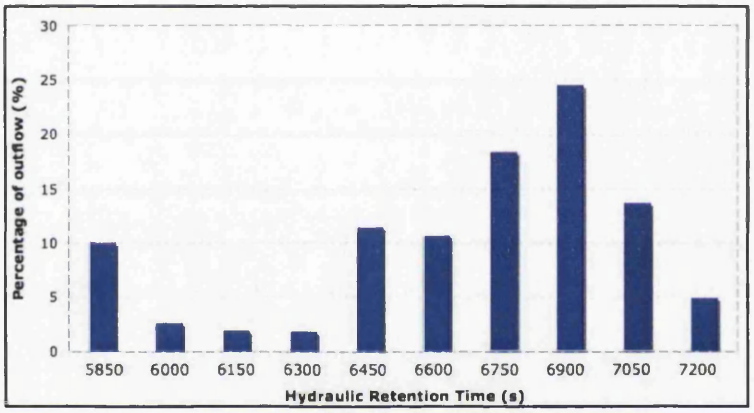


(b)

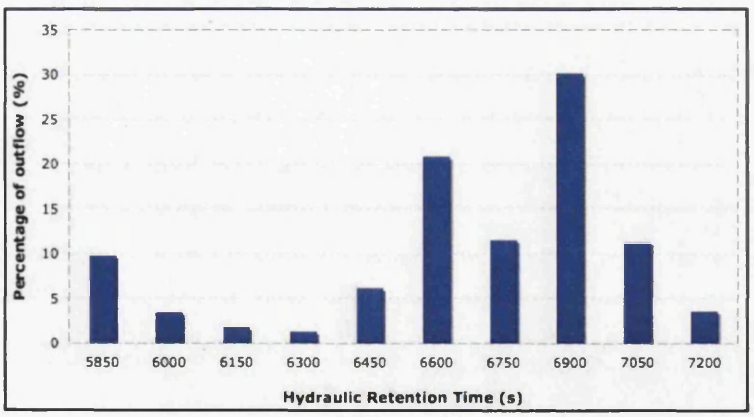


(c)

Figure 7.9: Case 2 - Charts of hydraulic retention time for (a) 5.2 NTU, (b) 10.7 NTU, and (c) 20.0 NTU

### 7.4.3 Case 3 - Flow Rate 0.058 $m^3s^{-1}$

For this case, the downward flow velocity at the inlet is 1.4035 $ms^{-1}$. The initial mass residual 5.790 x $10^1$ and the simulations were run for 15250 iterations with a false timestep of 0.01. The resulting final mass residual for the simulations are tabulated below in Table 7.6.

| Turbidity (NTU) | Final Mass Residual |
|---|---|
| 5.2 | 2.811 x $10^{-2}$ |
| 10.7 | 2.741 x $10^{-2}$ |
| 20.0 | 1.599 x $10^{-2}$ |

Table 7.5: Case 3 - Final mass residual for each turbidity case

Results of the resultant velocity contour plots are as shown in Figure 7.10. The bar charts of the HRT of these simulations are presented in Figure 7.11.

### 7.4.4 Case 4 - Flow Rate 0.077 $m^3s^{-1}$

The velocity of the inflow of this case is 1.871 $ms^{-1}$. The initial mass residual for all the simulations were ar 7.718 x $10^1$. They were run for 13750 iterations with false timestep of 0.01 and the final mass residuals for each simulation are tabulated in Table 7.6.

Figure 7.12 presents the contour plots of the resultant velocity at different cross-sections of the tank and the HRT of each simulation are presented in bar charts in Figure 7.13.

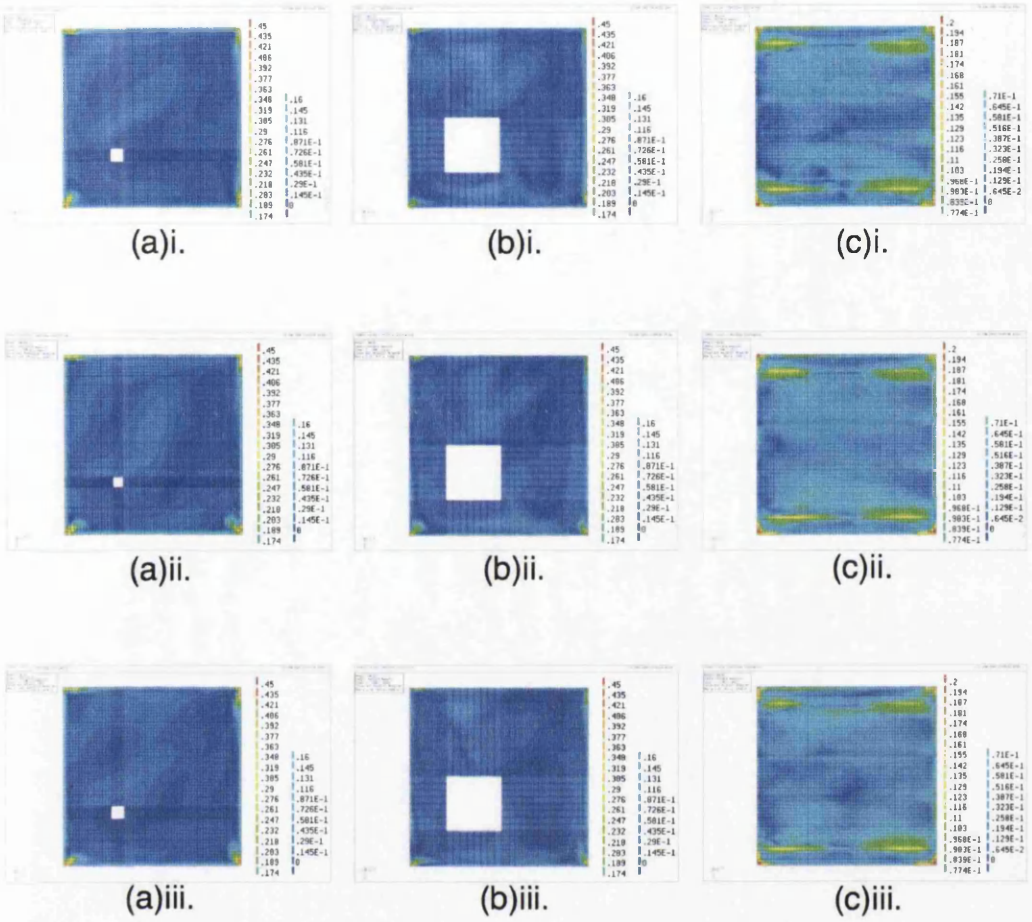


Figure 7.10: Invariant resultant velocity for Case 3 - Levels of tank: (a) 2 m below surface of sludge blanket, (b) top surface of sludge blanket, (c) bottom of troughs; turbidity: (i) 5.2 NTU, (ii) 10.7 NTU, (iii) 20.0 NTU.

| Turbidity (NTU) | Final Mass Residual |
|---|---|
| 5.2 | $4.670 \times 10^{-2}$ |
| 10.7 | $6.509 \times 10^{-2}$ |
| 20.0 | $4.687 \times 10^{-2}$ |

Table 7.6: Case 4 - Final mass residual for each turbidity case

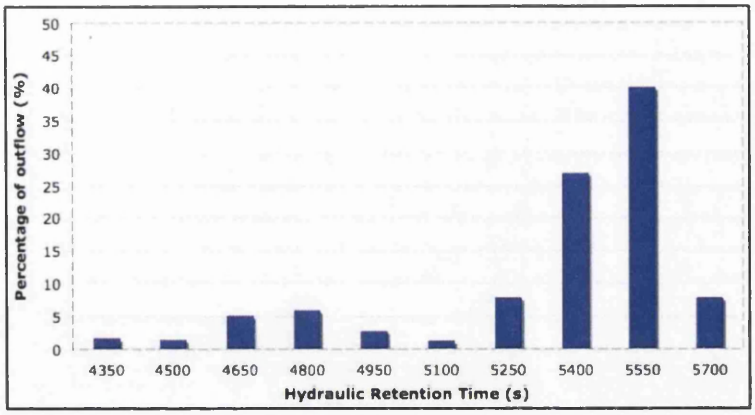


(a)

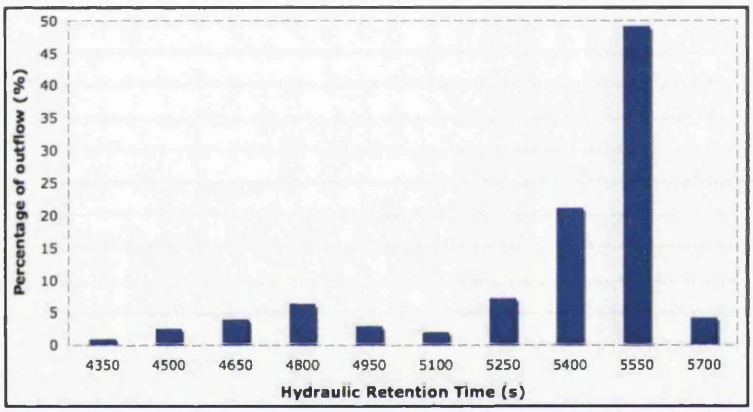


(b)

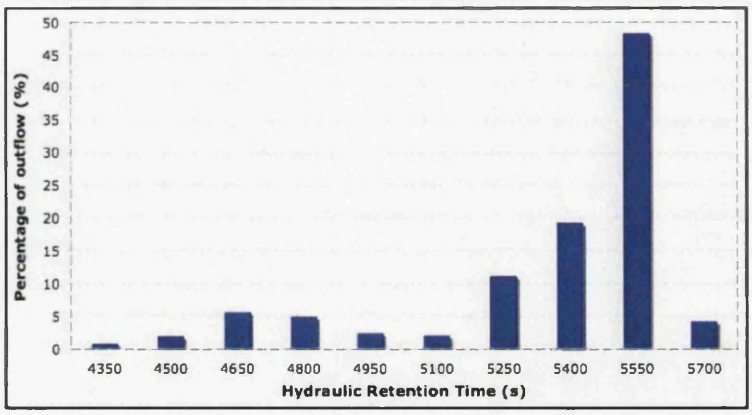


(c)

Figure 7.11: Case 3 - Charts of hydraulic retention time for (a) 5.2 NTU, (b) 10.7 NTU, and (c) 20.0 NTU

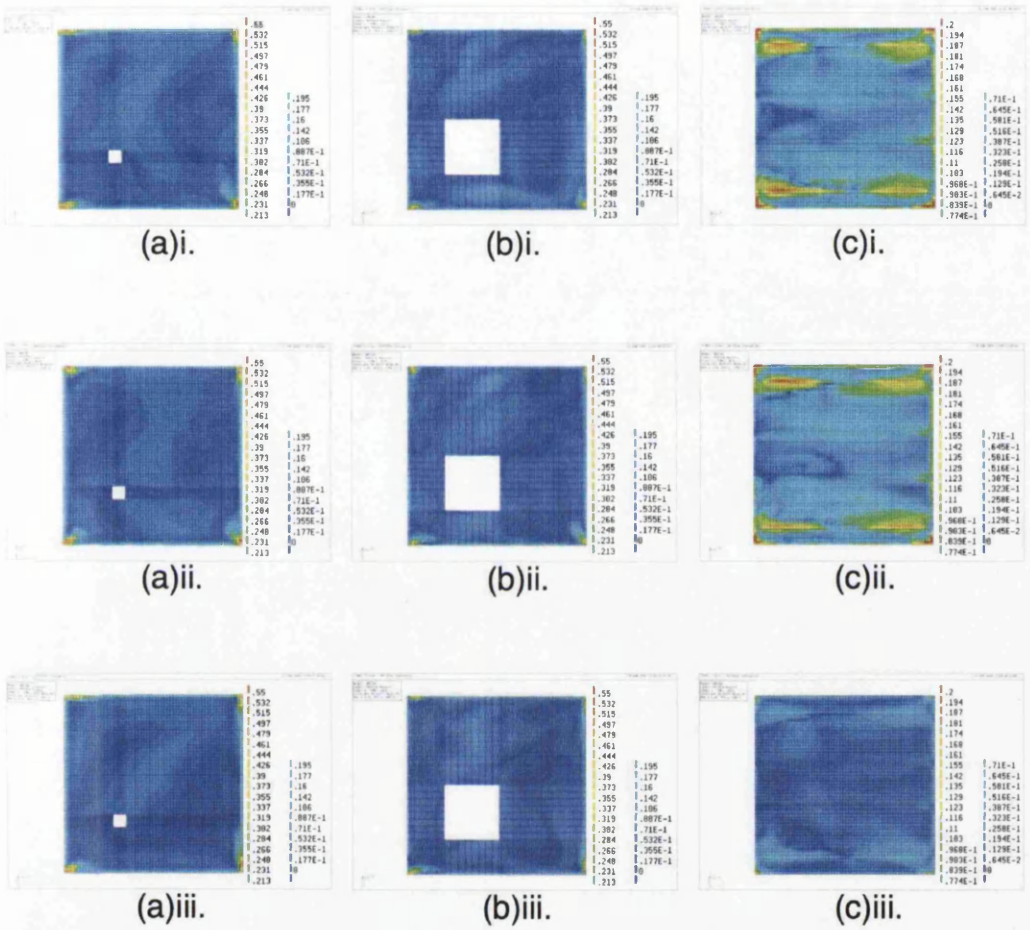


Figure 7.12: Invariant resultant velocity for Case 4 - Levels of tank: (a) 2 m below surface of sludge blanket, (b) top surface of sludge blanket, (c) bottom of troughs; turbidity: (i) 5.2 NTU, (ii) 10.7 NTU, (iii) 20.0 NTU.

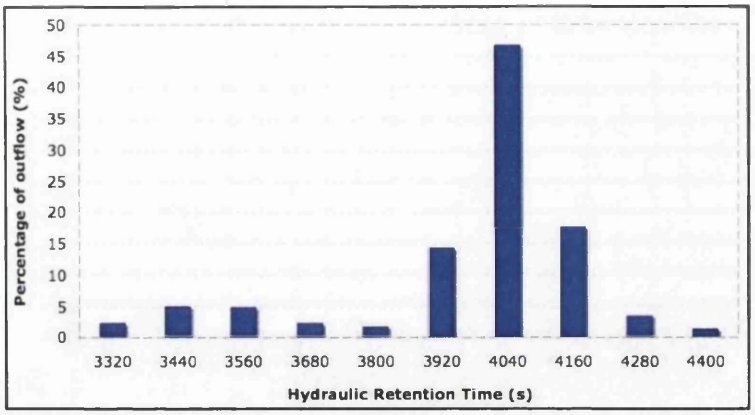


(a)

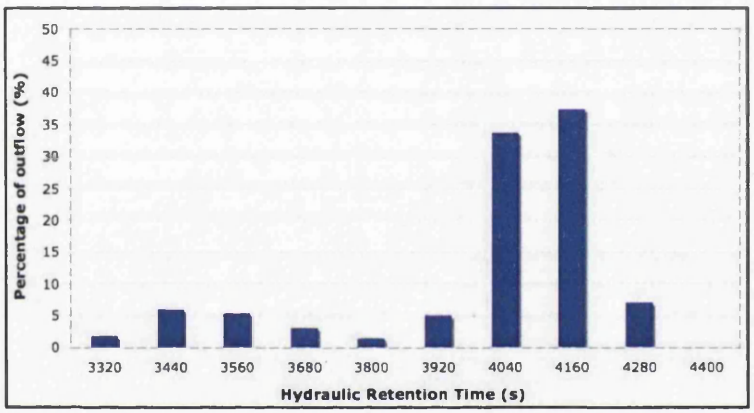


(b)

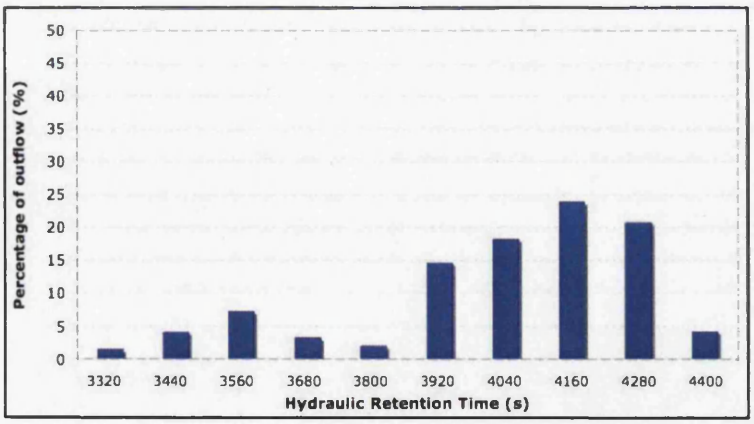


(c)

Figure 7.13: Case 4 - Charts of hydraulic retention time for (a) 5.2 NTU, (b) 10.7 NTU, and (c) 20.0 NTU

### 7.4.5 Case 5 - Flow Rate 0.117 $m^3s^{-1}$

For this case the corresponding velocity at the inlet is 2.807 $ms^{-1}$. The simulations started with mass residual of 1.157 x $10^2$ and were run for 13250 number of iterations with a false timestep of 0.01. The final mass residuals for each simulation are listed in Table 7.7.

| Turbidity (NTU) | Final Mass Residual |
|---|---|
| 5.2 | 1.082 x $10^{-1}$ |
| 10.7 | 1.986 x $10^{-1}$ |
| 20.0 | 1.397 x $10^{-1}$ |

Table 7.7: Case 5 - Final mass residual for each turbidity case

The contour plots for the resultant velocity of the simulations are presented in Figure 7.14. The chart representation of the HRT for all simulations are as shown in Figure 7.15.

## 7.5 Discussions

The contour plots of all the cases show some similarities in the flow pattern for all turbidities. The streaming of flow can be observed at the four corners of the tank at all the three levels of the tank. The area of this occurrence is reduced as the avereage velocity through the section decreases, i.e. at the surface of the sludge blanket. Near the outlet, although the flow is at its lowest speed, some streaming occurs along the length of the troughs, at the side of the tank. The flow at the corners of the tank is

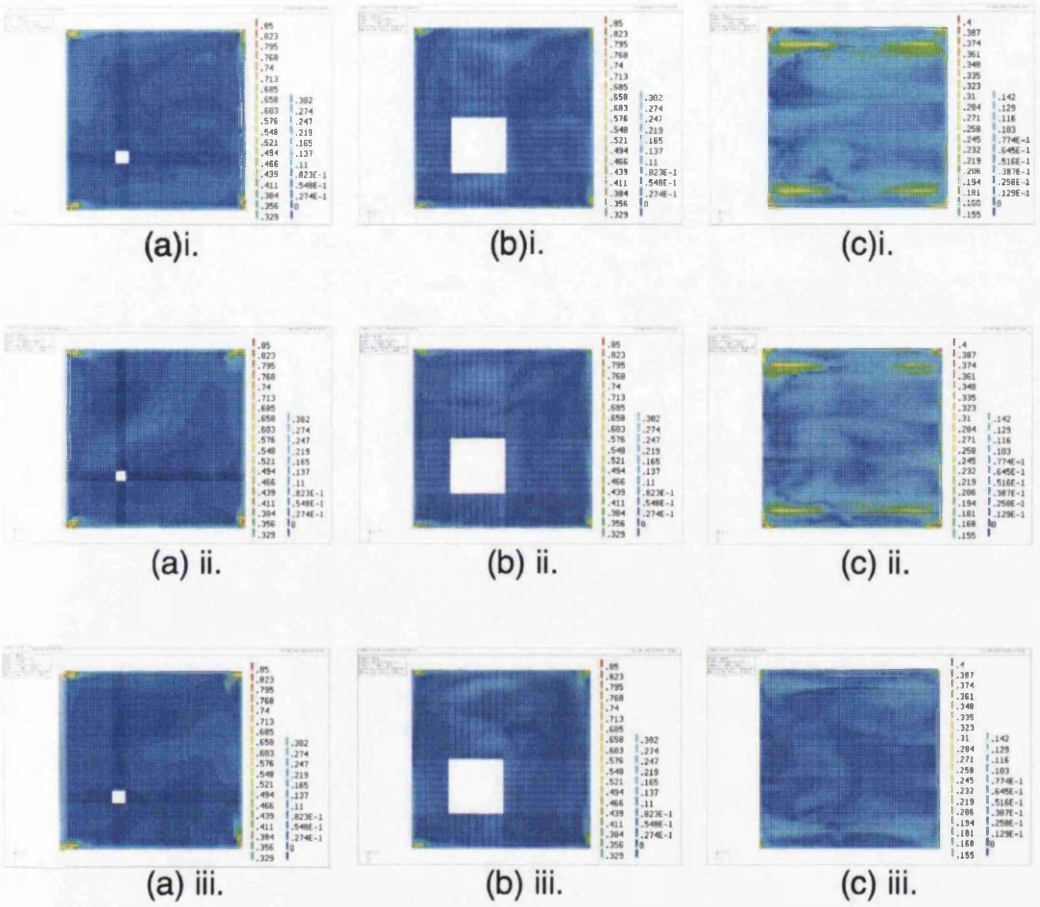


Figure 7.14: Invariant resultant velocity for Case 5 - Levels of tank: (a) 2 m below surface of sludge blanket, (b) top surface of sludge blanket, (c) bottom of troughs; turbidity: (i) 5.2 NTU, (ii) 10.7 NTU, (iii) 20.0 NTU.

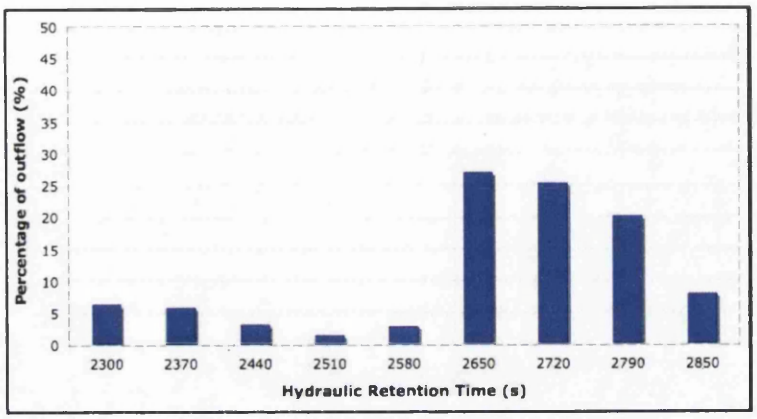


(a)

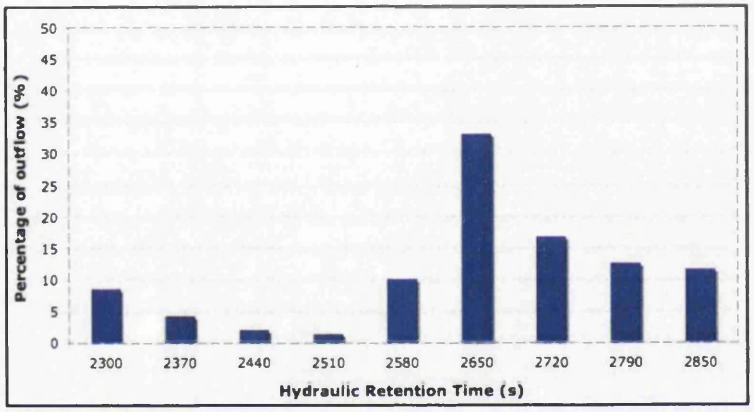


(b)

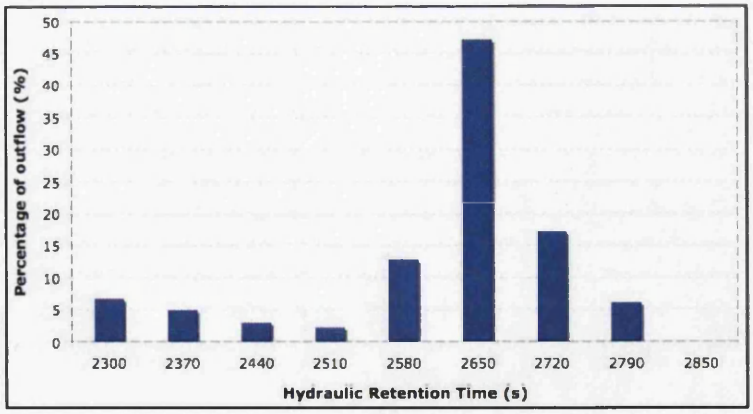


(c)

Figure 7.15: Case 5 - Charts of hydraulic retention time for (a) 5.2 NTU, (b) 10.7 NTU, and (c) 20.0 NTU

still the fastest at this level.

As the turbidity of the inflow increases, the streaming of flow can be seen to decrease, especially for the flow just under the troughs. The area of very slow flow is less for inflow with higher turbidity and this is more evident for cases with high flow rate.

The charts of HRT of Case 1 in Figure 7.7 show that almost half of the outflow has the HRT of between 9600 s to 9900 s. As the turbidity of the inflow increases, so does the percentage of the outflow that has HRT of above this range.

As for Case 2, in Figure 7.9, the charts show that the HRT for about 10% of the outflow lies in the range of 5850 s to 6000 s. The amount of flow that has HRT of between 6900 s to 7050 s increases as the turbidity of the inflow increases, while the percentage of flow with HRT of 6750 s to 6900 s decreases.

The charts for Case 3 presented in Figure 7.11 show a similar pattern of that of Case 2. As the turbidity of the inflow increases, the percentage of outflow that has the HRT of 5550 s to 5700 s increases but those that has a lower HRT that lies in the range of 4650 s to 4950 s decreases.

The HRT for UFC of Case 4 settings vary more compared to cases of lower flow rates. From the chart (a) shown in Figure 7.13, almost half of the outflow has the HRT of between 4040 s to 4160 s. This decreases as the turbidity of the inflow increases as the percentage of outflow that has the HRT of higher than this range increases. The amount of flow that has low HRT, which is between 3440 s and 3680 s also increases with the the tubidity of the inflow.

The percentage of outflow that has HRT higher than 2720 s in for Case 5 simulations decreases as the turbidity of the inflow increases, as shown in Figure 7.15. With the decrease, the amount of flow that has HRT of between 2650 s and 2720 s increases.

## 7.6 Conclusions

In this section, the three-dimensional model of the UFC presented in 6 is referred to as Model 1 and Model 2 represents the three-dimensional model of UFC presented in this chapter. This is to provide a clearer explanation when comparing the results obtained from the simulations of both models.

The simulations of Model 2 have produced a different results of flow pattern when compared to the results of the simulations of Model 1. This can be observed from the contour plots obtained from the simulation of both models, where Model 1 has flow streaming around the desludging cone, except for the simulations of Case 5. However, the contour plot results of Model 2 show that the streaming of flow at the corners of the tank is more significant.

Another difference in the results is that the magnitude of the resultant flow through the tank of Model 2 is higher than that predicted in the previous investigation. This is true for all the cases and at the three different levels of observation. The comparison of the magnitude of flow at the three different levels are presented in Table 7.8, Table 7.9 and Table 7.10.

The difference in the magnitude, albeit having the same flow rate is due to the difference in the viscosity of the sludge blanket in the two models. With Model 1, the viscosity of the imposed blanket is 1.0 x $10^{-3}$ $m^2s^{-1}$, which is nearly a thousand times higher than that of Model 2, which ranges from the viscosity of water up to 1.008 x $10^{-6}$ $m^2s^{-1}$, as evaluated from the equation 7.3. The high viscosity of the sludge blanket in Model 1 contributes a greater resistance to flow, causing the speed of flow to be much lower than that found in Model 1. The big difference in the viscosity of the fluid in the region of the sludge blanket may also be the cause of the different flow pattern in Model 1, as it has a different flow profile near the walls.

| Case | Model 1 ($ms^{-1}$) | Model 2 ($ms^{-1}$) |
|---|---|---|
| 1 | 0.0015 | 0.30 |
| 2 | 0.0050 | 0.40 |
| 3 | 0.0200 | 0.45 |
| 4 | 0.4000 | 0.55 |
| 5 | 0.6000 | 0.85 |

Table 7.8: Highest velocity of the resultant velocity at 2 m below the top of sludge blanket.

From the simulations of flow presented in this study, the HRT calculated for each of them have shown that the HRT of a UFC tank is a distribution. The HRT charts for all cases in this study show that there is a huge portion of the domain that has the HRT of the same range. This range lies in near the high end of the full range of HRT calculated for the outflow.

| Case | Model 1 ($ms^{-1}$) | Model 2 ($ms^{-1}$) |
|---|---|---|
| 1 | 0.0003 | 0.20 |
| 2 | 0.0004 | 0.25 |
| 3 | 0.0020 | 0.35 |
| 4 | 0.0055 | 0.45 |
| 5 | 0.5000 | 0.70 |

Table 7.9: Highest velocity of the resultant velocity at the top of sludge blanket.

The regions of the outflow where the HRT is lower are associated with flow that has streamed through the tank. These lower values are associated with the regions at the corners of the tank, where water flows through the tank at a higher speed. On average, the HRT for this portion of the outflow is about 15% to 20% lower than the HRT of most of the outflow. While this may seem insignificant for cases with high flow rates, considering Case 1, which is operating flow rate of Littleton Treatment Works, the difference in residence time is 1200 s or 20 minutes.

The streaming of flow at the corners of the tank may be the evidence of the lack of stability of the sludge blanket in those areas. This is because the higher speed of flow could disrupt the sludge blanket and thus carry over the flocs to the outlet. The lower HRT of this portion of flow also may affect the overall quality of the clarified water as the shorter residence time means shorter contact time within the sludge blanket for the clarifying process.

The HRT profiles obtained from this study are used in the next chapter to demon-

| Case | Model 1 ($ms^{-1}$) | Model 2 ($ms^{-1}$) |
|---|---|---|
| 1 | 0.00010 | 0.10 |
| 2 | 0.00025 | 0.15 |
| 3 | 0.00070 | 0.20 |
| 4 | 0.00250 | 0.20 |
| 5 | 0.30000 | 0.40 |

Table 7.10: Highest velocity of the resultant velocity at the outlet (Model 1) and under the troughs (Model 2).

strate the effect of incorporating the CFD findings of the UFC model into the process model in OTTER.

# Chapter 8

# Coupling of OTTER and CFD

This chapter presents the implementation of the coupling of the modelling abilities of both CFD and OTTER. The main goal of this work is to investigate the effect of integrating the analysis of HRT profile obtained from CFD simulations of the HBC into OTTER on the simulation results that OTTER produced. The HRT of HBC for different flow and water quality settings are obtained from the CFD modelling work presented in the previous chapter.

At this stage, the scope of this research only extends to the testing the effect of the integrating the results of CFD analysis into OTTER without changing the source code of OTTER. Hence, the HRT determined by the CFD analysis needs to be conveyed to the HBC model in OTTER through the user interface. A simple method used in this study to achieve this is explained in the following section.

## 8.1 Methodology

For every simulation case, two OTTER simulations are done. One with a HBC model that has the same dimensions as the real HBC tank, and the other, with a HBC model built based on the specified HRT. For the latter, the details are explained later in this section.

The results of these two simulations, specifically the turbidity of the clarified water, were compared to observe the difference in the results obtained. The effect of the coupling of the CFD analysis and the OTTER simulation of the clarification process was then investigated.

The treatment works model built on OTTER for the purpose of this study only consists of a raw water source, a pump, a coagulator, followed by a HBC. This is illustrated in Figure 8.1 below. No other treatment process tank was included in the works model so that only the quality of clarified water would be predicted, thus saving time.

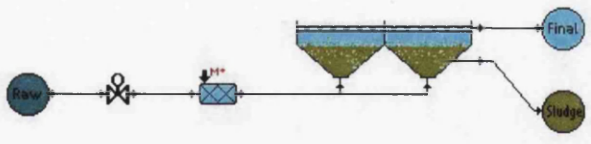


Figure 8.1: Works model built in OTTER to compare turbidity of clarified water.

### 8.1.1 Computing the Height of the Hopper Section

The solids removal model simulated in OTTER is a time dependent process. In order to translate the HRT of the HBC found from the CFD analysis, the average of the HRT of the HBC is used to determine the height of the hopper section of the HBC tank model built in OTTER. This is because the solids removal process is only simulated at this section of the tank. The height of the hopper section of the tank affects the residence time of the flow within the sludge blanket. Hence, this allows the clarification process simulated to be run for the length of the specified retention time.

The rest of the tank dimensions are kept constant, but the height of the troughs is neglected. The width of the tank are kept the same so that the cross-sectional area for the flow in both models are the same.The slowest flow through the tank occurs at the upper section of the tank, which is the section just above the sludge blanket where the walls are straight-sided. The flow in this section is assumed to be uniform due to the small variation in flow across the area.

As mentioned before, the hydraulics of the HBC model in OTTER is characterised by the number of CSTR model of the solids removal equation. The higher the number of CSTR, the more the flow through the tank behaves like a plug flow. For the purpose of this study, the number of CSTR used is five, which is the default value. Having a near plug flow, ensures that the HRT of the tank is basically the volume of the inflow divided by the flow rate of the tank.

The volume of the tank that has the average HRT as found from the CFD analysis

is simply the product of the flow rate and the average HRT. Deducting the volume of the upper section of the tank, which has the dimensions of 1.234 m x 8.23 m x 8.23 m, this gives the volume of the hopper section of the tank.

The volume of the hopper section, $V_{hopper}$ is given by the equation [39]:

$$V_{hopper} = \frac{h_i}{3}\left[\frac{z_0^3}{z_0 - z_i} - \frac{z_i^2 z_0}{z_0 - z_i} + z_i^2\right] \tag{8.1}$$

where $V_{hopper}$ is the volume of the hopper section of HBC, $z_0$ is the width of the top of HBC, $z_i$ is the width of the base of HBC.

From the equation above, the height of the hopper section of the tank with the desired HRT is evaluated.

The desludging of the sludge blanket is set to be intermittent, so as to ensure that the sludge blanket in the model is always stable.

## 8.2 Simulation Cases and Results

This investigation was executed on four cases, Case 1 to Case 4. This could not be done on Case 5 due to the very high upflow through the tank that disrupts the stability of the sludge blanket. The speed of the upflow in Case 5 causes carryover of the sludge blanket. When the simulation of Case 5 was attempted, even with the highest desludging rate allowed in OTTER, a stable sludge blanket could not be achieved.

In this investigation, the results of Case 1 are compared with the real data, as its

| Inflow Turbidity (NTU) | Average HRT (s) | Height of hopper section of tank (m) | Outflow Turbidity (before coupling) (NTU) | Outflow Turbidity (after coupling) (NTU) |
|---|---|---|---|---|
| 5.2 | 9255 | 8.70 | 0.80 | 0.53 |
| 10.7 | 9234 | 8.72 | 1.36 | 0.89 |
| 20.0 | 9235 | 8.72 | 1.76 | 1.17 |

Table 8.1: Case 1 - Details of HBC model in OTTER and predicted results before and after coupling.

flow rate setting is that of the operating flow rate in Littleton Treatment Works.

### 8.2.1 Case 1 - Flow Rate 0.033 $m^3s-1$

The detail of the the HBC model built in OTTER for this case is tabulated in Table 8.1 together with the results of the simulation.

#### 8.2.1.1 Validation of the CFD Model

A direct validation of the CFD model of the HBC is unfortunately not possible at the time of the study. This is due to the lack of equipment available and time constraints. However, PHYSICA is a CFD software package that has been validated for many of their analysis in simulating flow. Given that the calibration of the model is correct, a good simulation can be achieved.

| Inflow Turbidity (NTU) | Outflow Turbidity (OTTER) (NTU) | Outflow Turbidity (real data) (NTU) |
|---|---|---|
| 5.2 | 0.53 | 0.48 |
| 10.7 | 0.89 | 0.41 |
| 20.0 | 1.17 | 0.44 |

Table 8.2: Comparison of predicted turbidity of clarifier water with real data.

In this study, the model, is therefore, indirectly validated. This is done by comparing the results of the turbidity of the clarified water obtained from the OTTER simulation, with the coupling effect. The comparison, however, only serves the purpose of justifying the coupling effect. It could not be strictly done due to the restrictions of disclosing the type and dosage of the polyelectrolyte used in Littleton Treatment Works. The amount of polyelectrolyte dose also varies with the inflow turbidity and coagulant dose, where the chemical doses are increased if the turbidity of the inflow increases. This is to ensure that the turbidity of clarified water does not exceed a certain standard value.

The predicted turbidity of the clarified water from the OTTER simulation is compared to the average turbidity of clarified water of the real data for each inflow turbidity used in this study. The average value of the real data was used because there is some fluctuations in the data given. The comparison is shown in Table 8.2.

The predicted results for the simulation with inflow turbidity of 5.2 NTU is the nearest to the real data. With the increase in the turbidity in the inflow, the results obtained from OTTER simulation also show an increase in the turbidity of the clarified

water. However, with the increase in the dose of polyelectrolyte, the real data shows that the solids removal have increased when the raw water quality deteriorates, resulting in lower turbidities of clarified water.

Although these results cannot be strictly compared due to the constraints in calibrating the model, a significant change can be seen from the results predicted by the HBC model in OTTER after the coupling. The simulation of the clarification process of the HBC in Littleton by OTTER underestimates the performance of the HBC. This could be probably due to the lack of information to fully calibrate the model and the weaknesses of the model. However, the coupling of the findings from the CFD analysis with the OTTER simulation of the HBC have shown an effect on the results, giving a closer prediction to the real data.

### 8.2.2 Case 2 - Flow Rate 0.046 $m^3s-1$

The details of the HBC model built for this case in OTTER are tabulated in Table 8.3. The results of the OTTER simulation before and after the coupling, for this case is also presented in the same table below.

### 8.2.3 Case 3 - Flow Rate 0.058 $m^3s-1$

For this case, the details of the HBC model in OTTER and the predicted results for simulations of both before and after the coupling is listed in Table 8.4.

| Inflow Turbidity (NTU) | Average HRT (s) | Height of hopper section of tank (m) | Outflow Turbidity (before coupling) (NTU) | Outflow Turbidity (after coupling) (NTU) |
|---|---|---|---|---|
| 5.2 | 6577 | 8.69 | 2.53 | 2.31 |
| 10.7 | 6579 | 8.69 | 3.19 | 2.81 |
| 20.0 | 6573 | 8.68 | 3.85 | 3.31 |

Table 8.3: Case 2 - Details of HBC model in OTTER and predicted results before and after coupling.

| Inflow Turbidity (NTU) | Average HRT (s) | Height of hopper section of tank (m) | Outflow Turbidity (before coupling) (NTU) | Outflow Turbidity (after coupling) (NTU) |
|---|---|---|---|---|
| 5.2 | 5279 | 8.72 | 2.67 | 2.27 |
| 10.7 | 5284 | 8.74 | 3.67 | 2.97 |
| 20.0 | 5280 | 8.73 | 3.90 | 3.64 |

Table 8.4: Case 3 - Details of HBC model in OTTER and predicted results before and after coupling.

| Inflow Turbidity (NTU) | Average HRT (s) | Height of hopper section of tank (m) | Outflow Turbidity (before coupling) (NTU) | Outflow Turbidity (after coupling) (NTU) |
|---|---|---|---|---|
| 5.2 | 3920 | 8.60 | 3.61 | 2.93 |
| 10.7 | 3948 | 8.68 | 5.40 | 4.22 |
| 20.0 | 3968 | 8.75 | 7.26 | 3.93 |

Table 8.5: Case 4 - Details of HBC model in OTTER and predicted results before and after coupling.

### 8.2.4 Case 4 - Flow Rate 0.077 $m^3s-1$

Table 8.5 lists the details of the HBC model in OTTER built for the simulation of this case. Results of the prediction of the clarified water before and after the coupling are also presented.

## 8.3 Discussions and Conclusions

The results presented for all cases have shown that the coupling of the findings of CFD with the HBC model in OTTER predict that the performance of the HBC is better, as the predicted turbidity of the outflow is lower than that predicted by OTTER before coupling. The percentage of reduction in the predicted turbidity of the clarified water is listed in Table 8.6.

The better performance of the clarification process predicted by OTTER after cou-

| Case | Inflow Turbidity (NTU) | Outflow Turbidity (before coupling) (NTU) | Outflow Turbidity (after coupling) (NTU) | Percentage of reduction (%) |
|---|---|---|---|---|
| 1 | 5.2 | 0.80 | 0.53 | 67.5 |
| | 10.7 | 1.36 | 0.89 | 34.6 |
| | 20.0 | 1.76 | 1.17 | 33.5 |
| 2 | 5.2 | 2.53 | 2.31 | 8.7 |
| | 10.7 | 3.19 | 2.81 | 11.9 |
| | 20.0 | 3.85 | 3.31 | 14.2 |
| 3 | 5.2 | 2.67 | 2.27 | 15.0 |
| | 10.7 | 3.67 | 2.97 | 19.1 |
| | 20.0 | 3.90 | 3.64 | 6.9 |
| 4 | 5.2 | 3.61 | 2.93 | 18.8 |
| | 10.7 | 5.40 | 4.22 | 22.2 |
| | 20.0 | 7.26 | 3.93 | 45.9 |

Table 8.6: Comparison and percentage of difference in turbidity of clarifier water before and after coupling.

pling is due to the higher contact time of the flow through the sludge blanket. The effect of the coupling varies as the flow rate and quality of the inflow vary, in no particular trend. The effect is particularly high, with at least a third in reduction of turbidity for Case 1.

The comparison of the results of Case 1 with real data show that it is only when the turbidity of the inflow is low that the predicted results come close. This is possibly due to the change in the polyelectrolyte dose made by the operators in Littleton Treatment Works whenever there is a rise in the raw water turbidity. For raw water with higher turbidity, higher polyelectrolyte dose is provided in order to improve the removal of solids during the clarification process. Because only the type of polyelectrolyte can be specified and not its dosage, when using OTTER, the amount of polyelectrolyte that is taken into account in a simulation may differ from that used in Littleton.

The results predicted from OTTER simulations without coupling, as can be seen from this work show that OTTER under predicts the performance of the HBC process as clearly shown in Case 1. This does not only highlight the significance of the consideration of the HRT in process simulators, but also the lack of accuracy could lead to over designing of real process tank in practice, that leads to an increase in construction and operating costs.

Results of this study demonstrates that with the consideration of the HRT of the HBC obtained from the CFD analysis of the model, gives a different prediction of the clarification process. The lack of accuracy of the simulation may be due to several reasons. As mentioned earlier in the thesis, the HBC model simulator has been ac-

knowledged to be needing improvement [1] and the CSTR model of the clarification process had only been validated with a flat-bottomed clarifier [30]. Further more, the coupling work at this stage is not thorough.

Although the comparison of the outflow turbidity shows that it is encouraging, the average HRT found from the CFD analysis is inconsistent with what was initially expected at the beginning of the research. The higher HRT given by the CFD analysis of the HBC model denotes that the tank has a higher effective volume than that calculated in OTTER.

The reason for this is uncertain, but it could possibly due to the difference in the way the volume of water contained in the HBC model. The CFD model of the HBC imitates the damping of the flow of water through the sludge by assigning a higher viscosity, having no effect on the volume of water. OTTER, on the other hand is able to evaluate the volume of water in the sludge blanket from the solids concentration of the blanket.

Another possible reason to this is that the CFD model does not simulate the desludging of the sludge blanket. Desludging of the sludge blanket would mean that some of the flow in the tank exits to the cone, reducing the amount of outflow through the tank. The reduction in the amount of flow thus will lead to faster outflow.

With this finding, despite the effect of the coupling appearing to be positive, further investigation on the reliability of the CFD model of the HBC is therefore still needed.

# Chapter 9

# Conclusions and Future Work

## 9.1 Conclusions

The course of this research started off by exploring the two modelling tools used in this study, OTTER and CFD analysis with the use of the PHYSICA package. Two out of several of the shortcomings found in OTTER, specifically the UFC model are that the simulation of the clarification process was only tested for flat-bottomed clarifier and the hydraulics of the tank is simply represented by the CSTR model. As for CFD modelling of the HBC, although the usage of this tool has been widely used since 1995 in modelling water treatment processes [22], no published work was found to have applied CFD in modelling the HBC process tank.

The capability of CFD modelling was explored with some initial modelling of a

simple tank with different internal designs. Results of the simulations have shown that the flow pattern determines the HRT of the tank, and flow simulation through a tank can be used to calculate the HRT of the tank. The work was then carried on to model the HBC tank, based on a operating HBC tank in Littleton Treatment Works of Bristol Water. The model was built stage by stage and covers a large section in this research.

The CFD model of the HBC used in this research does not simulate the complex mechanism of the flocculation and clarification process within the HBC tank. The sludge blanket is represented by the mass balance equation of the rate of solids removal in the sludge blanket that is used in OTTER to simulate the clarification process that takes place within the sludge blanket. The employment of this equation has simplified the model to enable a quick evaluation of the viscosity of the sludge blanket at different levels. This has hence, allow a close approximation to the flow through the tank and thus the calculation of the HRT.

The coupling of the abilities of the two modelling tools was done in a simplistic way as it was restricted to be done on the user interface. With the obtained results from the CFD analysis, which in this case, is the HRT of the HBC tank, it was used as the design retention time for the UFC tank built in OTTER. Results from the simulation of the HBC process tank in OTTER with and without the coupling work was compared. This has demonstrated the effect of the coupling of the results from both modelling tools. The results of the coupling investigation was also compared with real data.

This research has shown that the predicted performances of the HBC at different conditions, with and without coupling, are significantly different. The results of this

investigation have shown that the prediction after the coupling gives a closer results to the available real data. It has shown that OTTER under predicts the performance of the clarifier. This is important to know as it leads to over designing of tanks. It will also leads to over-dosing of chemicals, e.g. coagulant, and both of these consequences results in the undesirable higher costs.

Moreover, the expectation from the users of process treatment simulators has been raised [1]. Process models are now expected to be highly accurate. A more accurate model is able to provide better insights into the process, especially for training purposes, which is what OTTER is mostly used for.

The modelling of HBC with CFD, although has been attempted [25], has not been published and therefore the details of the findings and modelling settings are not known. The work of incorporating the findings of CFD analysis with a process model has not been knowingly done to this date.

## 9.2 Future Work Suggestions

Clearly, there is still much work needed to enhance the ability of simulating the HBC process tank in OTTER. Following the encouraging finding outlined in this thesis, future work can include the information of the HRT into the source code of the OTTER software. With the established use of the CFD modelling in other treatment processes, the information of the HRT of these processes can also be used in developing OTTER.

Due to the high computational costs of CFD modelling, this can be done for a few variations of the generic designs of process tank for different flow rates. The relationships of flow rate and the tank sizes can then be derived and used as an input into the codings of OTTER.

As for the CFD model of the HBC, the encouraging development in the modelling of the other types of clarifiers in the water treatment provides a positive lead for its development. For example, the model can be incorporated with solids population balance and turbulence model, which are currently already used in the application of clarifiers in sewage water treatment.

Like other CFD work that has been done, the HBC model also can be used for design purposes. Modification or additional design to the process tank can be tested to observe the effect that it has on the flow pattern.

# Appendix A

# Appendix

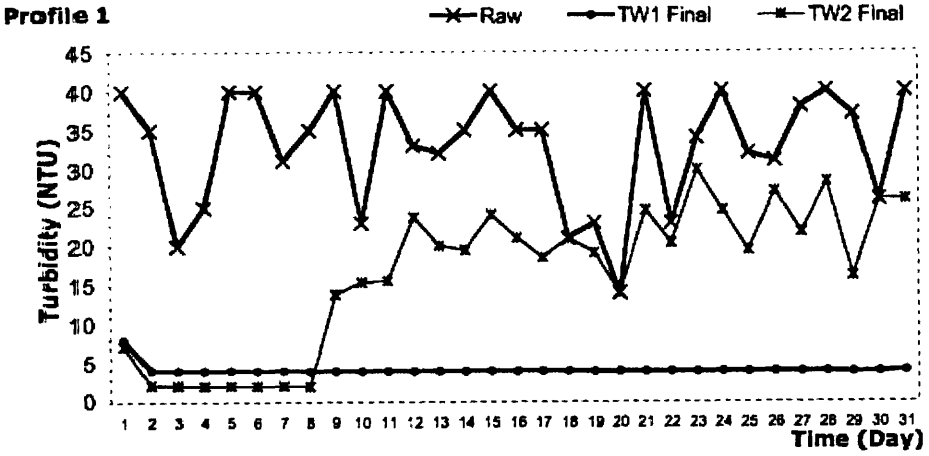
Profile 1
Raw
TW1 Final
TW2 Final
Turbidity (NTU)
Time (Day)

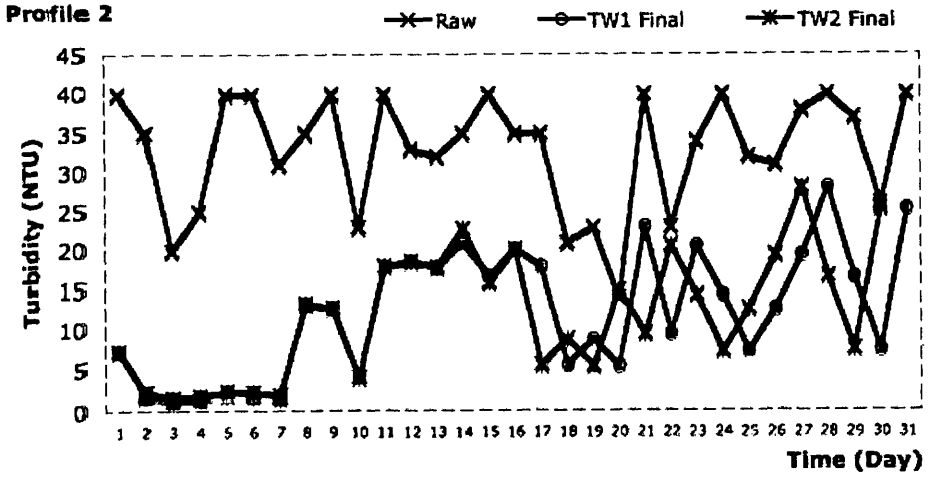
Profile 2
Raw
TW1 Final
TW2 Final
Turbidity (NTU)
Time (Day)

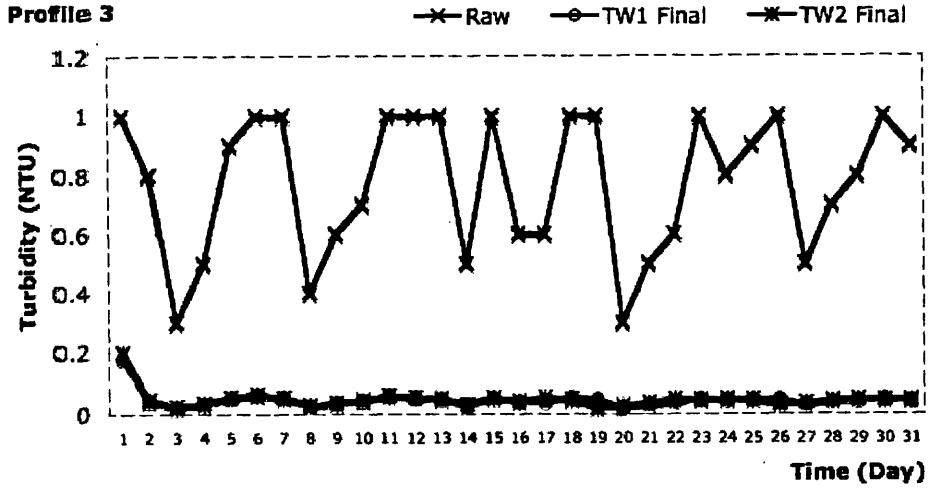
Profile 3
Raw
TW1 Final
TW2 Final
Turbidity (NTU)
Time (Day)

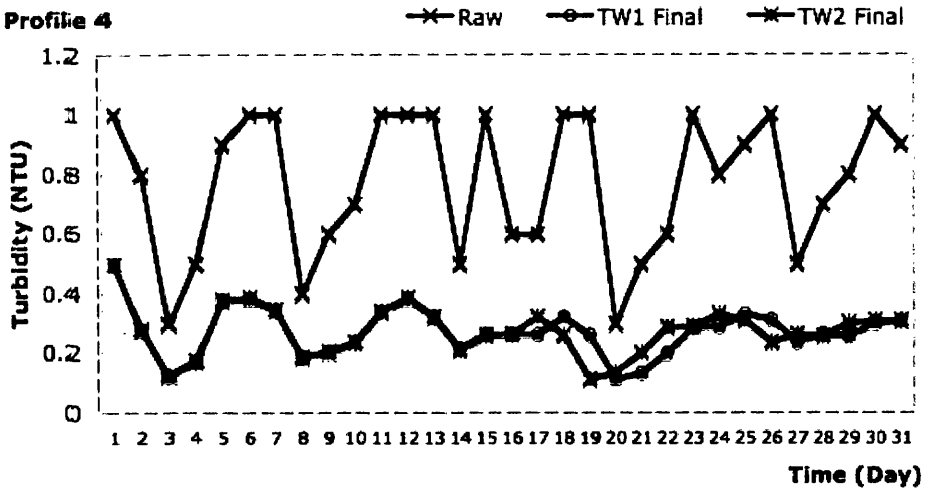
Profile 4
Raw
TW1 Final
TW2 Final
Turbidity (NTU)
1.2
1
0.8
0.6
0.4
0.2
0
1 2 3 4 5 6 7 8 9 10 11 12 13 14 15 16 17 18 19 20 21 22 23 24 25 26 27 28 29 30 31
Time (Day)

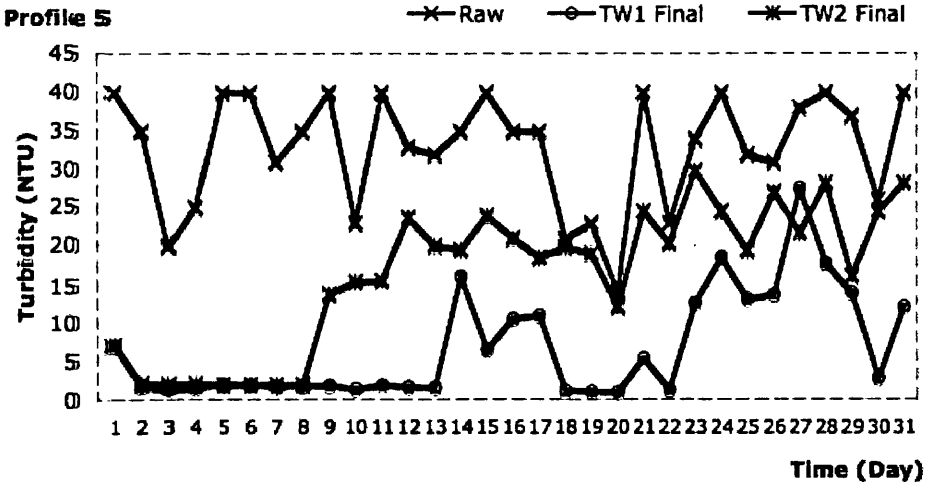
Profile 5
Raw
TW1 Final
TW2 Final
Turbidity (NTU)
45
40
35
30
25
20
15
10
5
0
1 2 3 4 5 6 7 8 9 10 11 12 13 14 15 16 17 18 19 20 21 22 23 24 25 26 27 28 29 30 31
Time (Day)

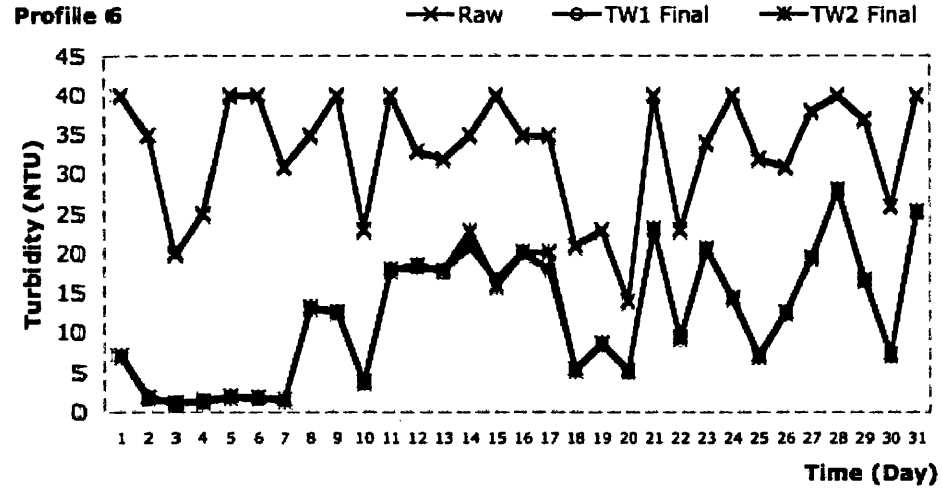
Profile 6
Raw
TW1 Final
TW2 Final
Turbidity (NTU)
45
40
35
30
25
20
15
10
5
0
1 2 3 4 5 6 7 8 9 10 11 12 13 14 15 16 17 18 19 20 21 22 23 24 25 26 27 28 29 30 31
Time (Day)

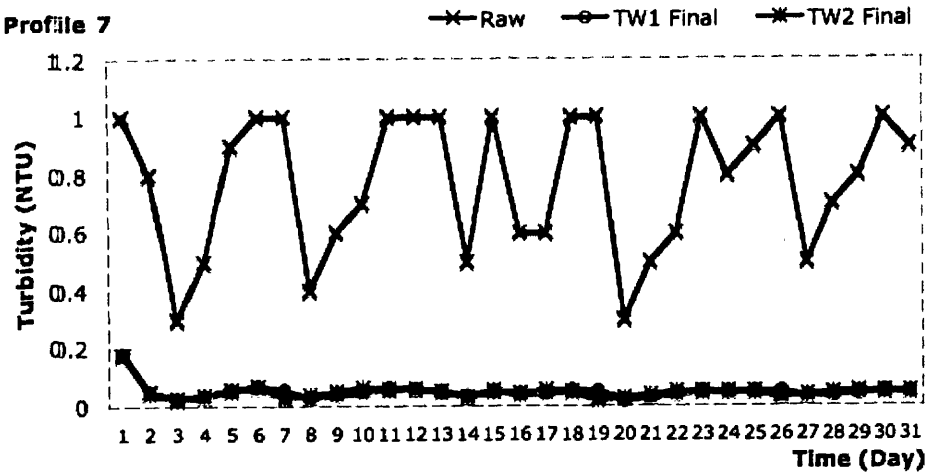
Profile 7
Raw
TW1 Final
TW2 Final
Turbidity (NTU)
1.2
1
0.8
0.6
0.4
0.2
0
1 2 3 4 5 6 7 8 9 10 11 12 13 14 15 16 17 18 19 20 21 22 23 24 25 26 27 28 29 30 31
Time (Day)

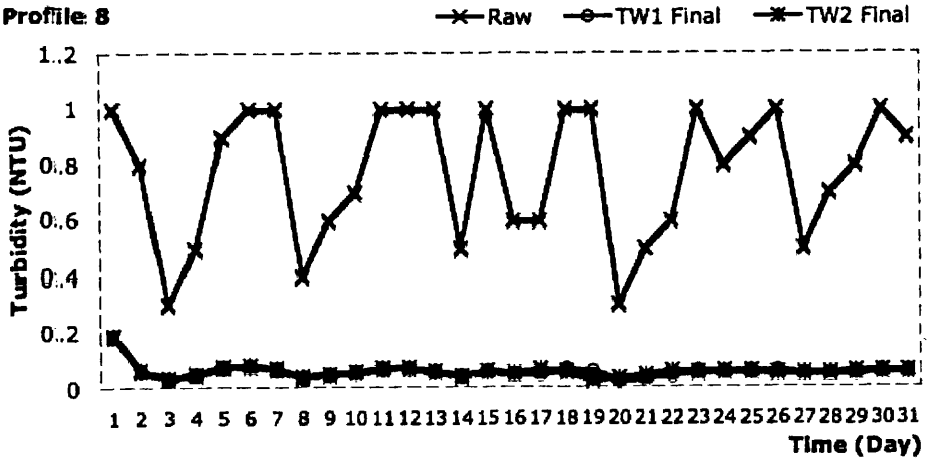
Profile 8
Raw
TW1 Final
TW2 Final
Turbidity (NTU)
1.2
1
0.8
0.6
0.4
0.2
0
1 2 3 4 5 6 7 8 9 10 11 12 13 14 15 16 17 18 19 20 21 22 23 24 25 26 27 28 29 30 31
Time (Day)

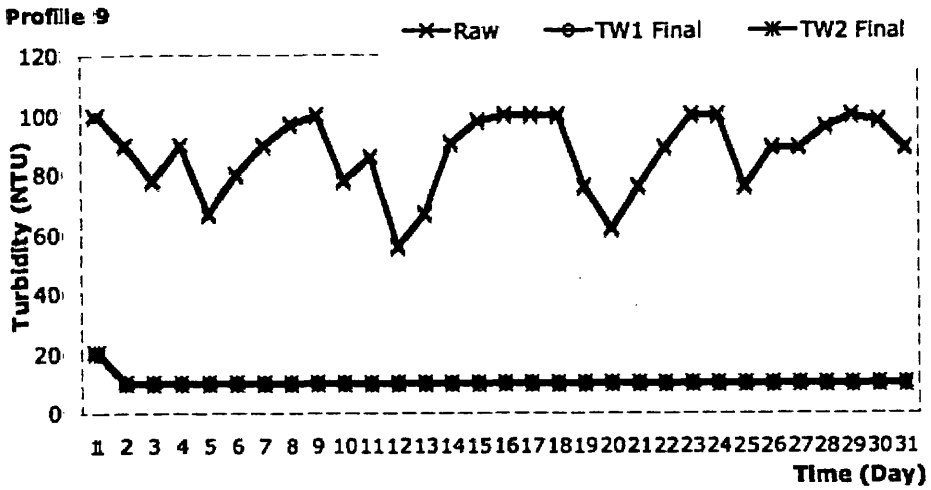
Profile 9
Raw
TW1 Final
TW2 Final
Turbidity (NTU)
120
100
80
60
40
20
0
1 2 3 4 5 6 7 8 9 10 11 12 13 14 15 16 17 18 19 20 21 22 23 24 25 26 27 28 29 30 31
Time (Day)

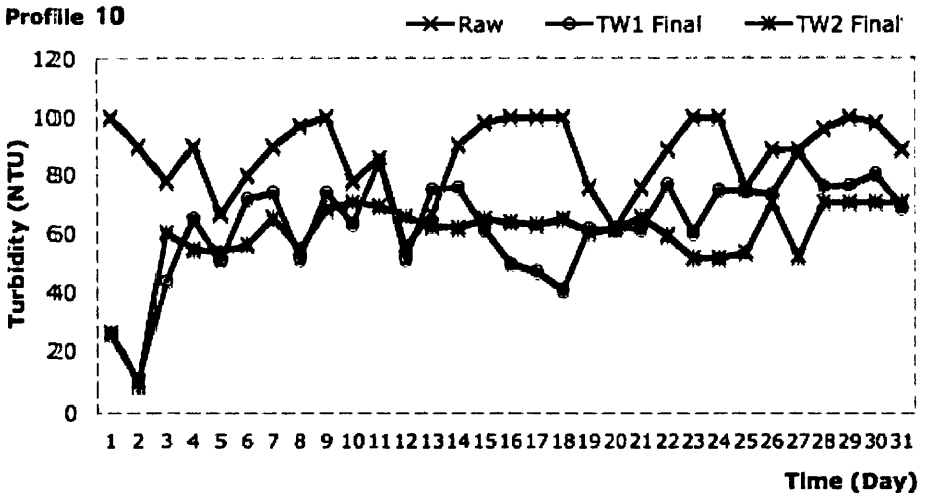
Profile 10
Raw
TW1 Final
TW2 Final
Turbidity (NTU)
120
100
80
60
40
20
0
1 2 3 4 5 6 7 8 9 10 11 12 13 14 15 16 17 18 19 20 21 22 23 24 25 26 27 28 29 30 31
Time (Day)

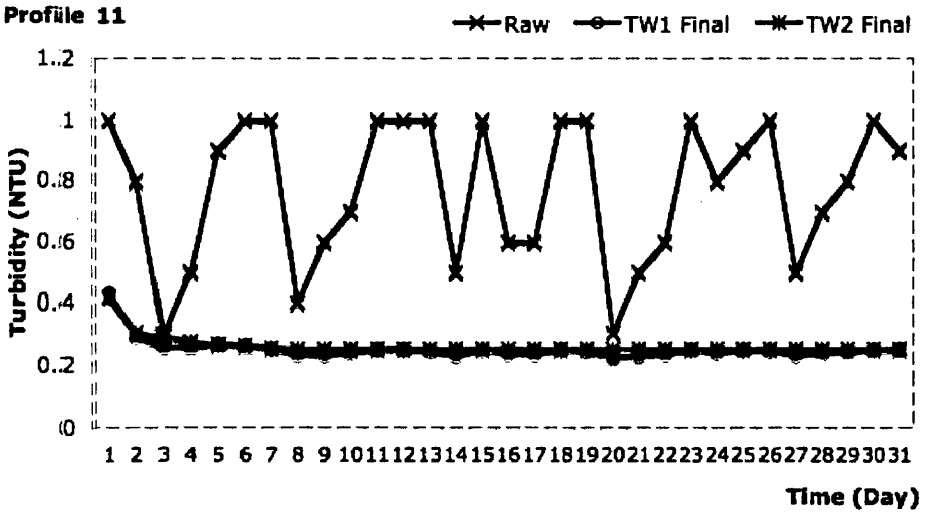
Profile 11
Raw
TW1 Final
TW2 Final
Turbidity (NTU)
1.2
1
0.8
0.6
0.4
0.2
0
1 2 3 4 5 6 7 8 9 10 11 12 13 14 15 16 17 18 19 20 21 22 23 24 25 26 27 28 29 30 31
Time (Day)

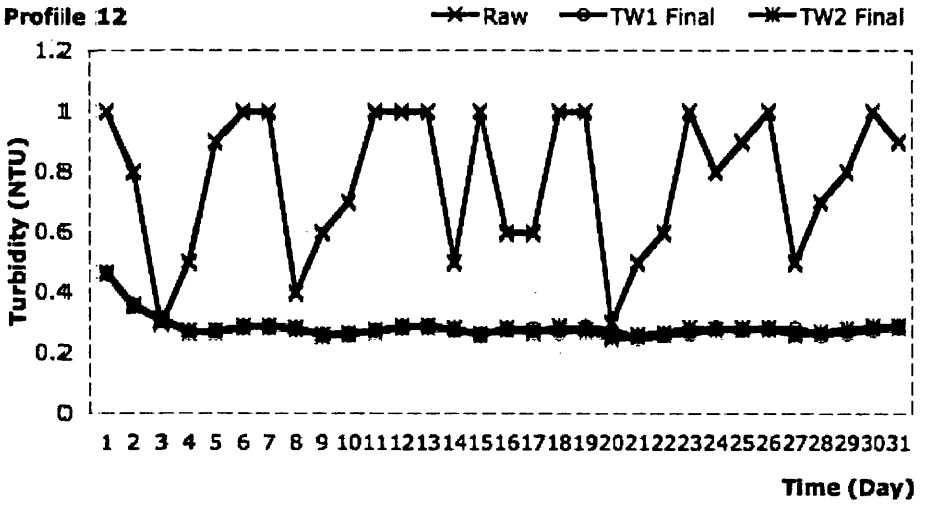
Profile 12
Raw
TW1 Final
TW2 Final
Turbidity (NTU)
1.2
1
0.8
0.6
0.4
0.2
0
1 2 3 4 5 6 7 8 9 10 11 12 13 14 15 16 17 18 19 20 21 22 23 24 25 26 27 28 29 30 31
Time (Day)

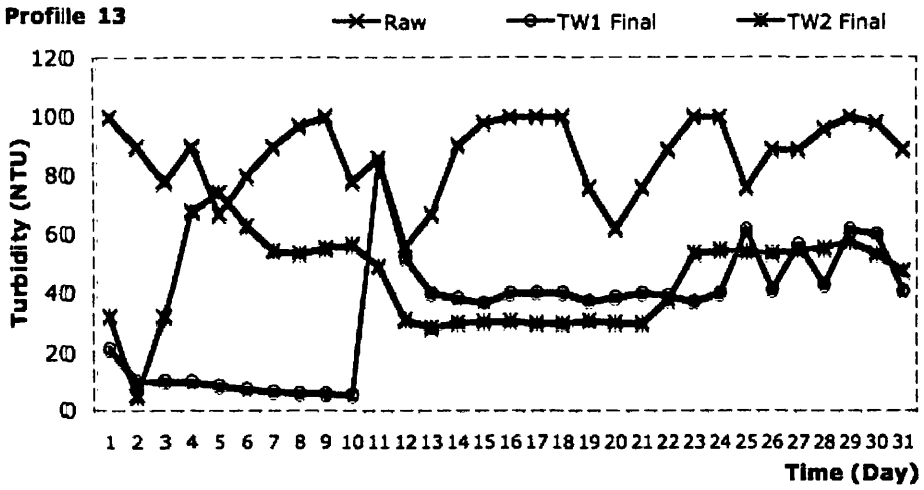
Profile 13
Raw
TW1 Final
TW2 Final
Turbidity (NTU)
120
100
80
60
40
20
0
1 2 3 4 5 6 7 8 9 10 11 12 13 14 15 16 17 18 19 20 21 22 23 24 25 26 27 28 29 30 31
Time (Day)

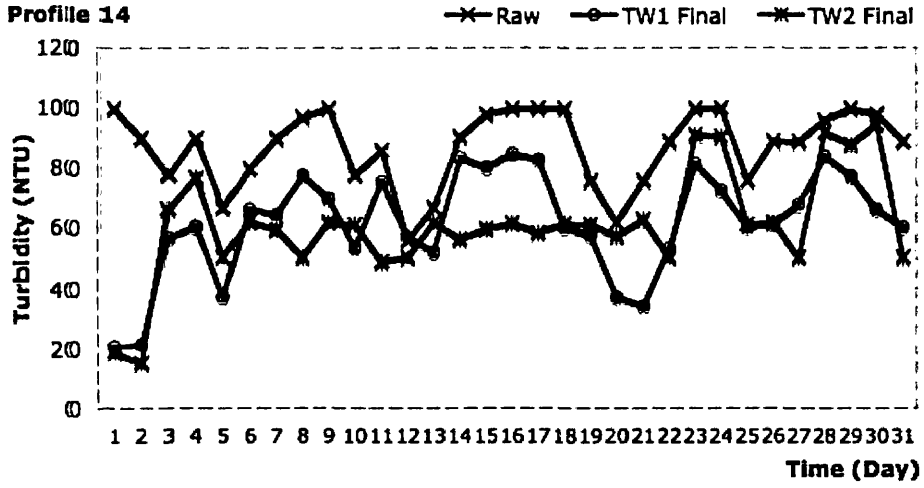
Profile 14
Raw
TW1 Final
TW2 Final
Turbidity (NTU)
120
100
80
60
40
20
0
1 2 3 4 5 6 7 8 9 10 11 12 13 14 15 16 17 18 19 20 21 22 23 24 25 26 27 28 29 30 31
Time (Day)

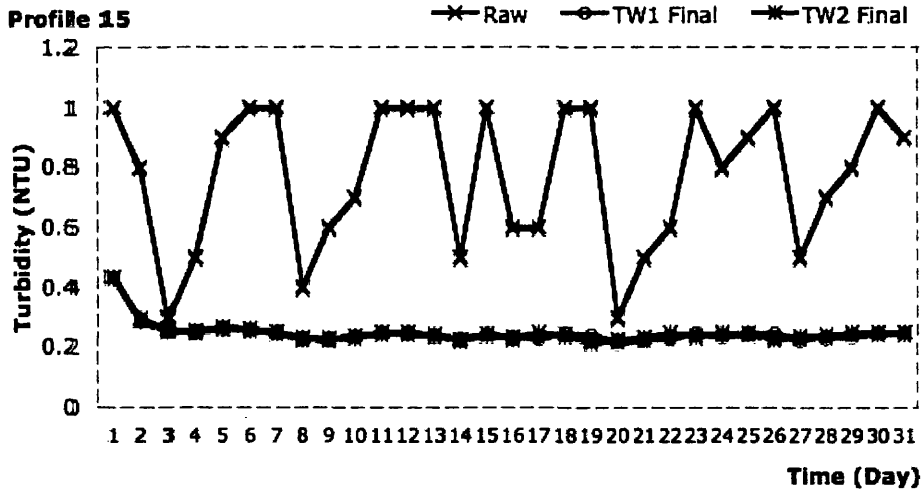
Profile 15
Raw
TW1 Final
TW2 Final
Turbidity (NTU)
1.2
1
0.8
0.6
0.4
0.2
0
1 2 3 4 5 6 7 8 9 10 11 12 13 14 15 16 17 18 19 20 21 22 23 24 25 26 27 28 29 30 31
Time (Day)

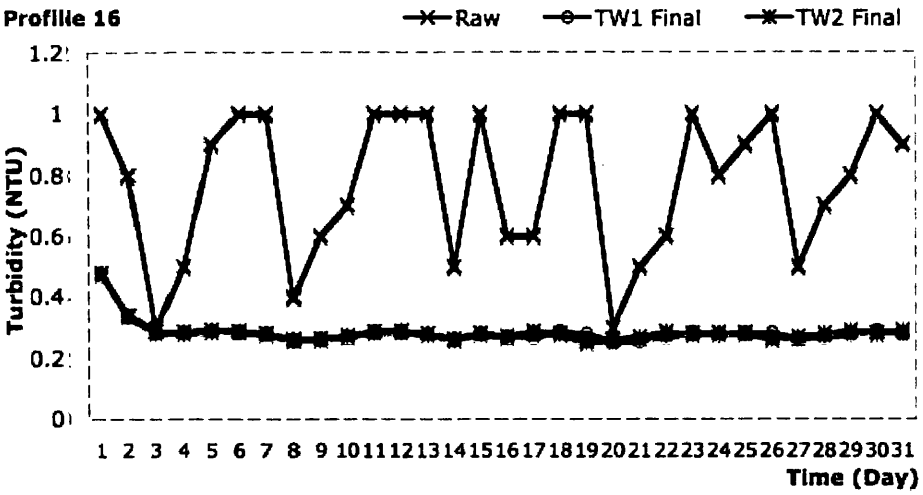
Profile 16
Raw
TW1 Final
TW2 Final
Turbidity (NTU)
Time (Day)

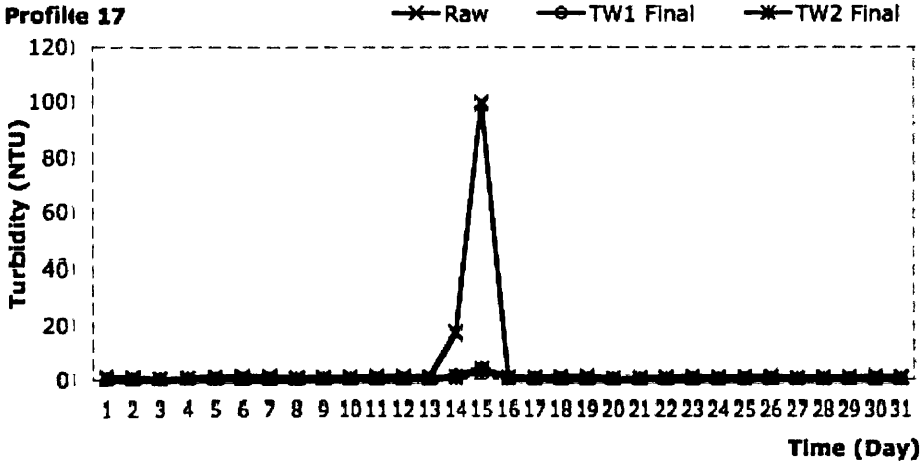
Profile 17
Raw
TW1 Final
TW2 Final
Turbidity (NTU)
Time (Day)

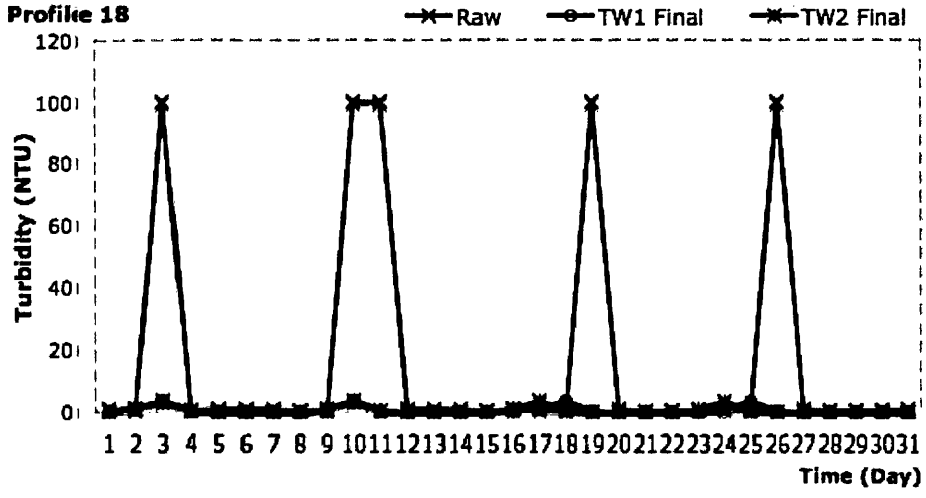
Profile 18
Raw
TW1 Final
TW2 Final
Turbidity (NTU)
Time (Day)

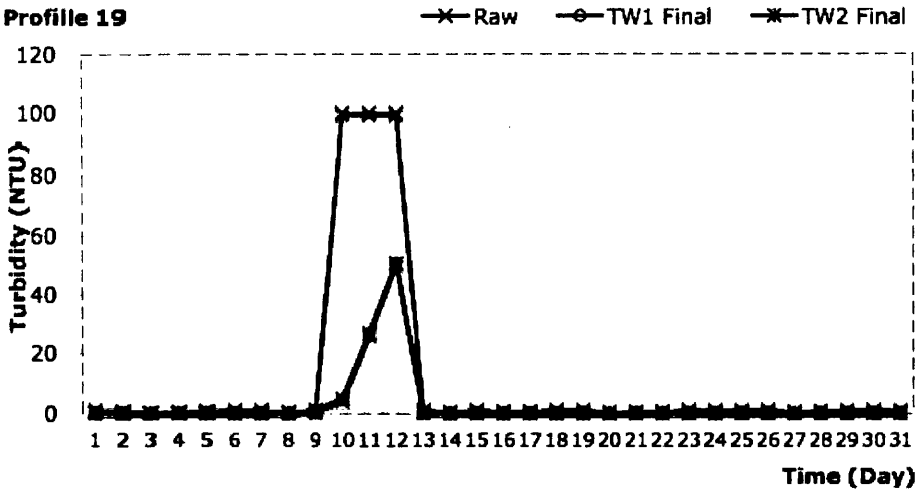
Profile 19
Raw
TW1 Final
TW2 Final
Turbidity (NTU)
120
100
80
60
40
20
0
1 2 3 4 5 6 7 8 9 10 11 12 13 14 15 16 17 18 19 20 21 22 23 24 25 26 27 28 29 30 31
Time (Day)

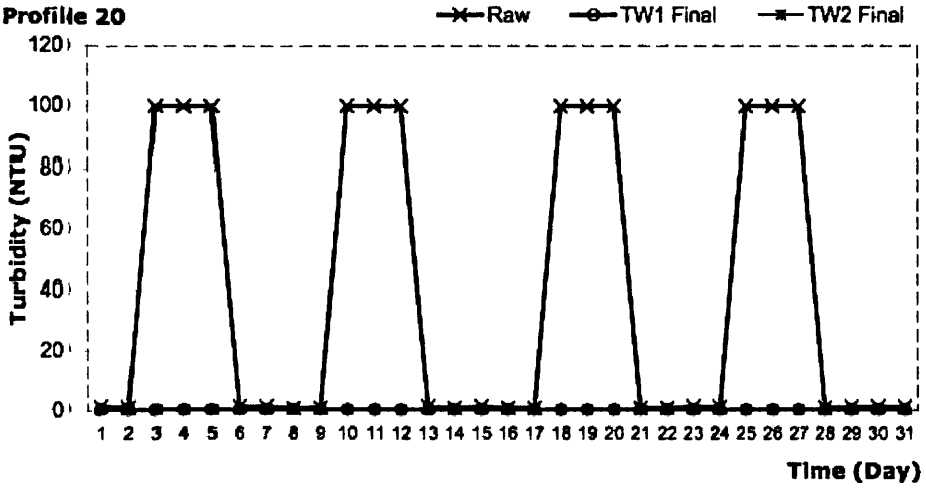
Profile 20
Raw
TW1 Final
TW2 Final
Turbidity (NTU)
120
100
80
60
40
20
0
1 2 3 4 5 6 7 8 9 10 11 12 13 14 15 16 17 18 19 20 21 22 23 24 25 26 27 28 29 30 31
Time (Day)

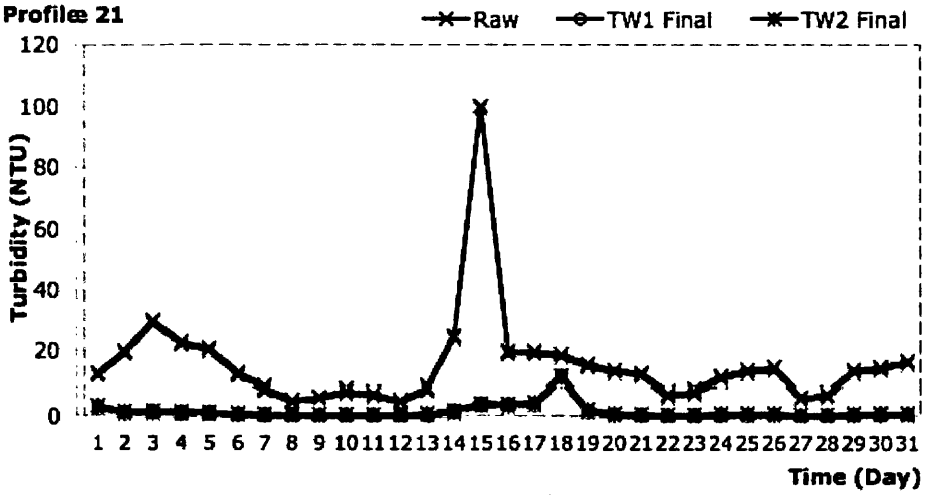
Profile 21
Raw
TW1 Final
TW2 Final
Turbidity (NTU)
120
100
80
60
40
20
0
1 2 3 4 5 6 7 8 9 10 11 12 13 14 15 16 17 18 19 20 21 22 23 24 25 26 27 28 29 30 31
Time (Day)

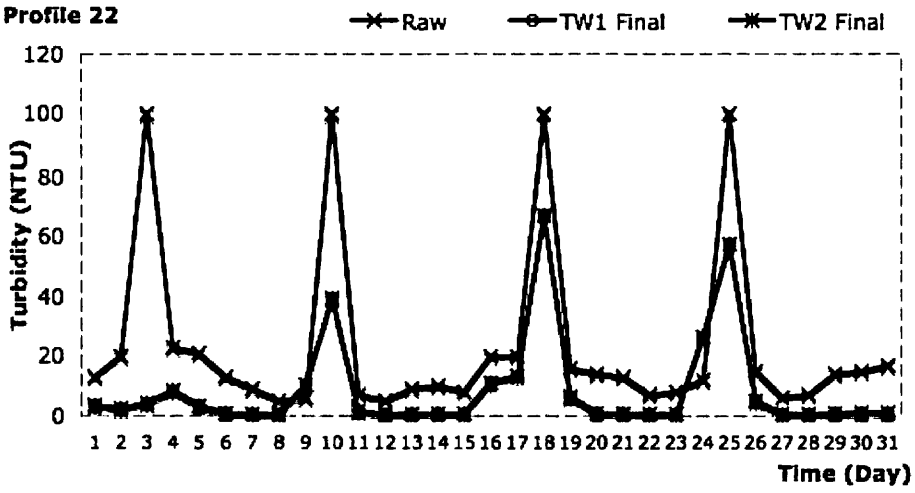
Profile 22
Raw
TW1 Final
TW2 Final
Turbidity (NTU)
Time (Day)

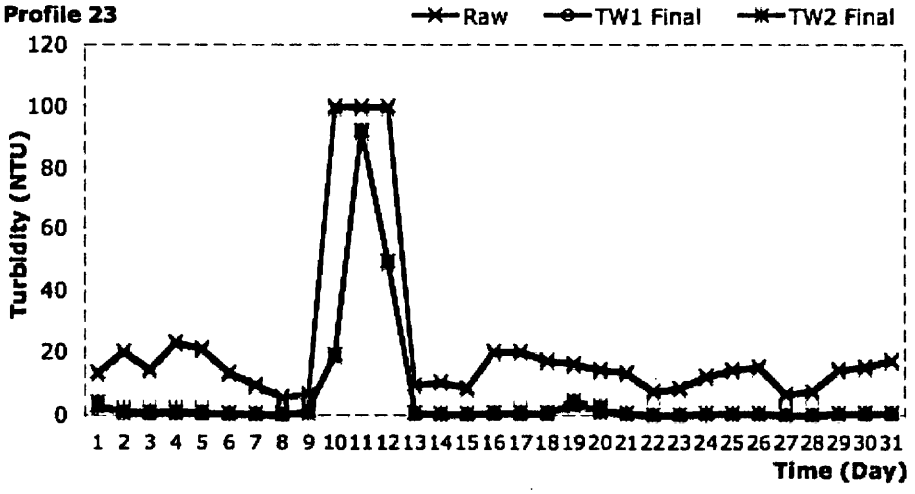
Profile 23
Raw
TW1 Final
TW2 Final
Turbidity (NTU)
Time (Day)

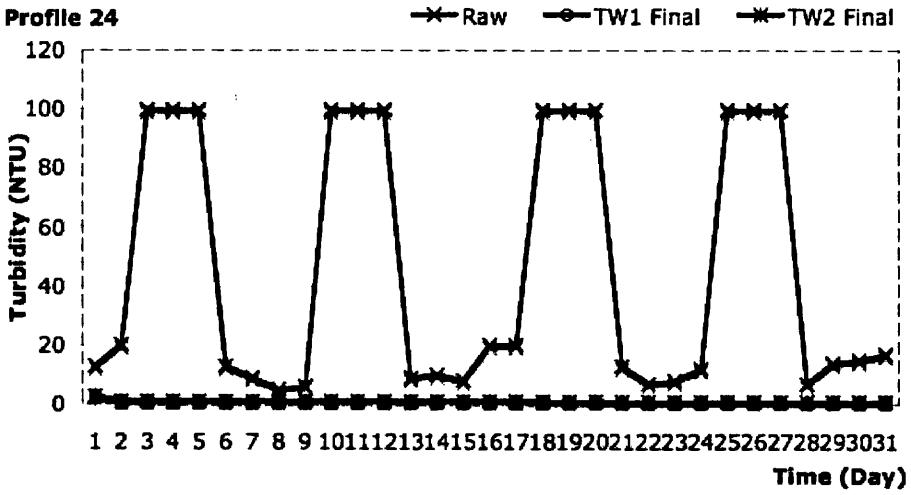
Profile 24
Raw
TW1 Final
TW2 Final
Turbidity (NTU)
Time (Day)

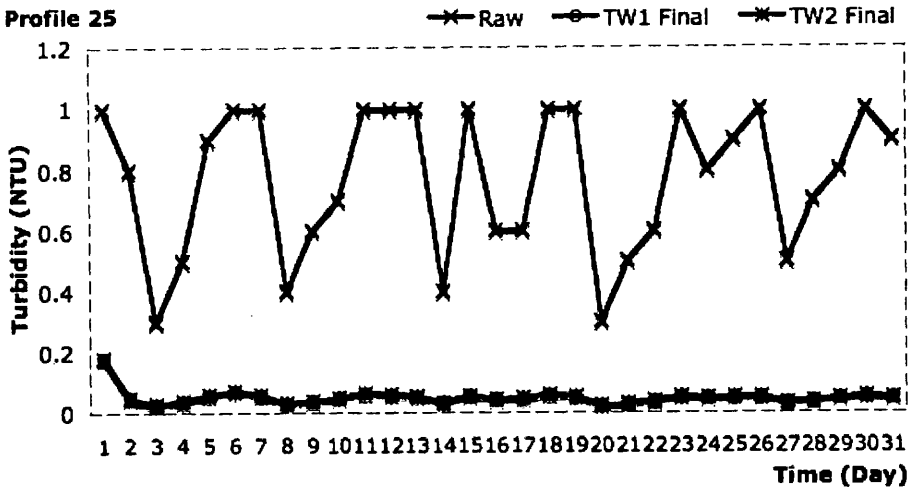
Profile 25
Raw
TW1 Final
TW2 Final
Turbidity (NTU)
1.2
1
0.8
0.6
0.4
0.2
0
1 2 3 4 5 6 7 8 9 10 11 12 13 14 15 16 17 18 19 20 21 22 23 24 25 26 27 28 29 30 31
Time (Day)

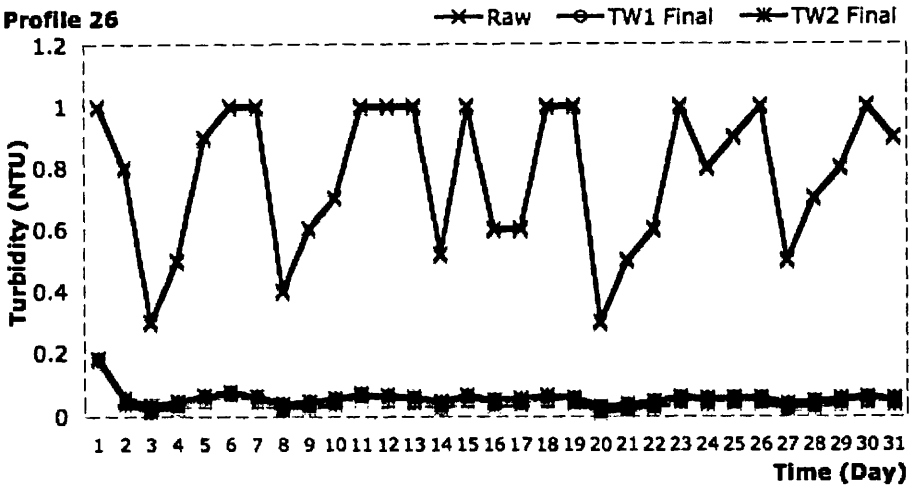
Profile 26
Raw
TW1 Final
TW2 Final
Turbidity (NTU)
1.2
1
0.8
0.6
0.4
0.2
0
1 2 3 4 5 6 7 8 9 10 11 12 13 14 15 16 17 18 19 20 21 22 23 24 25 26 27 28 29 30 31
Time (Day)

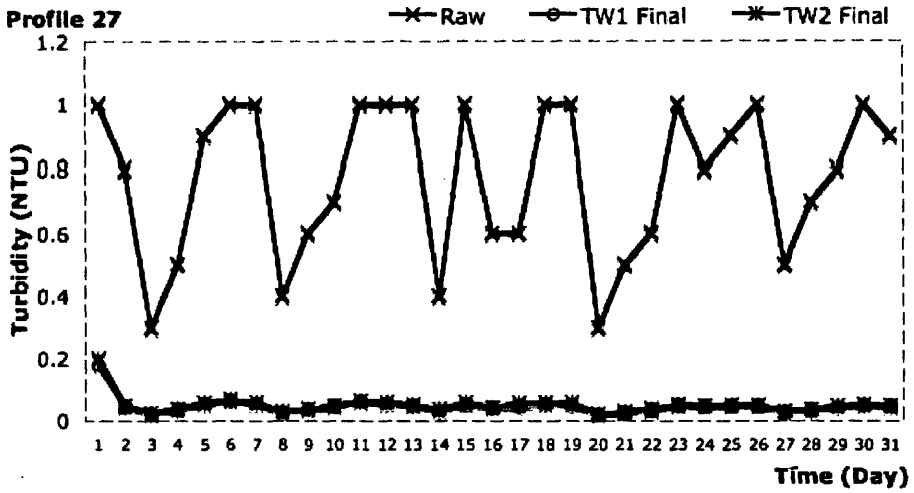
Profile 27
Raw
TW1 Final
TW2 Final
Turbidity (NTU)
1.2
1
0.8
0.6
0.4
0.2
0
1 2 3 4 5 6 7 8 9 10 11 12 13 14 15 16 17 18 19 20 21 22 23 24 25 26 27 28 29 30 31
Time (Day)

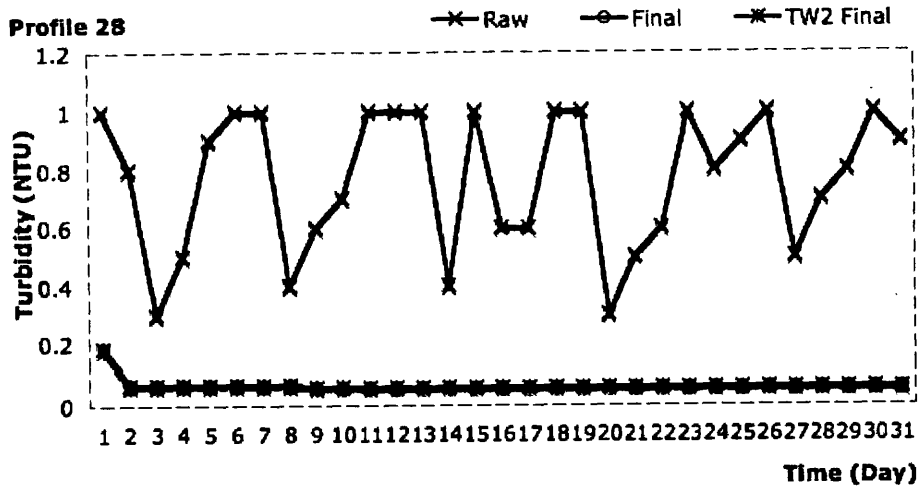
Profile 28
Raw
Final
TW2 Final
Turbidity (NTU)
1.2
1
0.8
0.6
0.4
0.2
0
1 2 3 4 5 6 7 8 9 10 11 12 13 14 15 16 17 18 19 20 21 22 23 24 25 26 27 28 29 30 31
Time (Day)

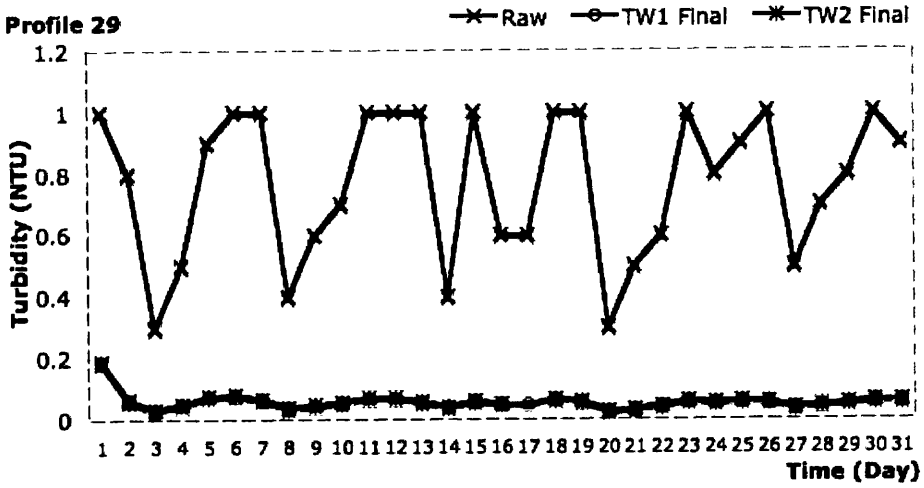
Profile 29
Raw
TW1 Final
TW2 Final
Turbidity (NTU)
1.2
1
0.8
0.6
0.4
0.2
0
1 2 3 4 5 6 7 8 9 10 11 12 13 14 15 16 17 18 19 20 21 22 23 24 25 26 27 28 29 30 31
Time (Day)

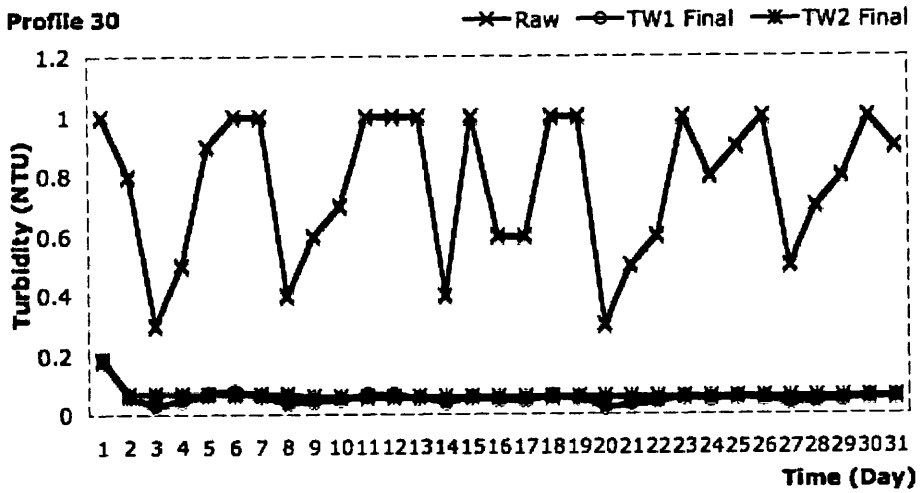
Profile 30
Raw
TW1 Final
TW2 Final
Turbidity (NTU)
1.2
1
0.8
0.6
0.4
0.2
0
1 2 3 4 5 6 7 8 9 10 11 12 13 14 15 16 17 18 19 20 21 22 23 24 25 26 27 28 29 30 31
Time (Day)

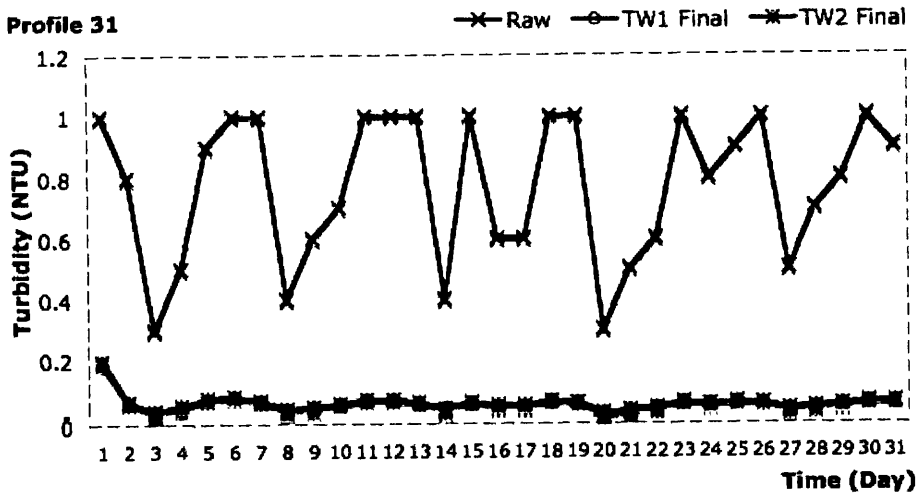
Profile 31
Raw
TW1 Final
TW2 Final
Turbidity (NTU)
1.2
1
0.8
0.6
0.4
0.2
0
1 2 3 4 5 6 7 8 9 10 11 12 13 14 15 16 17 18 19 20 21 22 23 24 25 26 27 28 29 30 31
Time (Day)

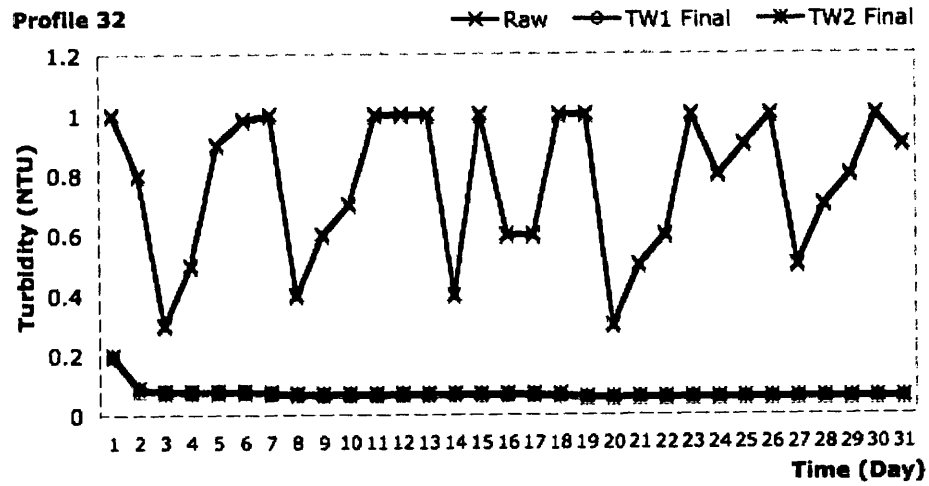
Profile 32
Raw
TW1 Final
TW2 Final
Turbidity (NTU)
1.2
1
0.8
0.6
0.4
0.2
0
1 2 3 4 5 6 7 8 9 10 11 12 13 14 15 16 17 18 19 20 21 22 23 24 25 26 27 28 29 30 31
Time (Day)

# References


[1] J. Dudley, G. Dillon, and L.C. Rietveld. Water treatment simulators. *Journal of Water Supply: Reseach and Technology*, 2008. TU Delft Water Workshop. 2, 4, 5, 6, 7, 8, 23, 40, 171, 174

[2] B.C.T. Lee, T.N. Croft, and C.R. Hayes. Computational fluid dynamics (cfd) modelling of disinfection tanks and water storage structures. In *CIWEM: Disinfection For Water Supply - UV Or Not UV?*, October 2006. 4

[3] Stimela website. Delft University of Technology, [Online] Available http://www.stimela.com. Acessed: 9 June 2009. 5

[4] Mälzer, H-J, and A Nahrstedt. Modellierung mehrstufiger trinkwasseraufbereitungsanlagen mittels eines expertensystem-basierten simulationsmodells (metrex) am beispiel von oberflächenwasser. IWW, 2002. 5

[5] Watpro website. Hydromantis, Inc., [Online] Available: http://www.hydromantis.com/WatPro.html. Acessed: 9 June 2009. 5

[6] A. W. C. van der Helm and L. C. Rietveld. Modelling of drinking water treatment

processes within stimela environment. *Water Science and Technology: Water Supply*, pages 87 – 93, 2002. 6

[7] Water treatment plant model for ms windows 3.1 web guide. US EPA, [Online] Available http://yosemite.epa.gov/water/owrccatalog.nsf/065ca07e299b464685256ce50075c11a/80acea46c3412a1185256b06007259ee!OpenDocument. 6

[8] G. W. Harrington, Z. K. Chowdhury, and D. M. Owen. Developing a computer model to simulate dbp formation during water treatment. *Journal of American Water Works Association*, 84:78 – 87, 1992. 6

[9] Watpro version 2 users' manual. Supplied with WatPro. 7

[10] L. Rietveld, P. Ross, and J. Dudley. Techneau water treatment simulator: Modelling framework (version 1.0). Technical report, TECHNEAU, September 2008. 7

[11] Anastasios J. Stamou. Improving the hydraulic efficiency of water process tanks using cfd models. *Chemical Engineering and Processing: Process Intensification*, 47:1179 – 1189, August 2007. 7

[12] T. Matko, N. Fawcett, A. Sharp, and T. Stephenson. Recent progress in the numerical modelling of wastewater sedimentation tanks. Technical report, Institution of Chemical Engineers, 2005. 7

[13] P. Larsen. On the hydraulics of rectangular settling basins. Technical report, Department of Water Research Engineering, Lund Institute of Technology, 1977. 8

[14] M. Al-Sammarraee, A. Chan, S.M. Salim, and U.S. Mahabaleswar. Large-eddy simulations of particle sedimentation in a longitudinal sedimentation basin of a water treatment plant. part 1: Particle settling performance. *Chemical Engineering Journal*, Article in press, 2009. 8

[15] D.J. Burt and J. Ganeshalingam. Design and optimisation of final clarifier performance with cfd modelling. In *CIWEM/Aqua Enviro Joint Conference*, 2005. 8

[16] Athanasia M. Goula, Margaritis Kostogrou, Thodoris D. Karapantrios, and Anastasios T. Zoubolis. A cfd methodology for the design of sedimentation tanks in potable water treatment: A case study- the influence of a feed flow control baffle. *Chemical Engineering Journal*, 140:110 –121, July 2008. 8

[17] M. Al-Sammarraee, A. Chan., S.M. Salim, and U.S. Mahabaleswar. Large-eddy simulations of particle sedimentation in a longitudinal sedimentation basin of a water treatment plant. part 2: The effects of baffles. *Chemical Engineering Journal*, Article in press, 2009. 8

[18] N.G. Wright and D.M. Hargreaves. The use of cfd in the evaluation of uv treatment systems. *Hournal of Hydroinformatics*, 2001. 8

[19] K. Craig, C. De Traversy, B.Bowen, K. Essemiani, C. Levecq, and R. Naylor. Hydraulic study and optimisation of water treatment processes using numerical solution. *International Water Association, World Water Congress No. 3 Melbourne*, 2(5 -6):135 –142, 2002. 8

[20] C.T. Ta and J. Hague. A two-phase computational fluid dynamics model for

ozone tank design and troubleshooting in water treatment. *Ozone: Science and Engineering*, 26(4):403 – 411, August 2004. 8

[21] K. Essemiani and C. De Traversy. Optimisation of the flocculation process using cfd. In *Chemical water and wastewater treatment*, volume VII, pages 41 – 50. IWA Publishing, 2002. 8

[22] J. Bridgeman, B. Jefferson, and S.A. Parsons. The development and application of cfd models for water treatment flocculators. In Press, 2009. 8, 9, 10, 172

[23] Seokjong Byun, Jeongik Oh, Bo-Young Lee, and Seockheon Lee. Improvement of coagulation efficiency using instantaneous flash mixer for water treatment. *Colloids and Surfaces A: Physiochemical and Engineering Aspects*, 268:104 – 110, 2005. 9

[24] Rome-Ming Wu, tsung Hao Lee, and Wen-Jie Yang. Study of flow in a blanket clarifier using computational fluid dynamics. *Journal of Environmental Engineering*, pages 443 – 455, June 2008. 9

[25] Bhr group website. BHR Group, [Online] Available http://www.bhrgroup.co.uk/. Acessed: 14 June 2009. 9, 174

[26] Cfd modelling of clarifier innocation by bhr group. BHR Group, [Online] Available http://www.bhrgroup.co.uk/cases/water12.htm. Acessed 14 June 2009. 9

[27] Tuan C Ta. Current cfd tool for water and waste water treatment process. *ASME Pressure Vessels Piping div Publ PVP*, 396:79 – 85, 1999. 9

[28] K.J. Ives. Theory of operation of sludge blanket clarifiers. *Proc. Institution of Civil Engineers*, 1968. 10

[29] R. Gregory. Floc blanket clarification. Technical report, WRc, March 1979. Technical Report TR 111. 10, 20, 21, 132

[30] Richard Head, Jem Hart, and Nigel Graham. Simulating the effect of blanket characteristics on the floc blanket clarification process. *Water Science and Technology*, 36(4):77–84, 1997. 10, 11, 28, 171

[31] Bernard W. Gould. Upflow clarifiers - flow flexibility related to concentrator size. *Effluent and Water Treatment Journal*, 14:621–631, 1974. 10, 28, 29

[32] T. Hall and R. A. Hyde., editors. *Water Treatment Processes and Practices.* WRc, 1992. 13, 14, 15, 16, 19, 21

[33] Council directive 98/83/ec. Eur-Lex, [Online] Available: http://eur-lex.europa.eu/LexUriServ/LexUriServ.do?uri=CELEX:31998L0083:EN:NOT. Accessed: 30 June 2009. 14

[34] United States Environmental Protection Agency. The history of drinking water treatment. Technical report, Office of Water, United States Environmental Protection Agency, February 2000. 14

[35] Gerard Kiely. *Environmental Engineering.* McGraw-Hill International Editions, 1998. 15

[36] T. H. Y. Tebutt. *Principles of Water Quality Control.* Butterworth-Heinemann, 5th edition, 1998. 15, 16

[37] Ladislav Svarovsky. *Solid-Liquid Separation.* Butterworth-Heinemann, 4 edition, 2000. 17

[38] R. Head, D. Shepherd, G. Butt, and G. Buck. Otter mathematical process simulation of potable water treatment. *Water Science and Technology: Water Supply*, pages 95 –101, 2002. 23

[39] WRc. *OTTER Documentation.* 23, 27, 30, 163

[40] M Butler. The analysis and modelling of two water treatment works. Master's thesis, Water Resources Technology and Management, Birmingham University, 1998. 23

[41] Z. Gallis. Modelling and simulation of water treatment plants. Master's thesis, Department of Civil and Environmental Engineering, University of London, 1999. 23

[42] Q. G. Guo and N. Sankararamakirshnan. Development of a numerical model for assessing the impact of raw water on conventional drinking water treatment. Technical report, New Jersey Department of Environmental Protection, Trenton, New Jersey, 2003. 23

[43] Barnea E and Mizrahi J. A generalised approach to the fluid dynamics of particulate systems:parti - general correlation for fluidisaion and sedimentation in solid multiparticle systems. *Chemical Engineering Journal*, 5:171–189, 1973. 29

[44] H K Versteg and W Malalasekera. *An Introduction to Computational Fluid Dynamics: The Finite Volume Method.* Pearson Prentice Hall, 1995. 47, 49, 50

[45] Diane McBride, Nick Croft, and Mark Cross. Combined vertex-based - cell-centered finite volume method for flows in complex geometries. In *Third In-*

*ternational Conference on CFD in the Minerals and Process Industries.* CSIRO, Melbourne, Australia, 2003. 50

[46] Femgv website. TNO Diana, [Online] Available: http://www.tnodiana.com. Accessed: 22 May 2009. 51

[47] Physica website. PHYSICA Ltd, [Online] Available: http://www.physica.co.uk. Accessed: 22 May 2009. 52

[48] C. M. Rhie and W. L. Chow. Numerical study of the turbulent flow past an airfoil with trailing edge separation. *AIAA*, 21:1525 – 1532, 1983. 52, 53

[49] S.V. Patankar. A calculation for two dimensional elliptic situations. *Numerical Heat Transfer*, 1979. 53

[50] Physica theory guide. PHYSICA, [Online] Available http://www.greenwich.ac.uk/~physica/phy3.00/theory/. Last assessed: 30 June 2009. 53

[51] M. Cross, T. N. Croft, G. Djambazov, and K. Pericleous. Computational modelling of bubble, droplets and particles in metals reduction and refining. *Applied Mathematical Modelling*, 30:1445 – 1458, 2006. 55

[52] John Gregory. The density of particle aggregates. *Water Science and Technology*, 36(4):1–13, 1997. 77, 78

[53] A. L. Lagvankar and R. S. Gemmell. A size-density relationship for flocs. *Journal of American Water Works Association*, 60:1040–1046, 1968. 77

[54] N. Tambo and Y. Watanabe. Physical aspects of flocculation. the floc density function and aluminium floc. *Water Research*, 13:409 – 419, 1979. 77, 78

[55] Desmond F. Lawler. Particle size distributions in treatment processes: Theory and practice. *Water Science and Technology*, 36(4):15–23, 1997. 78

[56] P. S. Monteiro. The influence of the anaerobic digestion process on the sewage sludges rheological behaviour. *Water Science and Technology*, 36:61 – 67, 1997. 135

[57] Slatter P. T. The rheological characterisationi of sludges. *Water Science and Technology*, 36:9 – 18, 1997. 135

[58] N. Tixier, G. Guibaud, and M. Baudu. Determination of some rheological parameters for the characterization of acitvated sludge. *Bioresource Technology*, 90:215 – 220, 2003. 135

[59] Warden J. H. Sludge treatment plant for waterworks. Technical Report TR 189, WRc, March 1989. 137